



Published in final edited form as:

J Med Chem. 2022 February 24; 65(4): 2880–2904. doi:10.1021/acs.jmedchem.1c00598.

Structure-based optimization of ML300 derived, non-covalent inhibitors targeting the severe acute respiratory syndrome coronavirus 3CL protease (SARS-CoV-2 3CL^{pro})

Sang Hoon Han^{a,#}, Christopher M. Goins^{a,#}, Tarun Arya^a, Woo-Jin Shin^b, Joshua Maw^a, Alice Hooper^a, Dhiraj P. Sonawane^a, Matthew R. Porter^a, Breyanne E. Bannister^c, Rachel D. Crouch^c, A. Abigail Lindsey^a, Gabriella Lakatos^a, Steven R. Martinez^a, Joseph Alvarado^a, Wendell S. Akers^c, Nancy S. Wang^a, Jae U. Jung^{d,e}, Jonathan D. Macdonald^a, Shaun R. Stauffer^{a,*}

^aCenter for Therapeutics Discovery, Lerner Research Institute, Cleveland Clinic, Cleveland, OH, 44195, USA

^bCleveland Clinic Florida Research & Innovation Center, Port St. Lucie, FL, 34987, USA

^cDepartment of Pharmaceutical Science, Lipscomb University College of Pharmacy, Nashville, TN, 37204, USA

^dDepartment of Cancer Biology, Lerner Research Institute, Cleveland Clinic, Cleveland, OH, 44195, USA

^eCenter for Global and Emerging Pathogens Research, Lerner Research Institute, Cleveland Clinic, Cleveland, OH, 44195, USA

Abstract

Starting from the MLPCN probe compound ML300 a structure-based optimization campaign was initiated against the recent severe acute respiratory syndrome coronavirus (SARS-CoV-2) main protease (3CL^{pro}). X-ray structures of SARS-CoV-1 and CoV-2 3CL^{pro} enzymes in complex with multiple ML300 based inhibitors, including the original probe ML300, were obtained and proved instrumental in guiding chemistry towards probe compound **41** (CCF0058981). The inhibitors disclosed utilize a non-covalent mode of action and complex in a non-canonical binding mode not observed by peptidic 3CL^{pro} inhibitors. *In vitro* DMPK profiling highlight key areas where

*Corresponding author, stauffs2@ccf.org.

#These authors contributed equally

Associated Content

Supporting Information

The Supporting Information is available free of charge on the ACS Publications website at DOI:

- Supplemental Figures, SARS-CoV-1 3CL^{pro} X-ray structures; Tier 1 DMPK Summary; Human S9 generated metabolites and MS fragmentation; X-ray data collection and refinement statistics; ligand electron density maps.
- Molecular-formula strings
- UV-based HPLC chromatograms of final compounds
- **41** CPE SARS-CoV-2 infected Vero E6 concentration-response-curve and Table

PDB ID Codes

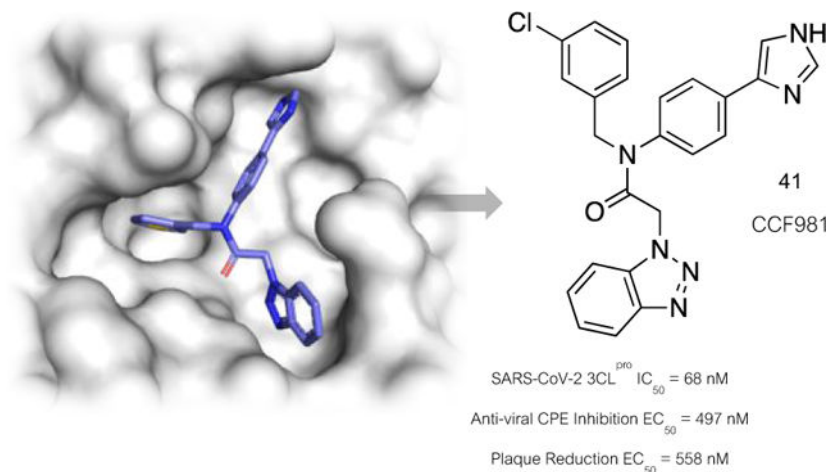
SARS-CoV-2 complexes: **1** PDB: 7LME; **19** PDB: 7LMD; **21** PDB: 7LMF.

SARS-CoV-1 complexes: **8** PDB: 7LMH; **19** PDB: 7LMI; **21** PDB: 7LMG; **35** PDB: 7LMJ.

Authors will release the atomic coordinates and experimental data upon article publication.

further optimization in the series is required to obtain useful in vivo probes. Anti-viral activity was established using a SARS-CoV-2 infected Vero E6 cell viability assay, and in a plaque formation assay. Compound **41** demonstrates nanomolar activity in these respective assays, comparable in potency to remdesivir. These findings have implications towards antiviral development to combat current and future SARS-like zoonotic coronavirus outbreaks.

Graphical Abstract



Keywords

3CL^{pro}; M^{pro}; SARS-CoV-2; COVID-19; coronavirus

Introduction

Coronaviruses (CoV) are a family of enveloped positive-strand RNA pathogenic viruses that can cause acute and chronic conditions including central nervous system disorders, the common cold, lower respiratory tract infections, and diarrhea.¹ The 229E and OC43 strains were among the first characterized human CoV strains starting in 1965.² The novel severe acute respiratory syndrome CoV reported in 2003,^{3,4} that is now identified as SARS-CoV-1, became the first global human CoV pandemic leading to progressive respiratory failure in over 8,000 individuals and 916 deaths (fatality rate of 10–15%).⁵ In the eight years that followed, significantly less lethal human coronaviruses NL64 and HKU1 were identified and characterized.^{6,7} Subsequently in 2012 the SARS-like MERS (Middle East Respiratory Syndrome) was identified and found to have a low transmission rate, but significant lethality with a total of 2567 patients with confirmed infection worldwide, of which 882 (34% fatality) died from 2012 through February 2nd, 2021. To date, most confirmed MERS cases have been reported from Saudi Arabia.⁸ Like the SARS-CoV of 2003 and MERS of 2012, the ongoing novel SARS-CoV pandemic of 2020, known as SARS-CoV-2, the causative agent of COVID-19, presents a worldwide threat due to its ability to rapidly spread person-to-person via respiratory droplets and its remarkable capacity to suppress human immune surveillance.⁹ Unfortunately SARS CoV-2 has been much more extensive than that of MERS and SARS CoV-1 in its spread, with current worldwide infections, as of March 29,

2021 exceeding 126 million confirmed cases of COVID-19 and 2,778,619 confirmed deaths (fatality rate of ~2%) according to the World Health Organization (WHO).¹⁰

The coronavirus SARS-CoV-2,¹¹ encodes multiple enzymes that are essential for viral replication.^{12,13} As potential therapeutic antiviral targets, the two cysteine proteases – the chymotrypsin-like or main protease (3CL^{pro} or M^{pro}), and the papain-like protease (PL^{pro}) – have garnered significant attention.^{14–16} Both SARS-CoV-1 and CoV-2 genomes encode a large polyprotein that is proteolytically processed by these respective cysteine proteases. In solution, 3CL^{pro} exists primarily as a dimer and has been confirmed to be the catalytically active species.¹⁷ 3CL^{pro} is responsible for processing at 11 different cleavage sites within the coronavirus polyprotein and PL^{pro} is responsible for cleavage at three other unique sites. Without these essential proteases replication is impaired and shuts down the viral life cycle.¹⁸ CoV 3CL^{pro} enzymes contain three structural domains connected by flexible loops. Domains I and II are β -barrel domains and contain the catalytic active site region, whereas domain III is an α -helical domain shown to be critical for dimerization.¹⁹ The active site contains a catalytic dyad consisting of a cysteine residue (Cys-145) that acts as a nucleophile and a histidine residue (His-41) that acts as the general acid-base.

Many published inhibitors of SARS-CoV-1 3CL^{pro}, and more recently for SARS-CoV-2 3CL^{pro} have been peptide-like, and often include a reactive center targeted toward a covalent interaction with the catalytic cysteine, Cys145. In collaboration with Mesecar and co-workers, and other member teams from NIH MLPCN, including the Scripps Research Institute Molecular Screening Center (SRIMSC) and the Vanderbilt Specialized Chemistry Center (VSCC), we participated in efforts to develop inhibitors of a coronavirus 3CL^{pro} in the aftermath of the SARS-CoV-1 outbreak, with a particular focus on the development of non-covalent inhibitors, leading to ML300 and ML188 (**1** and **2**, Figure 1).^{20–21} Examples of *de novo*, non-covalent inhibitors designed towards SARS-CoV-2 3CL^{pro} include the recently disclosed pyridone, **3**.²² In the course of the COVID-19 pandemic, two covalent inhibitors previously discovered, **4** (GC-376)²³ and **5** (PF-00835231)²⁴ have advanced into clinical trials in 2020. The phosphate pro-drug of **5**, PF-07304814 is also under clinical evaluation.²⁵

Among human novel CoV's the highest sequence homology for the 3CL^{pro} protease exists between SARS-CoV-1 and SARS-CoV-2, with an overall 96% sequence identity and 100% identity in the active site, giving rise to similar substrate specificity,²⁶ thus providing the field with an advanced starting point for the development of SARS-CoV-2 3CL^{pro} inhibitors. Structural biology has played a critical role in 3CL^{pro} protease inhibitor development, beginning with the first X-ray structure in 2003 with a hexapeptidyl chloromethyl ketone inhibitor bound to TGEV 3CL^{pro} (PDB: 1P9U)²⁷ and SARS-CoV-1 3CL^{pro} (PDB: 1UK4).²⁸ Today, a multitude of X-ray crystal structures have emerged comparing CoV 3CL^{pro}'s including SARS-CoV-2 to aid and galvanize inhibitor design efforts. High impact early contributions in the context of the ongoing pandemic include those from the Diamond Light Source XChem X-ray fragment screening program,²⁹ Shanghai Tech University N3-peptide,³⁰ University of Lübeck dicarbonyl compound 13b,²⁶ peptide based aldehydes similar to **5** reported by Dai and co-workers at the Chinese Academy of Sciences,³¹ and baicalein and related natural products from University of Chinese Academy of Sciences.³² More recent developments include evidence from a March 2020 Science report from Qiao

and co-workers³³ at Sichuan University demonstrating preclinical *in vivo* efficacy in a human angiotensin converting enzyme 2 (hACE2) transgenic SARS-CoV-2 murine model. Using a moderate infection threshold the Sichuan team developed a peptidyl aldehyde based upon a Boceprevir design. One of the lead orally bioavailable inhibitors, MI-09, was administered at 100 mg/kg BID 1h prior to virus inoculation and then continuing for 5 days post infection. In this study compound MI-09 demonstrated significant viral RNA load reduction within 3 days, with almost no virus detected by day 5, thus setting the stage as a comparator for emerging tool compounds to be evaluated and assessed against for their efficacy and overall PK-PD.

Our focus was directed to the synthesis and further optimization of non-peptidic, non-covalent inhibitors of SARS-CoV-2 3CL^{pro} that are derived from ML300.²¹ We were intrigued to investigate the ML300 series against SARS-CoV-2 for several reasons. Notably, in contrast to ML188 and prior peptidomimetics bound to 3CL^{pro} in a canonical binding mode wherein the inhibitor accommodates substrate sub-pockets in the enzyme active-site, the SARS-CoV-1 3CL^{pro} X-ray structure of the ML300 series HTS hit, **6** (Figure 2A) favors an induced-fit complex where key flexible amino acid side chains in the binding pocket, specifically Gln189 and Met49, take on distinct conformations and in tandem reorganize the S4 and S2 binding surface. The observed induced-fit allows the bis-aniline to occupy a newly formed channel proximal between what is traditionally the canonical S1' and S2 pockets (S2_c = S2 channel). Conversely, the pyrrole ring of **6** exists in a deeper sub-pocket of S2 (S2_{sp}) that is more proximal to the traditional S4 pocket.³⁴ Secondly, while the original ML300 series achieved nM inhibition against SARS-CoV-1, leading to compounds such as **7** and **8** (Figure 2C), the series was far from optimized. For example, only a handful of amide replacements presumed to occupy the upper rim of the S2_c were explored. In the S2_{sp} region, which the ML300 3-thienyl ring was presumed to act as an P2_{sp} group (Figure 2B), only these two π -excessive heterocycles were examined during hit expansion. Moreover, cellular antiviral structure-activity relationships (SAR) of the ML300 series against SARS CoV's remained largely unknown, although the potential for broad spectrum utility was precedent based upon studies examining ML300 series analogs targeting HKU4, a suspected reservoir host for MERS.³⁵ Lastly, *in vitro* ADME properties of ML300 revealed significant hurdles including metabolic instability with no knowledge of the mechanism or site of metabolism. Based on these fundamental gaps and our interest to contribute to understanding if the benzotriazole based ML300 series may have potential as a lead for COVID-19 or future broad spectrum 3CL^{pro}-based CoV antiviral therapies we assembled a team highly focused on the above goals.

The compounds disclosed herein provide significantly improved characteristics in several areas from the original ML300 report, achieving robust nanomolar biochemical inhibition against SARS-CoV-2 3CL^{pro}, sub-micromolar antiviral and plaque formation inhibition against the SARS-CoV-2 live virus, and a systematic DMPK and metabolite profile to support directions for future optimization. In addition, we compare and contrast several new X-ray structures of inhibitors bound to SARS-CoV-1 and CoV-2 3CL^{pro}, including ML300 and a number of analogs generated using structure-based design.

Results and Discussion

Our efforts began by initially synthesizing **1** (ML300), **7** and **8** and re-screening against SARS-CoV-1 3CL^{pro} (SC1), obtaining for **1** an IC₅₀ of 4.45 μM (Table 1), which was in agreement with reported data; a similar IC₅₀ value against SARS-CoV-2 3CL^{pro} (SC2) was also obtained. However, to our surprise, the previously published biphenyl derivative, **7**²¹ did not reconfirm its prior published value of 51 nM, and in fact was drastically less potent. Based on the concentration-response-curves (CRC) of compound **7** an SC1 IC₅₀ of 16.8 μM, and SC2 IC₅₀ of 31.2 μM was calculated, which represents potency more similar to the truncated compound, **9** (Table 1). In contrast, the 3-pyridyl congener **8** maintained an IC₅₀ between 930–950 nM for both SC1 and SC2 enzymes that mirrored the initial report from 2013. Relative to **1** the pyridyl biaryl **8** results in ligand efficiency (LE) enhancement from 0.23 to 0.27 respectively based upon SC2 mean IC₅₀ values. Since our findings regarding biphenyl **7** stand in contrast to the original work, we carefully examined our assay reagents, protocols, and compound fidelity. For each 3CL^{pro} construct we utilized the native sequence of the enzyme that represents the *in vivo*, post-proteolytic form using the protocol and conditions reported by Mesecar and co-workers.³⁶ We also utilized the same FRET-based 3CL^{pro} peptide substrate as reported and achieved excellent plate uniformity using a 384-well plate format, Z-prime > 0.8. Compound CRC's were generated and tested from at least three experiments using 384-well plate format with technical replicates on each plate. SC1 and SC2 reported IC₅₀ values reported in Tables 1–3 reflect n = 3, with further repeats as required until CV < 0.3 was achieved. The standard deviation is reported and shown for reference. As per published protocols, 0.01% Triton X-100 was included in the assay buffer to remove potential promiscuous inhibition caused by aggregation. At this time the >300-fold SC1 IC₅₀ discrepancy for biphenyl **7** cannot be fully explained; however, it is clear that inherent high lipophilicity of this molecule may have been a contributing factor based on its calculated physicochemical properties (**7** cLogP = 5.61, LogS = -6.85, ChemDraw 19.0) and behavior in FRET CRC measurements. For example, Figure 3 shows a comparison of the SC1 and SC2 3CL^{pro} FRET inhibition curves for **1**, **7**, and **8**. Incomplete inhibition is observed for compound **7** based on the curve profile when tested up to 100 μM maximum (Figure 3, 4-fold serial dilution). In addition, there is a clear plateau of inhibition that appears to be begin at concentrations from 25 μM onward, suggesting a likely solubility limit. In contrast, compound **8** behaves well up to a top assay concentration of 100 μM, achieving complete inhibition.

Encouraged by the sub-micromolar SC1 and SC2 inhibitory activity of pyridyl **8** we pursued a series of X-ray crystal studies and obtained high resolution structures of **8** bound to SC1 3CL^{pro} at 1.85 Å via soaking method, in addition to a co-crystal of **1** (ML300) bound to SC2 3CL^{pro} at 2.1 Å resolution via co-crystallization. Shown in Figure 4 is a depiction of key residues and the binding poses of **1** – SC2 3CL^{pro} (panel A) and **8** – SC1 3CL^{pro} (panel B).

Comparison of **6** – SC1 3CL^{pro}, **1** – SC2 3CL^{pro}, and **5** – SC2 3CL^{pro} X-ray structures

Overall the binding orientation of **1** in the SC2 3CL^{pro} binding pocket (Figure 4A) retains many of the key interactions found in the **6** – SC1 3CL^{pro} complex (Figure 2B); however, key distinctions are observed within the binding site which illuminate prior SAR trends.²¹

In general, removal of the P3 amide of **6** as the major difference versus inhibitor **1** does not grossly effect the ligand bioactive conformation, leaving the solvent exposed S3 pocket unoccupied. In the S1 pocket, identical to **6** – SC1 3CL^{PRO}, the benzotriazole of **1** forms neighboring putative H-bonding interactions with His163 and Cys145, at 2.8 and 3.6 Å, respectively. Similarly, the amide carbonyl oxygen retains a key anchoring hydrogen bond with the backbone NH of Glu166. Within the S2 pocket, as seen previously within the compound **6** – SC1 3CL^{PRO} complex, the dynamic nature of the Gln189 loop allows a new S2_{sp} to form to accommodate the thiophene ring, resulting in the thiophene sulfur being sandwiched between Met165 and Met49. Interestingly, the *N*-methyl pyrrole and thiophene conformationally present distinctly within the S2_{sp}. For example, the bulkier *N*-methyl pyrrole adopts an 18° torsion to reach into the S2_{sp} pocket, while the thiophene side chain of **6** adopts a 98° torsion with respect to the aniline ring. In addition, there is a slight frame shift of the *N*-benzyl amide backbone resulting in rotational shift of the aniline vector towards the S2_c upper rim that appears to favorably accommodate the larger cyclopropyl amide. Relative to **5** – SC2 3CL^{PRO} peptide **5** complex (see Supplemental Figure S1, PDB: 6XHM); **5** and **1** share common H-bond interactions with Glu166 and His163 in the S1 region; however, **5** forms a covalent interaction with the catalytic Cys145 and occupies the solvent exposed S3 pocket. In contrast to **6** – SC1 3CL^{PRO} complex, for ligand **1** in chain A of the asymmetric unit the cyclopropyl anilido amide moiety maintains a rotamer in the S2_c channel which positions the carbonyl at a 50° torsion from co-planarity relative to the central aniline ring, giving rise to a unique hydrogen bond with the side-chain of Ser46 (Figure 4, left). In chain B in the asymmetric unit the cyclopropyl moiety points further from the pocket towards solvent; however, for chain B, the B-factor values indicate significant motion versus the chain A inhibitor. Interestingly, this observed hydrogen bonding interaction represents an amino acid difference between the SC1 and SC2 3CL^{PRO} enzymes, namely an Ala46 in SC1 for Ser46 in SC2. Residue 46 defines part of a short helix-loop-helix motif spanning Arg40 through Lue50. Peptidomimetics efforts to date with a canonical mode of inhibition acknowledge that amino acids within the active-site between SC1 and SC2 3CL^{PRO} are 100% sequence identical. In regard to a tailored inhibitor design versus a broad spectrum inhibitor strategy, the observed interactions and residue differences noted within and near S2_c for this ML300-based series may present unique challenges as well as opportunities not available to traditional inhibitor scaffolds.

Comparison of **1** – SC2 3CL^{PRO} and **8** – SC1 3CL^{PRO}- **8** X-ray structures

Relative to **1** – SC2 3CL^{PRO} complex, the **8** – SC1 3CL^{PRO} binding pose and interactions are otherwise identical with the exception of distinctions within the S2_c upper rim region (Figure 4, right versus left). In regard to nearby polar residues that might engage the pyridyl nitrogen, Thr25 side chain is the closest residue in proximity; however, the distance measured at 3.8 angstroms would indicate this is less than favorable. Furthermore, no apparent water mediated interactions were observed with the ligand. In terms of π -interactions with the pyridyl ring of **8**, a Ala46 backbone amide- π interaction is apparent based upon proximity and distances from the backbone carbonyl carbon and the pyridyl centroid (3.5–3.8 Å). This stacking interaction may contribute to the beneficial boost in potency of **8** versus biphenyl **7**.

With the above new structural information and encouraging potency for compound **8** in hand we investigated more extensive amide variants and heterocyclic modifications (Table 1). The reverse amide of ML300, **11** had a 3-fold reduction in activity versus the parent, while the primary amide, **10**, displayed nanomolar inhibition against both proteases. Sulfonamides **12–13** both measured low micromolar inhibition. Reviewing the SC1 3CL^{pro} X-ray structure of **8**, while we did not observe any obvious direct hydrogen bonding interactions between the pyridyl group and the protein, it was clear that the orientation of this compound series was directed toward multiple residues for potential interaction. Additional isomeric analogs such as 4-pyridyl **14** and 2-pyridyl **15** were within 2-fold of the activity of **8** for both SC1 and SC2 3CL^{pro}. 2-Methoxy-pyridyl **16** lost 3–5 fold for both enzymes, while pyridone **17** was essentially equipotent to compound **8**. Encouraged by **17** and the observed interactions of **1** within the S_{2c} upper rim we continued to design and pursue modifications in the S_{2c} exploring various H-bond donors both neutral and potentially charged in nature. To our delight a significant enhancement was found with the *NH*-pyrazole and imidazole derivatives, **19** and **21**, reaching an IC₅₀ of 60 nM versus SC2 3CL^{pro} in the case of imidazole **21**. Potency of *N*-methyl analogs **18** and **20** was drastically diminished, between 160–185-fold versus their non-methylated analogs, underscoring the importance of the presence and nature of a H-bond donor in the P_{2c} group

Obtained X-ray co-crystal structures of **19** and **21** in SC2 3CL^{pro} indeed demonstrate the potential for multiple H-bonding interactions from these heterocyclic azole nitrogens (Figure 5, A and B). There are prospective H-bonds with both the hydroxyl side chain of Thr25 and backbone carbonyl of Cys44. The bound pose of the azole heterocycle is co-planar with the central phenyl in both cases and juxtaposed between the residues with distances from the closest nitrogen within acceptable inter-heteroatom H-bonding distances of 2.8 to 3.0 angstroms. The hydrogen bonding array revealed in both structures would suggest the azole is acting as hydrogen bond donor to the carbonyl of Cys44 and then an acceptor from Thr25. We also obtained X-ray structures of these same two compounds in SC1 3CL^{pro}, and in both cases we observed an almost identical binding pose – and binding site orientation – with the exception of a subtle difference in the S_{2sp} region (Supplemental Figure S1A). Here, there is movement of the unstructured loop, and rotation of Gln189, which leads to a small difference in the thiophene ring torsion (86° vs. 64°). This observation is presumed to be driven by different crystallization conditions used for the two proteins; SC2 was co-crystallized, while compounds for SC1 were soaked into apo-3CL^{pro} with increasing amounts of glycerol in the buffer solution. Indeed, density for a glycerol unit is found in the nearby S4 region for all our solved SC1 3CL^{pro} structures.

Simultaneously to the synthesis of our first series expanding the scope of the biaryl **8** SAR, we explored thiophene replacements at P_{2sp} (Table 2) holding the P_{2c} group constant as 3-pyridyl. A range of acyclic and cyclic aliphatic groups were targeted, including **22–26**, with the cyclobutyl derivative **24** affording a slight improvement relative to the parent **8**. Introduction of an ether oxygen via tetrahydrofuran **26** was highly deleterious. Thiazole analog, **27**, offered similar inhibition within two-fold of **8** and **24** with early evidence of an improvement in microsomal stability compared to **8** (*vide infra*). It was quickly established that a 3-chlorophenyl group led to a significant potency increase against both SC1 and SC2,

namely compound **28**, and subsequent analogs explored SAR of this ring in more depth, **29–34**. A 3,4-substitution pattern was clearly not tolerated (**29**, **30**), an observation that was consistent with our emerging X-ray structures and docking studies suggesting a limited steric bulk near the loop residue Arg188. This observation is in contrast to mobility in the loop region near Asn189. A 3,5-substitution afforded examples with inhibition below 200 nM, including analogs **31** and **32**, with the 5-fluoro derivative **31** among the most potent in this subseries with IC₅₀ values ranging 74–119 nM. The addition of a pyridine nitrogen to improve the physicochemical properties of this sub-series was tolerated, but with a reduction in SC2 inhibition to 540 nM.

Based on the above data, we elected to hold the P2_{sp} 3-chlorophenyl and P1 benzotriazole constant while exploring combinations P2_c pendant biaryls with a handful of aniline modifications (Table 3). Interestingly, a number of the prior P2_c favorable modifications, such as pyridone **17** and pyrazole **19**, led to active compounds **35** and **36**, however, differential SAR was noted. For example, within the pyridone sub-series 3-chlorophenyl (**35**) versus 3-thienyl (**17**) 3CL^{pro} inhibition is nearly identical. Within the more active pyrazole comparators (e.g. **36** versus **19**) there is a three-fold preference for the 3-thienyl sub-series which is in the opposing direction from that initially described in Table 1. This differential SAR is observed in both SC1 and SC2 3CL^{pro} data, suggesting a real phenomenon, highlighting dynamic SAR presumably resulting from the P2_c upper rim interactions identified. Relative to **36** modifications within aniline core such as methoxy analogs **37** and **38** are tolerated with 2-methoxy being slightly improved relative to **36** with an IC₅₀ = 197 nM for SC2 3CL^{pro}. A similar trend was noted for the central pyridyl congeners **39** and **40** with 2-pyridyl displaying identical 1.6-fold increases in potency for both SC1 and SC2 enzymes. Investigation of the 3-chlorophenyl P2_{sp} analog imidazole **21** afforded compound **41**. Once again like the pyrazole matched pairs described above, more potent P2_c modifications appear to engender differential SAR in context of the P2_{sp} group. In the case of SC1 3CL^{pro} an 8-fold boost in IC₅₀ is noted substituting 3-thienyl for 3-chlorophenyl (**21**, IC₅₀ = 148 nM versus **41**, IC₅₀ = 19 nM), respectively. However, in the case of SC2 3CL^{pro} we observe flat SAR with no real improvement in inhibition when the P2_c substituent is C4-imidazole.

As part of the ongoing optimization efforts we spot-checked compounds for DMPK properties throughout, including human and rat intrinsic clearance, plasma protein binding, MDCK passive permeability, and P450 isozyme reversible inhibition at 10 μM. A complete summary is presented in Supplemental Table S1. Beginning with **1** (ML300) and throughout most of the SAR presented, exceptionally high microsomal clearance has been observed, with hepatic clearance equivalent to hepatic blood-flow in both human and rat. We hypothesized that the P1-benzotriazole group may be a source of significant metabolism and indeed, the carbon-linked 3-pyridyl and 5-pyrimidyl analogs **42** and **43** (Figure 6) do show a noteworthy improvement in CL_{int}, with a 2- and 4-fold decrease compared to **36** in microsomes (human, rat) and in human S9 fraction. Unfortunately, these groups afforded a drop in primary biochemical potency back to micromolar levels, demonstrating further P1 optimization is required. The monodirectional cellular permeability is high, as measured in MDCK-MDR1 cells, across the series, and multiple examples have modest free fraction

at or above 1% unbound in human (e.g. **21** and **41**, Supplemental Table S1). We have also assessed an initial CYP inhibition profile for this series of compounds, and relatively high inhibition at 10 μM was noted in general with few exceptions (3A4, 2D6 \gg 50%). Given the structural features of these molecules, this finding was not unexpected, and further optimization is ongoing to mitigate P450 inhibition.

Subsequently, we initiated soft-spot metabolite ID analysis of a representative benzotriazole, namely 3-chlorobenzyl derivative **36**, to further understand the generally high hepatic oxidative metabolism observed and guide future target design. This analysis demonstrated that while there is NADPH-dependent oxidative metabolism of the benzotriazole moiety, this is a secondary metabolite in comparison to oxidation of the benzylic 3-chlorophenyl ring (Figure 7). The M1-metabolite is estimated at 60% based on UV total peak AUC, while M2 is 33%. We note that sample depletion was not observed in the absence of NADPH (data not shown), indicative of oxidative metabolism mediated by P450. A third, minor metabolite (M3, 7%) resulting from cleavage of the 3-chlorobenzyl group is also observed. Additional profiling of related compounds is ongoing to support this observation that benzylic P2_{sp} is the major soft spot in human hepatic S9 fractions. Strategies are underway to reduce oxidative metabolism and increase *in vitro* half-life.

We next turned to evaluation of promising compounds for their antiviral activity. The antiviral efficacy of compounds against infectious SARS-CoV-2 virus in Vero E6 cells was evaluated by cytopathic effect (CPE) inhibition and in a plaque reduction assay. The results are summarized in Table 4. The CPE inhibition assay was performed with 6-point dilution with three independent experiments for each compound, these results were then validated via a plaque reduction assay performed with between 4–6 concentrations of compound, dependent on the measured CPE inhibition.

The original declared MLPCN probe ML300 displayed weak activity in the high micromolar range (Table 4, CPE EC_{50} = 19.9 μM , Plaque reduction EC_{50} = 28 μM). The pyrazole and imidazole P2_{c} containing ML300 derivatives, **19** and **21**, which are among the more biochemically potent analogs, showed improved EC_{50} values between 1.7–8 μM in both assays. Interestingly, potency of the matched pair analogs **36** and **41** that substitute the P2_{sp} thienyl to 3-chlorophenyl are greatly improved with the EC_{50} of **41** sub-micromolar in both assays. In addition, the 50% cytotoxic concentration of **41** (CC_{50}) in the CPE antiviral assay was found $>$ 50 μM , indicating an excellent selectivity index ($\text{SI} > 100$, see Supplemental Figure S4 and Table S5). Comparison of $\text{EC}_{50}/\text{IC}_{50}$ ratios of the non-covalent compounds can help guide compound design in terms of estimating the required target IC_{50} in order to achieve a desired pharmacological effect. For example, for **19** and **21** the respective $\text{EC}_{50}/\text{IC}_{50}$ ratios are 52 and 29 respectively. These are far from a desired profile. In contrast, the 3-chlorophenyl analogs **36** and **41** have $\text{EC}_{50}/\text{IC}_{50}$ ratios of 7.3 and 7.4 respectively. To our knowledge, these values are equivalent to the best reported to-date non-covalent inhibitors of SC2 3CL^{PRO}. In addition, the efficacy of **41** was shown in our assays to be comparable to that of the clinically utilized polymerase inhibitor, remdesivir (Figure 8).^{37, 38}

Chemistry

The nature of our starting point, **1** (ML300), led to the possibility for modular and systematic exploration of SAR in different vectors of the 3CL^{Pro} binding pocket. Our initial focus was on optimization of the groups at P2_c, which was previously found to be a source of varied SAR.²¹ Here, the P2_{sp} group was fixed and thiophene-3-carbonyldehyde, **44**, was reacted with various anilines via reductive amination (Scheme 1). Amides **10** and **11**, the reverse amide relative to **1** were synthesized via benzoic acid intermediate **45**; while sulfonamides **12** and **13** were synthesized via the 1,4-dianiline intermediate, **46**. The aryl bromide, **47**, afforded a versatile intermediate that afforded bi-(hetero)aryl analogs **8**, **14–21** using Suzuki-Miyaura cross-coupling conditions. The pyridone example, **17**, was synthesized by hydrolysis of the fluoropyridine intermediate **48**. The *NH*-pyrazole could be introduced directly, without protection to afford **19**; however, reaction with the analogous *NH*-imidazole was unsuccessful. In this instance, we utilized 4-bromo-1-trityl-imidazole and the corresponding pinacol ester of **47** to furnish the desired product **21** after deprotection.

We simultaneously explored the nature of the P2_{sp}-substituent, with a desire to replace the thiophene moiety of ML-300 (Scheme 2). Here, various aldehydes were reacted with the biaryl aniline **51** via reductive amination, then amide bond formation with benzotriazole-1-acetic acid (**50**) in the presence of propylphosphonic anhydride (T3P) afforded compounds **22–34**.

Similar to our initial library, for compounds **35–43** the S2 3-chlorophenyl moiety was fixed as a thiophene replacement (Scheme 3). Reductive amination of 3-chlorophenylbenzaldehyde, **53**, with anilines afforded intermediates that follow a similar synthetic sequence as above. The bromo intermediate **58** provided synthetic flexibility, as subsequent Suzuki-Miyaura reaction, followed by T3P amide coupling, led to products **35**, **36**, **42** and **43**. Alternatively, the 1,2,3-benzotriazole moiety could be introduced first to give bromide **61**, which was then subjected to Miyaura-Ishiyama-Hartwig borylation and subsequent Suzuki-Miyaura cross-coupling conditions to afford **41** in acceptable yield.

Conclusions

As for many scientists around the globe, the huge effect on our lives caused by the COVID-19 pandemic instilled us to assess how we could have an impact, however large or small, in the study of this disease. Having prior experience targeting the 3CL-protease of SARS-CoV-1 working with leaders in the field we were compelled to further investigate ML300 as a starting point employing all disciplines within our newly formed Center and partnering with our CCF Institute virologist colleagues and experts in the field. After initial disappointment and intrigue, we found that the addition of H-bond donating azole heterocycles, in particular pyrazole and imidazole containing analogs, including **19** and **21**, directed to S2_c afforded an appreciable increase in potency. This discovery combined with the 3-chlorobenzyl modification in S2_{sp} advanced our optimization efforts to a series of compounds routinely reaching primary IC₅₀ SC2 3CL^{Pro} inhibition values below 500 nM. As such the ML300 amide series continues to display an interesting mode of action with differential SAR worthy of further investigation.

Historically the ML300 series has demonstrated basic DMPK properties that were not attractive for further development beyond *in vitro* studies. While we have observed improvements, the compounds disclosed still lack the properties needed for a full *in vivo* evaluation in animal models of SARS-CoV-2 infection. The addition of metabolite ID studies have highlighted key areas of the molecule for further optimization to improve the high clearance and metabolic turnover in the series. Similarly, while the unbound fraction and cellular permeability of these compounds is promising, a further hurdle these compounds must overcome is their high inhibition of CYP enzymes which is currently a major area of focus.

Non-covalent small molecule SARS-CoV-2 inhibitor **41** (CCF0058981) provides a significant advance from the original SARS-CoV-1 ML300-derived inhibitor, with low nanomolar biochemical inhibition and efficacy in cellular models comparable to the FDA-approved RNA polymerase inhibitor remdesivir. Optimization of the series of compounds is ongoing, with a particular focus on improving the DMPK profile, as well as further improving the biochemical and cellular efficacy. Further, we look forward to future opportunities to profile the series and compounds herein against a wider panel of coronaviruses, including MERS. We anticipate that investigators targeting SC1 and SC2 3CL^{pro} will benefit from the disclosed SAR and X-ray crystal structures. Furthermore, these findings have implications towards antiviral development to combat future SARS-like zoonotic coronavirus outbreaks.

Experimental Section

SARS-CoV-1/2 3CL^{pro} Protein Expression & Purification

SARS-CoV-1/2 3CL^{pro} enzymes were cloned using previously published methods.^{30,39} Briefly, genes encoding each protein were codon optimized for E.coli, synthesized, and inserted into a pGEX-6P-1 plasmid between the BamHI and XhoI cut sites (note that additional residues “AVLQ” and “GPHHHHHH-stop” were added to the N and C termini, respectively, of the proteins as previously described)^{30,39}. The resulting expression constructs yield unscarred, native enzymes following protein purification.

Both enzymes were recombinantly expressed using New England Biolabs T7 Express lysY/Iq cells transformed with 3CL^{pro} expression plasmids. The enzymes were expressed and purified using identical methods derived from previously published work.³⁰ Inoculated cultures of Lauri Broth media supplemented with ampicillin were grown at 37 °C with shaking to a density of 0.6–0.8 OD_{600nm}. The incubator/shaker temperature was then reduced to 16 °C and the cultures were induced with 0.5 mM IPTG. Following overnight induction, cells were harvested via centrifugation at 3900 RPM (Eppendorf 5810R, S-4–104 rotor) for 25 minutes and resuspended in 20 mM TRIS, 300 mM NaCl pH 8.0 buffer ([Buffer A](#)). Resuspended cells were lysed *via* sonication, centrifuged at 10,500 RPM (Eppendorf 5810R, FA45–6-30 rotor) for 30 minutes, and the clarified lysate loaded onto a 5 mL Ni-charged Nuvia IMAC column equilibrated with Buffer A. The column was washed with 10 column volumes (CV) of Buffer A and eluted with a 7 CV gradient of 0–100 % [Buffer B](#) (Buffer A + 500 mM imidazole). Fractions containing pure 3CL^{pro} were pooled, diluted in half with Buffer A, and dialyzed overnight at 4 °C with PreScission Protease against

a 50 mM TRIS, 150 mM NaCl, 1 mM DTT, pH 7.5 buffer. Cleaved protein was passed through a 5 mL Ni-charged Nuvia IMAC column equilibrated with a 50 mM TRIS, 150 mM NaCl pH 7.5 buffer. Collected flow through was concentrated to 5 mL using an Amicon Ultra 10k centrifugal filter and diluted to 25 mL with 50 mM TRIS pH 7.5. Diluted protein was passed through a 5 mL HiTrap Q FF anion exchange column equilibrated with 50 mM TRIS, 25 mM NaCl buffer pH 7.5 (**Buffer C**). The Q FF column was washed with 10 CV of Buffer C and bound proteins eluted with a 5 CV 0–100 % gradient of **Buffer D** (Buffer C + 1 M NaCl). Pure 3CL^{pro} was found to be in the non-bound and wash fractions from this chromatographic step. Final purity was assessed *via* Coomassie stained SDS-PAGE. The purified protein in a 50 mM TRIS and 25 mM NaCl pH 7.5 buffer was pooled, concentrated, aliquoted and frozen at –80 °C for biochemical assays, or used fresh for protein crystallography studies.

SARS-CoV-1/2 3CL^{pro} Biochemical Assay

Protease activity and subsequent 10-point IC₅₀ curves were spectroscopically determined using a scaled down, endpoint assay adapted from a previously described peptide-based Forster Resonance Energy Transfer (FRET) assay.^{20,40} Compounds (as 10 mM DMSO stock) were serially diluted 4-fold using 100% DMSO in a LabCyte 384-well LDV plate and acoustically transferred using a LabCyte ECHO 550 into Corning 384-well black NBS plates. Standard 10-point IC₅₀ 384-well plate layout is as follows: 100 μM of **8** was stamped into columns 1 and 24 (low control), DMSO was stamped into columns 2 and 23 (high control), and serially diluted compounds were stamped from high (100 μM) to low (0.38 nM) concentrations in columns 3–12 (replicate 1) and 13–22 (replicate 2). Protocol for running the assay is as follows: assay wells stamped with 0.25 μL of compound or DMSO were filled *via* a ThermoFisher Multidrop Combi liquid dispenser with 14.5 μL of 150 nM or 200 nM (concentration for 25 μL final reaction volume) of SARS-CoV-1 or SARS-CoV-2 3CL^{pro}, respectively, in assay buffer (50 mM HEPES, 0.1 mg/ml BSA, 0.01% v/v TRITON X100, 2 mM DTT, pH 7.5). Assay plates were then centrifuged at 1,000 RPM (Eppendorf 5810R, S-4–104 rotor) for 1 minute, covered, and incubated at room temperature for 15 minutes. Reactions were initiated using the Multidrop Combi liquid dispenser to titrate 10 μL of 2 μM (concentration for 25 μL final reaction volume) of fluorophore-quencher peptide substrate (HiyteFluor™-488ESATLQSGLRKAK-(QXL™)-NH₂ from AnaSpec, Inc. Catalog No. AS-65599) solubilized in assay buffer into each well. Assay plates were again centrifuged at 1,000 RPM for 1 minute, covered, and incubated at room temperature for 30 minutes. Biochemical assays were quenched through the addition of 5 μL of 500 mM acetic acid via Multidrop Combi liquid dispenser. Assay plates were then centrifuged at 1,000 RPM for 1 minute and resulting fluorescence intensity measured on a BioTek Cytation 5 multimode plate reader ($\lambda_{\text{ex}} = 485\text{nm}$, $\lambda_{\text{em}} = 528\text{nm}$).

Data analyses: Raw fluorescence values were normalized (RF_{norm}) by dividing each value by the average of DMSO control wells which represents the maximal fluorescence signal ($\text{RF}_{\text{norm}} = \text{RF}_{\text{sample}} / \text{Ave RF}_{\text{DMSO control}}$). Dose response curve fitting was performed using Dotmatics Studies (software version 5.4.2), which computes IC₅₀ values utilizing a four-parameter logistical fit. Reported values are average IC₅₀ from at least 3 independent experiments.

Protein Crystallization, Data Collection, and Structure Refinement

SARS-CoV-2 3CL^{pro} was concentrated to 6.5 mg/ml and titrated with inhibitor to give a final concentration of 3% v/v inhibitor (10 mM DMSO stocks of **19** and **21**, and 20 mM DMSO stock of **1**). Protein-inhibitor complexes were left at room temp for 1 hour prior to setting up crystallization drops. Diffraction quality crystals were obtained by hanging drop vapor diffusion experiments comprised of 1 μ L protein/inhibitor mix and 1 μ L crystallization solution drops incubated at 16 °C. The Hampton Research Index Screen (HR2–144) yielded a high rate of crystal formation, with optimal crystals forming in either 0.2 M lithium or ammonium sulfate, 0.1 M Bis-TRIS or HEPES pH 6.5–7.5, and 25 % polyethylene glycol 3350 conditions. Protein crystals were directly looped, flash frozen in liquid nitrogen, and shipped for remote X-ray diffraction data collection at the Advanced Photon Source LS-CAT beamline 21-ID-F. Diffraction data was indexed and scaled using HKL2000 and phased (Phaser-MR) using molecular replacement with the search molecule PDB: 6WQF.^{41–43} Inhibitor coordinates were generating using ELBOW and the resulting protein-inhibitor structures were refined and built using iterative rounds of refinement and manual manipulations with PHENIX Refine and COOT.^{44–46} X-ray diffraction and model refinement statistics are given in Supplemental Table 1. The final coordinates and electron density maps were deposited into the Protein Data Bank.

SARS-CoV-1 3CL^{pro} was concentrated to 6.0 mg/ml and titrated with inhibitor to give a final concentration of 4% v/v inhibitor (10 mM DMSO stocks of **35** and 25 mM DMSO stock of **1**). Protein-inhibitor complexes were left at room temp for 30 min prior to setting up crystallization drops. Diffraction quality crystals were obtained by hanging drop vapor diffusion experiments comprised of 1 μ L protein/inhibitor mix and 1 μ L crystallization solution drops incubated at 16 °C. The Hampton Research Index Screen (HR2–144) yielded a high rate of crystal formation, with optimal crystals forming in ammonium sulfate, HEPES pH 7.5, and 25 % polyethylene glycol 3350 conditions. For collecting X-ray diffraction data, the crystals were flash-cooled in liquid nitrogen followed by dragging the crystals through the crystallization solution. In another method, SARS-CoV-1 3CL^{pro} was crystallized at 20 °C using the hanging-drop vapor-diffusion method by mixing 6 mg/mL 3CL^{pro} in 1:1 ratio with 100 mM MES buffer in pH 5.5, 12–18% (w/v) polyethylene glycol 6000, 10% (v/v) glycerol, 2% (v/v) DMSO. Single crystals were transferred to 5 μ L of the mother liquor with 400 μ M inhibitor concentration (10 mM DMSO stocks of **8**, **19** and **21**). After incubation at 16 °C for 5 min, the crystals were looped and dragged out through the crystallization solution cryoprotected by 20% (v/v) glycerol. The crystals were then shipped for remote X-ray diffraction data collection at the Advanced Photon Source LS-CAT beamline 21-ID-F. Diffraction data was indexed and scaled using HKL2000 and phased with CCP4i molecular replacement program with the search molecule PDB: 3VB3.⁴⁷ Inhibitor coordinates were generating using ELBOW and the resulting protein-inhibitor structures were refined and built using iterative rounds of refinement and manual manipulations with Refmac (ccp4i)⁴⁸ and COOT. X-ray diffraction and model refinement statistics are given in Supplemental Table 2. The final coordinates and electron density maps were deposited into the Protein Data Bank.

Virus propagation and titration

The following reagent was deposited by the Centers for Disease Control and Prevention and obtained through BEI Resources, NIAID, NIH: SARS-Related Coronavirus 2, Isolate USA-WA1/2020, NR-52281. The virus was propagated in Vero E6 expressing ACE2 receptor (a gift from Dr. Younho Choi, Cleveland Clinic Lerner Research Institute) in a DMEM media supplemented with 1X penicillin-streptomycin (Gibco) and 0.5µg/ml TPCK-treated trypsin (Worthington Biochemical) at 37 °C in a humidified incubator with 5% CO₂. Propagated virus was aliquoted and stored at –80 °C until further use.

The virus titer was determined by plaque assay as previously described with a little modification.⁴⁹ Briefly, confluent monolayer Vero E6 ACE2 cells cultured in a 6-well plate were infected with 10-fold serial diluted virus inoculum incubated on a rocker for 45 min in 37 °C for virus adsorption. After the removal of virus solution, cells were overlaid with DMEM containing 1% low melting agarose and incubated in a humidified incubator at 37 °C and 5% CO₂ for 4 days. To visualize the plaques, the cells were fixed with 4% formaldehyde and stained with 0.2% crystal violet solution containing 20% ethanol.

Virus inhibition assays

Initial antiviral screening was done by using CPE inhibition assay.⁵⁰ Briefly, Vero E6 ACE2 cells were cultured in a 96-well flat-bottom plates at a density of 2×10^4 cells per well. Following infection of the cells with a 100 TCID₅₀ of SARS-CoV-2, the plates were incubated on a rocker in 37 °C for 45 min for virus adsorption. The cells were then washed with DMEM and added the medium containing the test compounds in the desired concentration. Both the uninfected cells and infected cells treated with 10 µM of Remdesivir were used as controls. The antiviral efficacy of test compounds was determined by the uptake and subsequent extraction of neutral red dye. After infection (68 h), cells were incubated with 0.034% neutral red dye for 3 h at 37 °C. Free dye was washed from the wells and the uptake dye was quantified using a microplate reader with absorbance at 540 nm. Absorbance values were expressed as percentages of uninfected control cells, and EC₅₀ values of the test compounds were determined using Prism software (GraphPad).

The validation of the initial CPE inhibition results was done by testing the compounds by plaque reduction assay.⁵¹ Confluent monolayers of Vero E6 ACE2 cells in 12-well plates were washed once with DMEM and infected with approximately 50 plaque forming units (PFUs) of SARS-CoV-2 in each well. The plates were incubated on a rocker in 37 °C for 45 min for virus adsorption. The virus inoculum was removed and replaced by overlay media (DMEM containing 1% low-melting agarose without serum) containing 3-fold serial dilutions of the test compounds and placed in 37 °C CO₂ incubator until plaques can be visualized under light. The cells were then fixed with 4% formaldehyde solution for at least 30 min and the overlaid agarose was removed and stained with 0.2% (w/v) crystal violet solution. The plaques were counted by visual examination and the required concentration to reduce 50% plaque number (EC₅₀) was calculated as relative to the control without test compounds.

Hepatic S9 Metabolic Stability Assessment of Compounds

The metabolic stability compounds were investigated in human hepatic S9 fractions pooled from 20 mixed gender donors (Xenotech, catalog # H0606.S9(AX) / lot 1710129) using substrate depletion methodology (percentage of parent compound remaining). Potassium phosphate-buffered (0.1 M, pH 7.4) solutions of test article (1 μ M) and S9 (2.5 mg/ml) were incubated at 37°C under ambient oxygenation in the presence or absence of NADPH (2 mM). Total incubation volumes were 0.4 mL with a final organic concentration of 0.5%. Mixtures lacking substrate were pre-incubated at 37 °C for 5 minutes. Reactions were initiated with addition of substrate, and at the designated times (t = 0, 3, 7, 15, 30, and 45 min), a 25 μ L aliquot of the incubation mixture was removed and precipitated by the addition of 4 volumes of ice-cold MeCN containing carbamazepine as an internal standard (50 nM). The mixtures were centrifuged at 3500 rcf (4 °C) for 10 min. The resulting supernatants were diluted 1:3 (supernatant-water) into 96-well plates in preparation for LC-MS/MS analysis. All samples were analyzed via electrospray ionization on an AB Sciex API-6500 QTrap (Applied Biosystems, Foster City, CA) instrument that was coupled with LC-20ADXR pumps (Shimadzu, Columbia, MD) and a CTC PAL autosampler (Leap Technologies, Carrboro, NC). Analytes were separated by gradient elution using a Phenomenex Kinetix C18 column (2.1 \times 50 mm, 1.7 μ m; Phenomenex, Torrance, CA) thermostated at 40 °C. HPLC mobile phase A was 0.1% formic acid in water (pH unadjusted); mobile phase B was 0.1% formic acid in acetonitrile (pH unadjusted). The gradient started at 5% B after a 0.2-min hold and was linearly increased to 90% B over 1.0 min, held at 90% B for 1.0 min, and returned to 5% B in 0.1 min followed by a re-equilibration (0.5 min). The total run time was 2.5 min, and the HPLC flow rate was 0.5 ml/min. The source temperature was set at 500 °C, and mass spectral analyses were performed using multiple reaction monitoring, with transitions and voltages specific for each compound using a Turbo Ion Spray source in positive ionization mode (4.5 kV spray voltage): **36**, m/z 443>124.9 CE 38; **40**, m/z 444>124.9 CE46; **42**, m/z 403>120 CE 34; **43**, m/z 404>125 CE 36; Verapamil, m/z 455.1>165.1 CE 40; Carbamazepine, m/z 237.1>194.0 CE 25. All data were analyzed using AB Sciex Analyst 1.5.1 software. Each compound was assayed in triplicate within the same 96-well plate. Hepatic intrinsic clearance (CL_{int} , mL/min/kg) was extrapolated from hepatic S9 using the substrate depletion method and Equation 1:⁵²

$$CL_{int} = \frac{\ln 2}{t_{1/2(min)}} \times \frac{mL}{2.5 \text{ mg protein}_{S9}} \times \frac{120.7 \text{ mg protein}_{S9}}{g \text{ liver weight}} \times \frac{21 \text{ g liver weight}}{kg \text{ body weight}} \quad (1)$$

Hepatic clearance (CL_{HEP} , mL/min/kg) was estimated using Equation 2, according to the well-stirred model, uncorrected for fraction unbound in plasma:⁵³

$$CL_{HEP} = \frac{Q_H \times f_u CL_{int}}{Q_H + f_u CL_{int}} \quad (2)$$

where Q_H represents human hepatic blood flow (21 mL/min/kg) and CL_{int} represents the intrinsic clearance calculated from Equation 1.

***In Vitro* Biotransformation of Compounds in Hepatic S9 Fractions.**

The *in vitro* metabolism of test articles was investigated using hepatic S9 fractions from Sprague-Dawley rats (62 males, pooled) and humans (150-donor UltraPool, BD Biosciences). A potassium phosphate-buffered reaction (0.1 M, pH 7.4) of test article (25 μ M), hepatic S9 fractions (5 mg/ml), and $MgCl_2$ (3 mM) was incubated at 37 °C in borosilicate glass test tubes under ambient oxygenation for 1 h with select experiments being fortified with NADPH (2 mM). All S9 reactions were initiated by the addition of NADHP to the *in vitro* milieu. Protein was precipitated by the addition of 2 volumes of MeCN with subsequent centrifugation (3000 rcf, 10 min). The supernatant was dried under a stream of nitrogen and reconstituted in 85:15 (v/v) ammonium formate (10 mM, pH 4.1)-MeCN in preparation for LC-MS analysis.

Liquid Chromatography-UV-Mass Spectrometry Analysis of Metabolites.

The LC-MS/MS system described in the hepatic S9 metabolic stability experiment was coupled to an Acquity BEH C18 column (2.1 μ m, 2.1 \times 100 mm; Waters, Billerica, MA). Solvent A was 10 mM (pH 4.1) ammonium formate, and solvent B was MeCN. The initial mobile phase was 85:15 A-B (v/v) and held for 5 min, and by linear gradient was transitioned to 20:80 A-B over 20 min. The flow rate was 0.400 ml/min. The HPLC eluent was first introduced into Shimadzu SPD-20A UV detector (single wavelength selected, 254 nm) followed by electrospray ionization-assisted introduction the 6500 QTrap mass spectrometer operated in the positive ion mode. The electrospray voltage was set at 4.5 kV with a source temperature of 500 °C. The collision energy was 25 when the mass spectrometer was operated in the MS/MS mode.

Compound Synthesis

General Experimental.—All chemical reagents and reaction solvents were purchased from commercial suppliers and used as received. Normal phase chromatography was performed on a Teledyne ISCO CombiFlash NextGen300 system using Teledyne RediSep[®] normal phase silica cartridges, with average particle size 35–70 micron. Preparative reversed-phase HPLC was performed using a Teledyne ACCQ-Prep HP150 equipped with Phenomenex Kinetex C18 columns, using gradients of MeCN in H_2O with 0.1% TFA additive. Compounds that are obtained as a TFA salt after purification were afforded as free base, by dissolving the salt in EtOAc and washing with sat. aq. K_2CO_3 , or by elution through a Biotage ISOLUTE[®] SCX-II cartridge, loading and washing with MeOH and eluting with 2N NH_3 in MeOH. Proton nuclear magnetic resonance (1H NMR) spectra were recorded 400 MHz on a Bruker spectrometer. For 1H NMR spectra, chemical shifts are reported in parts per million (ppm) and are reported relative to residual non-deuterated solvent signals. Coupling constants are reported in hertz (Hz). The following abbreviations (or a combination, thereof) are used to describe splitting patterns: s, singlet; d, doublet; t, triplet; q, quartet; pent, pentet; m, multiplet; br, broad. Analytical thin layer chromatography (TLC) was performed on Kieselgel 60 F254 glass plates precoated with a 0.25 mm thickness of silica gel. TLC plates were visualized with UV light and iodine.

All compounds were of 95% purity or higher, unless otherwise noted, as measured by analytical reversed-phase HPLC. Mass spectra were obtained on an Agilent 1290 series

6230 TOF. Detection methods are diode array (DAD) at 210, 254 nm and positive/negative electrospray ionization (ESI), mass range 100–1200 *m/z*. All methods use an Agilent InfinityLab Poroshell 120 EC-C18 column, dimensions 4.6 × 50 mm, 2.7 μM, fitted with Poroshell 120 EC-C18, 2.1 mm, 1.9 μM guard. Mobile phase A was 0.1% TFA in H₂O, mobile phase B was 0.1% TFA in MeCN.

Method A: The mobile phase B was 5% for 0.2 min, then a gradient of 5–95% B over 2.0 min, then hold 0.45 min (0.4 mL/min flow rate), using positive ESI.

Method B: The gradient was 40–95% B for 2.5 min, then hold 0.5 min (0.4 mL/min flow rate), using positive ESI.

2-(Benzotriazol-1-yl)-N-(4-phenylphenyl)-N-(3-thienylmethyl)acetamide (6).—

Synthesized according to published procedure.^{21,54} ¹H NMR (400 MHz, DMSO-*d*₆) δ 8.03 (d, *J* = 8.4 Hz, 1H), 7.84 – 7.73 (m, 3H), 7.70 (d, *J* = 7.6 Hz, 2H), 7.60 – 7.51 (m, 4H), 7.48 (t, *J* = 7.6 Hz, 2H), 7.44 – 7.36 (m, 2H), 7.33 (s, 1H), 7.05 – 6.99 (m, 1H), 5.47 (s, 2H), 4.92 (s, 2H); ¹³C NMR (101 MHz, DMSO) δ 165.6, 145.5, 140.6, 140.0, 139.4, 138.1, 134.3, 129.5, 129.2, 128.4, 128.3, 128.2, 127.6, 127.3, 127.1, 124.3, 123.8, 119.4, 111.6, 49.9, 48.7; Purity 95% by LCMS (Method A) *t*_R = 2.44 min, *m/z* = 425.14 [M+H]⁺; HRMS calculated for C₂₅H₂₁N₄OS [M+H]⁺ 425.1431, found 425.1450.

2-(1*H*-Benzo[*d*]1,2,3-triazol-1-yl)-N-(4-(pyridin-3-yl)phenyl)-N-(thiophen-3-ylmethyl)acetamide (7).

Step 1. 4-Bromo-N-(3-thienylmethyl)aniline.: To a solution of **44** (493 mg, 4.4 mmol) and 4-bromoaniline (929 mg, 5.4 mmol) in DCE (44 mL) was added NaBH(OAc)₃ (1.42 g, 6.7 mmol) and the mixture stirred for 1 h at rt. Sat. aq. NH₄Cl (50 mL) was added and DCE layer separated. The aqueous layer was extracted with EtOAc (3 × 40 mL) and concentrated, purified by flash chromatography to afford a product (1.18 g, 4.4 mmol, 99%). LCMS (Method A) *t*_R = 2.28 min, *m/z* = 269.98 [M+H]⁺.

Step 2. 2-(benzotriazol-1-yl)-N-(4-bromophenyl)-N-(3-thienylmethyl)acetamide.: To an ice-cold solution of **50** (1.27 g, 7.16 mmol) and Et₃N (2.00 mL, 14.32 mmol) in DCM (25 mL) was added HATU (2.72 g, 7.16 mmol) and the mixture stirred for 30 min before the addition of 4-bromo-*N*-(3-thienylmethyl)aniline (1.28 g, 4.77 mmol) in a single portion. The mixture was stirred for 20 h at rt then washed with water, brine, and concentrated. Purified by flash chromatography to afford a pale brown solid (1.13 g, 2.64 mmol, 55%). LCMS (Method A) *t*_R = 2.34 min, *m/z* = 429.02 [M+H]⁺; ¹H NMR (400 MHz, CDCl₃) δ 8.05 (d, *J* = 8.4 Hz, 1H), 7.56 (d, *J* = 8.6 Hz, 2H), 7.53 – 7.45 (m, 2H), 7.42 – 7.33 (m, 1H), 7.30 – 7.27 (m, 1H), 7.03 (s, 1H), 7.00 – 6.93 (m, 3H), 5.15 (s, 2H), 4.86 (s, 2H).

Step 3. 2-(1*H*-Benzo[*d*]1,2,3-triazol-1-yl)-N-(4-(pyridin-3-yl)phenyl)-N-(thiophen-3-ylmethyl)acetamide.: A vial was charged with **47** (128 mg, 0.30 mmol), pyridine-3-boronic acid (59 mg, 0.48 mmol) and Pd(PPh₃)₄ (35 mg, 0.03 mmol). THF (3 mL) and water (0.6 mL) was added into the vial. The mixture was stirred and purged with Ar. The vial was capped and heated at 100°C for 16 h. The reaction was allowed to cool to ambient

temperature, diluted with EtOAc, filtered with celite, purified by preparative RP-HPLC to afford a colorless solid (100 mg, 0.24 mmol, 78%). ¹H NMR (400 MHz, CD₃OD) δ 8.80 (d, *J* = 2.3 Hz, 1H), 8.55 (dd, *J* = 4.9, 1.6 Hz, 1H), 8.10 (dt, *J* = 8.2, 1.9 Hz, 1H), 7.97 (d, *J* = 8.4 Hz, 1H), 7.74 (d, *J* = 8.5 Hz, 2H), 7.66 (d, *J* = 8.4 Hz, 1H), 7.58 – 7.50 (m, 2H), 7.46 – 7.35 (m, 4H), 7.18 (s, 1H), 7.04 (d, *J* = 5.0 Hz, 1H), 5.45 (s, 2H), 4.98 (s, 2H); ¹³C NMR (101 MHz, CDCl₃) δ 165.08, 149.46, 148.49, 146.25, 140.41, 139.05, 137.06, 135.43, 134.78, 133.98, 129.31, 129.20, 128.55, 128.00, 126.66, 124.87, 124.27, 124.05, 120.37, 110.05, 50.25, 48.84; Purity 95% by LCMS (Method A) *t*_R = 1.68 min, *m/z* = 426.14 [M+H]⁺; HRMS calculated for C₂₄H₁₉N₅OS [M+H]⁺ 426.1394, found 426.1396.

2-(1*H*-benzo[*d*][1,2,3]triazol-1-yl)-*N*-phenyl-*N*-(thiophen-3-ylmethyl)acetamide (9).

Step 1. *N*-(thiophen-3-ylmethyl)aniline.: To a stirring solution of thiophene-3-carbaldehyde, **44** (88 μL, 1.0 mmol) and aniline (112 μL, 1.23 mmol) in DCE (10 mL) was added sodium triacetoxyborohydride (323 mg, 1.52 mmol). The mixture was stirred at rt for 2h, then sat. aq. NH₄Cl (20 mL) added and the DCE layer separated. The aqueous was extracted with DCM (3 × 30 mL), combined organics were dried (Na₂SO₄), concentrated and purified by flash chromatography to afford a colorless solid (188 mg, 1.1 mmol, 99%). LCMS (Method A) *t*_R = 1.57 min, *m/z* = 190.06 [M+H]⁺; ¹H NMR (400 MHz, CDCl₃) δ 7.34 – 7.28 (m, 1H), 7.23 – 7.15 (m, 3H), 7.12 – 7.06 (m, 1H), 6.74 (t, *J* = 7.4 Hz, 1H), 6.67 (d, *J* = 7.9 Hz, 2H), 4.34 (s, 2H), 4.20 (d, *J* = 20.9 Hz, 1H).

Step 2. 2-(1*H*-benzo[*d*][1,2,3]triazol-1-yl)-*N*-phenyl-*N*-(thiophen-3-ylmethyl)acetamide.: To a stirred solution of *N*-(thiophen-3-ylmethyl)aniline (208 mg, 1.1 mmol) and benzotriazol-1-ylacetic acid (195 mg, 1.1 mmol) in DMF (5.5 mL) was added T3P (50% in EtOAc) (1.31 mL, 2.2 mmol), followed by pyridine (266 μL, 3.3 mmol). The mixture was stirred at rt for 18 h, then sat. aq. NaHCO₃ (20 mL) added. The aqueous was extracted with DCM (3 × 30 mL), combined organics were dried (Na₂SO₄), concentrated and purified by flash chromatography to afford a colorless solid (325 mg, 1.1 mmol, 85%). ¹H NMR (400 MHz, CD₃OD) δ 7.98 (d, *J* = 8.4 Hz, 1H), 7.66 (d, *J* = 8.4 Hz, 1H), 7.60 – 7.52 (m, 1H), 7.52 – 7.40 (m, 4H), 7.36 (dd, *J* = 5.0, 2.9 Hz, 1H), 7.30 (d, *J* = 6.7 Hz, 2H), 7.13 (s, 1H), 6.99 (d, *J* = 4.9 Hz, 1H), 5.35 (s, 2H), 4.93 (s, 2H); ¹³C NMR (101 MHz, CDCl₃) δ 165.09, 146.25, 140.56, 137.18, 134.04, 130.62, 129.53, 128.68, 128.64, 128.01, 126.50, 124.84, 124.27, 120.38, 110.10, 50.23, 48.78; Purity 95% by LCMS (Method A) *t*_R = 2.18 min, *m/z* = 349.11 [M+H]⁺; HRMS calculated for C₁₉H₁₆N₄OS [M+H]⁺ 349.1129, found 349.1139.

4-[[2-(Benzotriazol-1-yl)acetyl]-(3-thienylmethyl)amino]benzamide (10).

Step 1. Ethyl 4-(3-thienylmethylamino)benzoate.: To a stirring solution of **44** (1.75 mL, 20 mmol) and ethyl 4-aminobenzoate (3.63 g, 22 mmol) in DCE (100 mL) was added sodium triacetoxyborohydride (5.09 g, 24 mmol). The mixture was stirred at rt for 12 h, then sat. aq. NaHCO₃ (100 mL) added and the DCE layer separated. The aqueous was extracted with DCM (3 × 50 mL), combined organics were dried (MgSO₄), concentrated and purified by flash chromatography to afford a colorless solid (1.67 g, 6.4 mmol, 32%). LCMS (Method A) *t*_R = 2.02 min, *m/z* = 262.09 [M+H]⁺; ¹H NMR (400 MHz, CDCl₃) δ 7.89 (d, *J*

= 8.3 Hz, 1H), 7.32 (dd, J = 5.0, 2.9 Hz, 1H), 7.22 – 7.18 (m, 1H), 7.07 (dd, J = 5.0, 1.4 Hz, 1H), 6.65 (d, J = 8.3 Hz, 1H), 4.40 (s, 1H), 4.32 (q, J = 7.1 Hz, 1H), 1.36 (t, J = 7.1 Hz, 2H).

Step 2. Ethyl 4-[[2-(benzotriazol-1-yl)acetyl]-(3-thienylmethyl)amino]benzoate.: To a stirred solution of ethyl 4-(3-thienylmethylamino)benzoate (1.67 g, 6.4 mmol) and benzotriazol-1-yl-acetic acid (1.24 g, 7.0 mmol) in EtOAc (12.75 mL) was added T3P (50% in EtOAc) (7.6 mL, 12.75 mmol), followed by pyridine (1.54 mL, 19.12 mmol). The mixture was stirred at rt for 16 h, then washed with water (20 mL) and brine (20 mL). Purification by flash column chromatography afforded a cream solid (2.52 g, 6.0 mmol, 94%). LCMS (Method A) t_R = 2.00 min, m/z = 421.04 [M+H]⁺.

Step 3. 4-[[2-(benzotriazol-1-yl)acetyl]-(3-thienylmethyl)amino]benzoic acid, (45).: To a solution of ethyl 4-[[2-(benzotriazol-1-yl)acetyl]-(3-thienylmethyl)amino]benzoate (2.52 g, 6.0 mmol) in THF (30 mL) was added 2M LiOH (15 mL, 30 mmol) and the mixture stirred at rt for 18 h. The mixture was acidified with 2M HCl (20 mL) and extracted with EtOAc, washed with brine, and concentrated. The crude material was purified by preparative RP-HPLC to afford a colorless solid (1.11 g, 2.83 mmol, 47%). LCMS (Method A) t_R = 1.89 min, m/z = 393.10 [M+H]⁺.

Step 4. 4-[[2-(Benzotriazol-1-yl)acetyl]-(3-thienylmethyl)amino]benzamide.: To **45** (100 mg, 0.25 mmol) in THF (1.3 mL) was added 1-ethyl-3-(3-dimethylaminopropyl)carbodiimide (98 mg, 0.51 mmol) and HOBt (41 mg, 0.31 mmol) and the mixture stirred at rt for 20 min before the addition of NH₄Cl (68 mg, 1.27 mmol) and Et₃N (0.35 mL, 2.55 mmol). The mixture was stirred for 18 h, then diluted with EtOAc and washed with sat. aq. NaCl. Purification by ISCO automated flash chromatography afforded title compound as a colorless solid (27 mg, 27%). ¹H NMR (400 MHz, CD₃OD) δ 7.88 (d, J = 8.4 Hz, 1H), 7.84 (d, J = 8.1 Hz, 1H), 7.56 (d, J = 8.4 Hz, 1H), 7.45 (t, J = 7.7 Hz, 1H), 7.34 (d, J = 7.7 Hz, 1H), 7.31–7.24 (m, 3H), 7.05 (br s, 1H), 6.90 (d, J = 4.9 Hz, 1H), 5.30 (s, 2H), 4.87 (s, 2H); ¹³C NMR (101 MHz, CD₃OD) δ 169.59, 165.61, 145.11, 142.97, 136.79, 134.17, 133.89, 129.10, 128.27, 127.53, 125.98, 124.20, 123.85, 118.49, 110.21, 49.45; Purity 95% by LCMS (Method A) t_R = 1.74 min, m/z = 392.12 [M+H]⁺; HRMS calculated for C₂₀H₁₇N₅O₂S [M+H]⁺ 392.1176, found 392.1163.

4-[[2-(Benzotriazol-1-yl)acetyl]-(3-thienylmethyl)amino]-N-cyclopropylbenzamide (11).—To a stirred solution of **45** (78 mg, 0.2 mmol) and cyclopropylamine (21 μ L, 0.3 mmol) in DCM (1 mL) was added COMU (128 mg, 0.3 mmol) and DIPEA (105 μ L, 0.6 mmol). The mixture was stirred at rt for 2 h, then washed with water and concentrated. Purification by RP-HPLC affords a colorless solid (15 mg, 35%). ¹H NMR (400 MHz, CD₃OD) δ 8.00 (d, J = 8.4 Hz, 1H), 7.88 (d, J = 8.2 Hz, 2H), 7.71 – 7.66 (m, 1H), 7.61 – 7.54 (m, 1H), 7.49 – 7.42 (m, 1H), 7.39 (d, J = 8.2 Hz, 2H), 7.15 (s, 1H), 7.01 (d, J = 4.9 Hz, 1H), 5.41 (s, 2H), 4.98 (s, 2H), 2.87 (dq, J = 7.2, 3.7 Hz, 1H), 0.83 (dt, J = 7.1, 3.6 Hz, 2H), 0.74 – 0.58 (m, 2H); ¹³C NMR (101 MHz, CD₃OD) δ 169.08, 165.59, 145.11, 142.73, 136.78, 134.64, 133.88, 128.72, 127.54, 125.97, 124.20, 123.85, 118.50, 110.22, 60.13, 49.44, 22.68, 5.15; Purity 95% by LCMS (Method A) t_R = 1.91 min, m/z = 432.15 [M+H]⁺; HRMS calculated for C₂₃H₂₁N₅O₂S [M+H]⁺ 432.1489, found 432.1506.

2-(1*H*-Benzo[*c*][1,2,3]triazol-1-yl)-*N*-(4-(methylsulfonylamino)phenyl)-*N*-(thiophen-3-ylmethyl)acetamide (12).

Step 1. *tert*-Butyl *N*-[4-(3-thienylmethylamino)phenyl]carbamate.: To a solution of **44** (493 mg, 4.4 mmol) and 4-(*tert*-butoxycarbonylamino)aniline (1125 mg, 5.4 mmol) in DCE (44 mL) was added NaBH(OAc)₃ (1.42 g, 6.7 mmol) and the mixture stirred for 1 h at rt. Sat. aq. NH₄Cl (50 mL) was added and DCE layer separated. The aqueous layer was extracted with EtOAc (3 × 40 mL) and concentrated, purified by flash chromatography to afford a colorless solid (1.23 g, 4.0 mmol, 92%). LCMS (Method A) *t*_R = 1.81 min, *m/z* = 305.13 [M+H]⁺.

Step 2. *tert*-Butyl *N*-[4-[[2-(benzotriazol-1-yl)acetyl]-(3-thienylmethyl)amino]phenyl]carbamate.: To an ice-cold solution of 2-(benzotriazol-1-yl)acetic acid (700 mg, 3.95 mmol) and Et₃N (1.10 mL, 7.90 mmol) in DCM (20 mL) was added HATU (1.50 g, 3.95 mmol) and the mixture stirred for 30 min before the addition of *tert*-butyl *N*-[4-(3-thienylmethylamino)phenyl]carbamate (802 mg, 2.63 mmol) in a single portion. The mixture was stirred for 16 h at rt then washed with water, brine, and concentrated. Purification by flash chromatography afforded title compound as a pale brown solid (1.08 g, 2.34 mmol, 89%). LCMS (Method A) *t*_R = 2.34 min, *m/z* = 464.18 [M+H]⁺; ¹H NMR (400 MHz, CDCl₃) δ 8.05 (d, *J* = 8.4 Hz, 1H), 7.50 – 7.47 (m, 2H), 7.44 (d, *J* = 8.7 Hz, 2H), 7.36 (ddd, *J* = 8.1, 5.6, 2.3 Hz, 1H), 7.26 – 7.23 (m, 1H), 7.05 – 6.99 (m, 3H), 6.97 (dd, *J* = 5.0, 1.3 Hz, 1H), 6.62 (s, 1H), 5.15 (s, 2H), 4.84 (s, 2H), 1.53 (s, 9H).

Step 3. *N*-(4-Aminophenyl)-2-(benzotriazol-1-yl)-*N*-(3-thienylmethyl)acetamide, (46**).:** To a solution of *tert*-butyl *N*-[4-[[2-(benzotriazol-1-yl)acetyl]-(3-thienylmethyl)amino]phenyl]carbamate (588 mg, 1.27 mmol) in DCM (3 mL) was added TFA (2 mL) and stirred for 1 h, then diluted with DCM (10 mL) and washed with sat. aq. K₂CO₃ (20 mL), water and sat. aq. NaCl affording a cream solid that was used without purification (436 mg, 1.20 mmol, 95%). LCMS (Method A) *t*_R = 1.70 min, *m/z* = 364.14 [M+H]⁺; ¹H NMR (400 MHz, CDCl₃) δ 8.05 (d, *J* = 8.4 Hz, 1H), 7.50 – 7.46 (m, 2H), 7.36 (ddd, *J* = 8.1, 5.1, 2.8 Hz, 1H), 7.25 – 7.22 (m, 1H), 7.04 (d, *J* = 2.9 Hz, 1H), 6.98 (dd, *J* = 5.0, 1.2 Hz, 1H), 6.86 (d, *J* = 8.6 Hz, 2H), 6.67 (d, *J* = 8.6 Hz, 2H), 5.17 (s, 2H), 4.82 (s, 2H), 3.84 (s, 2H).

Step 4. 2-(Benzotriazol-1-yl)-*N*-(4-(methanesulfonylamino)phenyl)-*N*-(3-thienylmethyl)acetamide.: To a solution of **46** (87 mg, 0.24 mmol) in DCM (2 mL) was added methanesulfonyl chloride (28 μL, 0.36 mmol) and Et₃N (509 μL, 3.6 mmol) and stirred for 2 h at rt. The mixture was washed with sat. aq. NH₄Cl and concentrated, purified by flash chromatography to afford a colorless solid (26 mg, 0.06 mmol, 25%). ¹H NMR (400 MHz, CDCl₃) δ 8.04 (d, *J* = 8.4 Hz, 1H), 7.51 (d, *J* = 3.9 Hz, 2H), 7.41 – 7.35 (m, 1H), 7.22 (d, *J* = 8.7 Hz, 2H), 7.05 – 6.98 (m, 3H), 6.97 (d, *J* = 4.9 Hz, 1H), 6.69 (s, 1H), 5.19 (s, 2H), 4.85 (s, 2H), 3.11 (s, 3H); ¹³C NMR (101 MHz, CDCl₃) δ 165.16, 146.24, 137.90, 137.02, 136.94, 133.90, 129.96, 128.51, 128.18, 126.74, 124.91, 124.45, 121.25, 120.40, 110.09, 50.55, 48.88, 40.46; Purity 95% by LCMS (Method A) *t*_R = 1.92 min, *m/z* = 442.12 [M+H]⁺; HRMS calculated for C₂₀H₁₉N₅O₃S₂ [M+H]⁺ 442.1013, found 442.1009.

2-(1*H*-Benzo[d][1,2,3]triazol-1-yl)-*N*-(4-(cyclopropanesulfonamido)phenyl)-*N*-(thiophen-3-ylmethyl)acetamide (13).—To a solution of **46** (36 mg, 0.1 mmol) in DCM (1 mL) was added cyclopropanesulfonyl chloride (12 μ L, 0.12 mmol) and Et₃N (509 μ L, 3.6 mmol) and stirred at rt for 1 h. The mixture was washed with sat. aq. NH₄Cl and concentrated, purified by preparative RP-HPLC, washed with aq. K₂CO₃ to remove TFA and concentrated to afford a colorless solid (8 mg, 0.02 mmol, 7%). ¹H NMR (400 MHz, CD₃OD) δ 7.98 (d, *J* = 8.4 Hz, 1H), 7.67 (d, *J* = 8.4 Hz, 1H), 7.56 (t, *J* = 7.7 Hz, 1H), 7.44 (t, *J* = 7.6 Hz, 1H), 7.39 – 7.29 (m, 3H), 7.22 (d, *J* = 8.8 Hz, 2H), 7.15 (s, 1H), 6.99 (d, *J* = 4.7 Hz, 1H), 5.38 (s, 2H), 4.91 (s, 2H), 2.65 – 2.56 (m, 1H), 1.10 – 1.03 (m, 2H), 1.00 – 0.93 (m, 2H); ¹³C NMR (101 MHz, CDCl₃) δ 165.19, 146.22, 138.22, 136.96 (two peaks overlap), 133.98, 129.77, 128.52, 128.18, 126.69, 124.89, 124.45, 122.32, 120.38, 110.15, 50.40, 48.84, 30.73, 6.20; Purity 95% by LCMS (Method A) *t*_R = 2.05 min, *m/z* = 468.12 [M+H]⁺; HRMS calculated for C₂₂H₂₁N₅O₃S₂ [M+H]⁺ 468.1170, found 468.1166.

2-(1*H*-Benzo[d][1,2,3]triazol-1-yl)-*N*-(4-(pyridin-4-yl)phenyl)-*N*-(thiophen-3-ylmethyl)acetamide (14).—An argon purged vial was charged with **47** (85 mg, 0.20 mmol), pyridine-4-boronic acid (39 mg, 0.32 mmol) and Pd(PPh₃)₄ (23 mg, 0.02 mmol). THF (2 mL) and water (0.4 mL) was added into the vial. The vial was capped and heated at 100°C for 16 h. The reaction was allowed to cool to ambient temperature, diluted with EtOAc, filtered with celite, and purified by preparative RP-HPLC to afford title compound as a colorless solid (52 mg, 0.12 mmol, 61%). ¹H NMR (400 MHz, CDCl₃) δ 8.72 (d, *J* = 6.3 Hz, 2H), 8.05 (d, *J* = 8.4 Hz, 1H), 7.69 (d, *J* = 8.6 Hz, 2H), 7.58 – 7.46 (m, 4H), 7.40 – 7.34 (m, 1H), 7.31 – 7.27 (m, 1H), 7.23 (d, *J* = 8.0 Hz, 2H), 7.07 (s, 1H), 7.00 (dd, *J* = 5.0, 1.3 Hz, 1H), 5.22 (s, 2H), 4.93 (s, 2H); ¹³C NMR (101 MHz, CDCl₃) δ 165.05, 150.62, 147.26, 146.29, 141.29, 139.31, 137.00, 133.99, 129.39, 129.18, 128.54, 128.07, 126.75, 124.94, 124.33, 121.99, 120.43, 110.06, 50.29, 48.86; Purity 95% by LCMS (Method A) *t*_R = 1.67 min, *m/z* = 426.13 [M+H]⁺; HRMS calculated for C₂₄H₁₉N₅OS [M+H]⁺ 426.1394, found 426.1390.

2-(1*H*-Benzo[d][1,2,3]triazol-1-yl)-*N*-(4-(pyridin-2-yl)phenyl)-*N*-(thiophen-3-ylmethyl)acetamide (15).—A vial was charged with **47** (86 mg, 0.20 mmol), 2-pyridinylboronic acid (49 mg, 0.40 mmol), CsCO₃ (261 mg, 0.80 mmol), CuCl (20 mg, 0.20 mmol), Pd(OAc)₂ (2 mg, 0.01 mmol) and 1,1-bis(diphenylphosphino)ferrocene (11 mg, 0.02 mmol). DMF (2 mL) was added into the vial. The mixture was stirred and purged with Ar. The vial was capped and heated at 100°C for 15 h. The reaction was allowed to cool to ambient temperature, diluted with EtOAc, filtered with celite, and purified by flash chromatography to afford title compound as a colorless solid (55 mg, 0.13 mmol, 65%). ¹H NMR (400 MHz, CD₃OD) δ 8.64 (d, *J* = 4.8 Hz, 1H), 8.05 (d, *J* = 8.1 Hz, 2H), 7.98 (d, *J* = 8.4 Hz, 1H), 7.95 – 7.85 (m, 2H), 7.68 (d, *J* = 8.4 Hz, 1H), 7.55 (t, *J* = 7.7 Hz, 1H), 7.46 – 7.34 (m, 5H), 7.18 (s, 1H), 7.03 (d, *J* = 4.9 Hz, 1H), 5.44 (s, 2H), 4.98 (s, 2H); ¹³C NMR (101 MHz, CDCl₃) δ 165.05, 156.12, 150.20, 146.25, 140.96, 140.56, 137.37, 137.05, 134.03, 129.06, 128.99, 128.60, 127.97, 126.55, 124.92, 124.21, 123.13, 121.03, 120.34, 110.04, 50.12, 48.71; Purity 95% by LCMS (Method A) *t*_R = 1.76 min, *m/z* = 426.14 [M+H]⁺; HRMS calculated for C₂₄H₁₉N₅OS [M+H]⁺ 426.1394, found 426.1397.

2-(1*H*-Benzo[d][1,2,3]triazol-1-yl)-*N*-(4-(2-methoxypyridin-3-yl)phenyl)-*N*-(thiophen-3-ylmethyl)acetamide (16).—A vial was charged with **47** (85 mg, 0.20 mmol), (2-methoxy-3-pyridyl)boronic acid (49 mg, 0.32 mmol) and Pd(PPh₃)₄ (23 mg, 0.02 mmol). THF (2 mL) and water (0.4 mL) was added into the vial. The mixture was stirred and purged with Ar. The vial was capped and heated at 100°C for 16 h. The reaction was allowed to cool to ambient temperature, diluted with EtOAc, filtered with celite, purified by flash chromatography to afford a colorless solid (90 mg, 0.20 mmol, 99%). ¹H NMR (400 MHz, CDCl₃) δ 8.21 (dd, *J* = 5.0, 1.9 Hz, 1H), 8.06 (d, *J* = 8.5 Hz, 1H), 7.69 – 7.60 (m, 3H), 7.53 – 7.47 (m, 2H), 7.41 – 7.33 (m, 1H), 7.31 – 7.27 (m, 1H), 7.18 (d, *J* = 8.3 Hz, 2H), 7.10 (s, 1H), 7.07 – 6.98 (m, 2H), 5.23 (s, 2H), 4.92 (s, 2H), 4.01 (s, 3H); ¹³C NMR (101 MHz, CDCl₃) δ 164.86, 160.71, 146.50, 145.98, 139.40, 138.66, 137.80, 136.98, 133.75, 130.97, 128.31, 128.03, 127.67, 126.21, 124.48, 123.91, 122.95, 120.07, 117.25, 109.77, 53.65, 49.94, 48.55; Purity 95% by LCMS (Method A) *t*_R = 2.23 min, *m/z* = 456.15 [M+H]⁺; HRMS calculated for C₂₅H₂₁N₅O₂S [M+H]⁺ 445.1489, found 456.1499.

2-(1*H*-Benzo[d][1,2,3]triazol-1-yl)-*N*-(4-(2-oxo-1,2-dihydropyridin-3-yl)phenyl)-*N*-(thiophen-3-ylmethyl)acetamide (17).

Step 1. 2-(benzotriazol-1-yl)-*N*-[4-(2-fluoro-3-pyridyl)phenyl]-*N*-(3-thienylmethyl)acetamide (48).: A vial was charged with **47** (85 mg, 0.20 mmol), 2-fluoropyridine-3-boronic acid (45 mg, 0.32 mmol) and Pd(PPh₃)₄ (23 mg, 0.02 mmol). THF (2 mL) and water (0.4 mL) was added into the vial. The mixture was stirred and purged with Ar. The vial was capped and heated at 100°C for 16 h. The reaction was allowed to cool to ambient temperature, diluted with EtOAc, filtered with celite, purified by RP-HPLC and flash chromatography to afford a colorless solid (80 mg, 0.18 mmol, 90%). LCMS (Method A) *t*_R = 2.16 min, *m/z* = 444.13 [M+H]⁺; ¹H NMR (400 MHz, CDCl₃) δ 8.25 (dt, *J* = 4.8, 1.6 Hz, 1H), 8.09 – 8.02 (m, 1H), 7.88 (ddd, *J* = 9.6, 7.5, 1.9 Hz, 1H), 7.67 – 7.60 (m, 2H), 7.53 – 7.47 (m, 2H), 7.41 – 7.31 (m, 2H), 7.30 – 7.27 (m, 1H), 7.21 (d, *J* = 8.1 Hz, 2H), 7.08 (s, 1H), 7.01 (dd, *J* = 5.0, 1.3 Hz, 1H), 5.23 (s, 2H), 4.93 (s, 2H).

Step 2. 2-(1*H*-benzo[d][1,2,3]triazol-1-yl)-*N*-(4-(2-oxo-1,2-dihydropyridin-3-yl)phenyl)-*N*-(thiophen-3-ylmethyl)acetamide.: To a solution of **48** (44 mg, 0.10 mmol) in dioxane (1 mL) was added conc. aq. HCl (0.08 mL, 1 mmol) and the mixture stirred for 16 h at 80°C. The reaction was allowed to cool to room temperature, concentrated, and purified by flash chromatography to afford a colorless solid (9.0 mg, 0.02 mmol, 20%). ¹H NMR (400 MHz, CDCl₃) δ 8.06 (d, *J* = 8.4 Hz, 1H), 7.83 (d, *J* = 8.3 Hz, 2H), 7.66 (dd, *J* = 7.1, 2.0 Hz, 1H), 7.53 – 7.47 (m, 2H), 7.43 (dd, *J* = 6.5, 2.0 Hz, 1H), 7.40 – 7.33 (m, 1H), 7.30 – 7.26 (m, 1H), 7.20 (d, *J* = 8.1 Hz, 2H), 7.09 (s, 1H), 7.03 (dd, *J* = 5.0, 1.3 Hz, 1H), 6.44 (t, *J* = 6.8 Hz, 1H), 5.22 (s, 2H), 4.91 (s, 2H); ¹³C NMR (101 MHz, CDCl₃) δ 165.20, 163.62, 146.30, 140.61, 140.03, 137.63, 137.30, 134.75, 134.08, 130.61, 130.28, 128.64, 128.46, 128.01, 126.53, 124.81, 124.25, 120.40, 110.11, 107.71, 50.26, 48.90; Purity 95% by LCMS (Method A) *t*_R = 1.65 min, *m/z* = 442.13 [M+H]⁺; HRMS calculated for C₂₄H₁₉N₅O₂S [M+H]⁺ 442.1343, found 442.1342.

2-(Benzotriazol-1-yl)-*N*-[4-(1-methylpyrazol-4-yl)phenyl]-*N*-(3-thienylmethyl)acetamide (18).—A vial was charged

with **47** (128 mg, 0.30 mmol), 1-methyl-1*H*-pyrazole-4-boronic acid, pinacol ester (75 mg, 0.36 mmol), 2M aq. K₂CO₃ (0.3 mL, 0.60 mmol) and Pd(dppf)Cl₂.DCM (12 mg, 0.02 mmol). 1,4-Dioxane (1.5 mL) was added and the mixture degassed under a stream of Ar for 15 mins then heated at 100 °C for 16 h. The reaction was diluted with DCM, washed with water, dried (Na₂SO₄) and concentrated *in vacuo*. Residue was purified by preparative RP-HPLC (5–95% MeCN in H₂O, 0.1% TFA), pure fractions were combined and concentrated *in vacuo*. The free base was obtained by SCX-II chromatography (load/wash MeOH, elution with 2N NH₃ in MeOH) to afford the title compound as a colorless solid (57 mg, 0.13 mmol, 44%). ¹H NMR (400 MHz, CD₃OD) δ 8.02 – 7.94 (m, 2H), 7.84 (s, 1H), 7.69 – 7.59 (m, 3H), 7.54 (t, *J* = 7.6 Hz, 1H), 7.46 – 7.39 (m, 1H), 7.37 (dd, *J* = 5.0, 2.9 Hz, 1H), 7.29 – 7.21 (m, 2H), 7.15 (d, *J* = 3.0 Hz, 1H), 7.04 – 6.98 (m, 1H), 5.40 (s, 2H), 4.93 (s, 2H), 3.93 (s, 3H); ¹³C NMR (101 MHz, DMSO-*d*₆) δ 165.62, 145.46, 138.26, 138.06, 136.79, 134.27, 133.35, 129.17, 128.66, 128.22, 127.62, 127.00, 126.54, 124.25, 123.88, 121.43, 119.41, 111.58, 49.82, 48.48, 39.19; Purity 95% by LCMS (Method A) *t*_R = 1.84 min, *m/z* = 429.15 [M+H]⁺; HRMS calculated for C₂₃H₂₀N₆OS [M+H]⁺ 429.1492, found 429.1497.

2-(Benzotriazol-1-yl)-N-[4-(1*H*-pyrazol-4-yl)phenyl]-N-(3-thienylmethyl)acetamide (19).—A vial was

charged with **46** (128 mg, 0.30 mmol), 4-(4,4,5,5-tetramethyl-1,3,2-dioxaborolan-2-yl)-1*H*-pyrazole (70 mg, 0.36 mmol), 2M K₂CO₃ (0.3 mL, 0.60 mmol) and Pd(dppf)Cl₂.DCM (12 mg, 0.02 mmol). 1,4-Dioxane (1.5 mL, 0.2 M) was added and degassed under a stream of Ar for 15 min then heated at 110 °C for 4 h. The reaction mixture was filtered through celite with EtOAc. The filtrate was washed with water, dried (Na₂SO₄) and concentrated *in vacuo*. The residue was purified by preparative RP-HPLC (5–95% MeCN in H₂O, 0.1% TFA). The pure fractions were combined and concentrated *in vacuo*. The free base was obtained by SCX-II chromatography (load/wash MeOH, elution with 2N NH₃ in MeOH) to afford the title compound as a colorless solid (63 mg, 0.15 mmol, 51%). ¹H NMR (400 MHz, CD₃OD) δ 8.01 – 7.76 (m, 3H), 7.45 (t, *J* = 7.6 Hz, 1H), 7.33 (t, *J* = 7.7 Hz, 1H), 7.27 (dd, *J* = 5.0, 2.9 Hz, 1H), 7.20 – 7.13 (m, 2H), 7.06 (d, *J* = 3.0 Hz, 1H), 6.92 (d, *J* = 4.9 Hz, 1H), 5.31 (s, 2H), 4.84 (s, 2H); ¹³C NMR (101 MHz, CD₃OD) δ 165.91, 153.23, 145.12, 137.87, 137.05, 133.91, 128.58, 127.67, 127.48, 126.61, 125.82, 124.17, 123.80, 121.07, 118.46, 110.23, 49.39; Purity 95% by LCMS (Method A) *t*_R = 1.71 min, *m/z* = 415.13 [M+H]⁺; HRMS calculated for C₂₂H₁₈N₆OS [M+H]⁺ 415.1336, found 415.1328.

2-(Benzotriazol-1-yl)-N-[4-(1-methylimidazol-4-yl)phenyl]-N-(3-thienylmethyl)acetamide (20).

Step 1. 2-(Benzotriazol-1-yl)-N-[4-(4,4,5,5-tetramethyl-1,3,2-dioxaborolan-2-yl)phenyl]-N-(3-thienylmethyl)acetamide.: Compound **47** (717 mg, 1.68 mmol), bis(pinacolato)diboron (511 mg, 2.01 mmol), Pd(dppf)Cl₂.DCM (68 mg, 0.08 mmol), and KOAc (494 mg, 5.03 mmol) were combined in dioxane (8 mL) and heated to 100 °C for 16 h. Upon cooling, the mixture was filtered, concentrated and purified by ISCO flash chromatography (0–100% EtOAc in hexanes) to afford a pale brown solid (650 mg, 1.37 mmol, 82%). LCMS (Method A) *t*_R = 2.22 min, *m/z* = 475.09 [M+H]⁺; ¹H NMR (400 MHz, CDCl₃) δ 8.05 (d, *J* = 8.2 Hz, 1H), 7.88 (d, *J* = 7.2 Hz, 2H), 7.53 – 7.44 (m, 2H), 7.36 (t, *J* =

7.0 Hz, 1H), 7.30 – 7.21 (m, 1H), 7.14 (d, $J = 7.5$ Hz, 2H), 7.02 (d, $J = 2.9$ Hz, 1H), 6.96 (d, $J = 4.9$ Hz, 1H), 5.14 (s, 2H), 4.89 (s, 2H), 1.36 (s, 12H).

Step 2. 2-(Benzotriazol-1-yl)-N-[4-(1-methylimidazol-4-yl)phenyl]-N-(3-thienylmethyl)acetamide: 2-(Benzotriazol-1-yl)-*N*-[4-(4,4,5,5-tetramethyl-1,3,2-dioxaborolan-2-yl)phenyl]-*N*-(3-thienylmethyl)acetamide (100 mg, 0.21 mmol), 4-bromo-1-methyl-1*H*-pyrazole (41 mg, 0.25 mmol), 2M aq. K_2CO_3 (0.21 mL, 0.42 mmol) and $Pd(dppf)Cl_2 \cdot DCM$ (9 mg, 0.01 mmol) were combined in 1,4-dioxane (1 mL), degassed under a stream of Ar for 15 mins then heated at 100 °C for 18 h. The reaction mixture was filtered through celite, washing with EtOAc. The filtrate was washed with water, dried (Na_2SO_4) and concentrated *in vacuo*. Residue was purified by preparative RP-HPLC (5–95% MeCN in H_2O , 0.1% TFA), pure fractions were combined and concentrated *in vacuo*. The free base was obtained by SCX-II chromatography (load/wash MeOH, elution with 2N NH_3 in MeOH) to afford the title compound as a colorless solid (36 mg, 0.08 mmol, 40%). 1H NMR (400 MHz, CD_3OD) δ 7.98 (d, $J = 8.4$ Hz, 1H), 7.80 (d, $J = 8.4$ Hz, 2H), 7.71 (s, 1H), 7.67 (d, $J = 8.4$ Hz, 1H), 7.59 – 7.51 (m, 2H), 7.43 (t, $J = 7.7$ Hz, 1H), 7.37 (dd, $J = 5.0, 2.9$ Hz, 1H), 7.28 (d, $J = 8.6$ Hz, 2H), 7.16 (s, 1H), 7.01 (d, $J = 5.0$ Hz, 1H), 5.41 (s, 2H), 4.94 (s, 2H), 3.78 (s, 3H); ^{13}C NMR (101 MHz, $DMSO-d_6$) δ 165.61, 145.47, 139.90, 139.18, 138.51, 138.05, 134.29, 128.90, 128.22, 127.64, 126.99, 125.78, 124.25, 123.88, 119.42, 118.22, 111.59, 49.80, 48.48, 33.68; Purity = 95% by LCMS (Method A) $t_R = 1.43$ min, $m/z = 429.03$ $[M+H]^+$; HRMS calculated for $C_{23}H_{20}N_6OS$ $[M+H]^+$ 429.1492, found 429.1497.

2-(Benzotriazol-1-yl)-N-[4-(1*H*-imidazol-4-yl)phenyl]-N-(3-thienylmethyl)acetamide (21).

Step 1: 2-(Benzotriazol-1-yl)-N-(3-thienylmethyl)-N-[4-(1-tritylimidazol-4-yl)phenyl]acetamide.: Compound **49** 2-(benzotriazol-1-yl)-*N*-[4-(4,4,5,5-tetramethyl-1,3,2-dioxaborolan-2-yl)phenyl]-*N*-(3-thienylmethyl)acetamide (122 mg, 0.31 mmol), 4-bromo-1-trityl-imidazole (178 mg, 0.38 mmol), 2M aq. K_2CO_3 (0.31 mL, 0.63 mmol) and $Pd(dppf)Cl_2 \cdot DCM$ (13 mg, 0.02 mmol) were combined in 1,4-dioxane (1.6 mL), degassed under a stream of Ar for 15 mins then heated at 100 °C for 18 h. The reaction mixture was filtered through celite, washing with EtOAc. The filtrate was washed with water, dried (Na_2SO_4) and concentrated *in vacuo*. Residue was purified by ISCO flash chromatography (24 g, 0–60% EtOAc in hexanes) to afford title compound (117 mg, 0.18 mmol, 57%). Purity = 85% by LCMS (210, 254 nm); $t_R = 1.78$ min, $m/z = 657.24$ $[M+H]^+$.

Step 2: 2-(Benzotriazol-1-yl)-N-[4-(1*H*-imidazol-4-yl)phenyl]-N-(3-thienylmethyl)acetamide.: Compound **49** (50 mg, 0.08 mmol) was dissolved in MeOH (380 μ L), acetic acid (95 μ L, 0.08 mmol) was added and the reaction mixture stirred at 65 °C for 2 h. The mixture was concentrated *in vacuo* then purified by preparative RP-HPLC (5–40% MeCN in H_2O , 0.1% TFA). The free base was obtained by SCX-II chromatography (load/wash MeOH, elution with 2N NH_3 in MeOH) to afford the title compound as a colorless solid (11 mg, 0.03 mmol, 35%). 1H NMR (400 MHz, CD_3OD) δ 9.04 – 9.00 (m, 1H), 8.01 – 7.94 (m, 2H), 7.80 (d, $J = 8.1$ Hz, 2H), 7.67 (s, 1H), 7.56 (t, $J = 7.7$ Hz, 1H), 7.46 – 7.35 (m, 4H), 7.16 (s, 1H), 7.02 (d, $J = 4.9$ Hz, 1H), 5.44 (s, 2H), 4.98

(s, 2H); ^{13}C NMR (101 MHz, CD_3OD) δ 165.61, 145.47, 138.38, 138.04, 136.75, 134.29, 128.90, 128.24, 127.64, 126.99, 125.86, 124.25, 123.92, 119.42, 111.59, 49.80, 48.45; Purity 95% by LCMS (Method A) $t_{\text{R}} = 1.65$ min, $m/z = 415.13$ $[\text{M}+\text{H}]^+$; HRMS calculated for $\text{C}_{22}\text{H}_{18}\text{N}_6\text{OS}$ $[\text{M}+\text{H}]^+$ 415.1336, found 415.1341.

2-(1*H*-Benzo[d][1,2,3]triazol-1-yl)-*N*-isopentyl-*N*-(4-(pyridin-3-yl)phenyl)acetamide (22).

Step 1. 4-(3-Pyridyl)aniline (51): To a vial containing 4-bromoaniline (1.72 g, 10 mmol), pyridine-3-boronic acid (1.47 g, 12 mmol), $\text{Pd}(\text{dppf})\text{Cl}\cdot\text{DCM}$ (203.66 mg, 0.25 mmol) and K_2CO_3 (2.76 g, 20 mmol) was added dioxane (25 mL) and water (5 mL). The mixture was heated to 100 °C for 18 h. The mixture was diluted with EtOAc and washed with water, brine, then dried over MgSO_4 and concentrated. The crude material was purified by flash chromatography to afford a pale brown solid (1.45 g, 8.54 mmol, 85%). LCMS (Method A) $t_{\text{R}} = 0.53$ min, $m/z = 171.03$ $[\text{M}+\text{H}]^+$.

Step 2. *N*-Isopentyl-4-(3-pyridyl)aniline: To a solution of isovaleraldehyde (0.05 mL, 0.50 mmol) and **51** (104 mg, 0.61 mmol) in DCE (5 mL) was added $\text{NaBH}(\text{OAc})_3$ (161 mg, 0.76 mmol) and the mixture stirred for 2 h at rt. Saturated aq. NH_4Cl (30 mL) was added and DCE layer separated. The aqueous layer was extracted with DCM (3×10 mL) and concentrated to dryness. Purification by flash chromatography afford a yellow solid (107 mg, 0.45 mmol, 89%). ^1H NMR (400 MHz, CDCl_3) δ 8.80 (s, 1H), 8.48 (dd, $J = 5.0, 1.6$ Hz, 1H), 7.82 (dt, $J = 8.1, 1.9$ Hz, 1H), 7.43 (d, $J = 8.7$ Hz, 2H), 7.31 (dd, $J = 8.0, 4.9$ Hz, 1H), 6.69 (d, $J = 8.7$ Hz, 2H), 3.18 (t, $J = 7.4$ Hz, 2H), 1.81 – 1.67 (m, 1H), 1.55 (q, $J = 7.2$ Hz, 2H), 0.97 (d, $J = 6.6$ Hz, 6H).

Step 3. 2-(1*H*-Benzo[d][1,2,3]triazol-1-yl)-*N*-isopentyl-*N*-(4-(pyridin-3-yl)phenyl)acetamide: To a stirred solution of *N*-isopentyl-4-(3-pyridyl)aniline (48 mg, 0.2 mmol) and **50** (35 mg, 0.2 mmol) in DMF (0.5 mL) was added T3P (50% in EtOAc) (238 μL , 0.4 mmol), followed by pyridine (48 μL , 0.6 mmol). The mixture was stirred at rt for 16 h, then directly purified by RP-HPLC to afford a colorless solid (30 mg, 0.08 mmol, 38%). ^1H NMR (400 MHz, CDCl_3) δ 8.88 (d, $J = 2.4$ Hz, 1H), 8.66 (dd, $J = 4.9, 1.7$ Hz, 1H), 8.04 (d, $J = 8.4$ Hz, 1H), 7.92 (dt, $J = 7.9, 2.0$ Hz, 1H), 7.71 (d, $J = 8.1$ Hz, 2H), 7.55 – 7.31 (m, 6H), 5.21 (s, 2H), 3.84 – 3.75 (m, 2H), 1.65 – 1.52 (m, 1H), 1.52 – 1.43 (m, 2H), 0.89 (d, $J = 6.6$ Hz, 6H); ^{13}C NMR (101 MHz, CDCl_3) δ 164.95, 149.43, 148.49, 146.28, 140.92, 138.92, 135.58, 134.90, 134.06, 129.39, 129.25, 128.00, 124.25, 124.12, 120.36, 110.17, 50.34, 49.09, 36.63, 26.37, 22.79; Purity 95% by LCMS (Method A) $t_{\text{R}} = 1.76$ min, $m/z = 400.21$ $[\text{M}+\text{H}]^+$; HRMS calculated for $\text{C}_{24}\text{H}_{25}\text{N}_5\text{O}$ $[\text{M}+\text{H}]^+$ 400.2143, found 400.2131.

2-(1*H*-Benzo[d][1,2,3]triazol-1-yl)-*N*-isopentyl-*N*-(4-(pyridin-3-yl)phenyl)acetamide (23).

Step 1. *N*-(Cyclopropylmethyl)-4-(3-pyridyl)aniline: To a solution of cyclopropanecarbaldehyde (0.04 mL, 0.50 mmol) and **51** (104 mg, 0.61 mmol) in DCE (5 mL) was added $\text{NaBH}(\text{OAc})_3$ (161.4 mg, 0.76 mmol) and the mixture stirred for 1.5 h at rt. Saturated aq. NH_4Cl (30 mL) was added and DCE layer separated. The aqueous layer was extracted with EtOAc (3×10 mL) and concentrated. Purification by flash chromatography

afforded a pale cream solid (100 mg, 0.45 mmol, 89%). ¹H NMR (400 MHz, CDCl₃) δ 8.80 (s, 1H), 8.52 – 8.46 (m, 1H), 7.81 (dt, *J* = 7.9, 2.0 Hz, 1H), 7.43 (d, *J* = 8.6 Hz, 2H), 7.30 (dd, *J* = 7.9, 4.8 Hz, 1H), 6.70 (d, *J* = 8.6 Hz, 2H), 4.03 (s, 1H), 3.01 (d, *J* = 6.9 Hz, 2H), 1.19 – 1.05 (m, 1H), 0.63 – 0.54 (m, 2H), 0.31 – 0.23 (m, 2H).

Step 2. 2-(1H-Benzo[d][1,2,3]triazol-1-yl)-N-isopentyl-N-(4-(pyridin-3-yl)phenyl)acetamide.: To a stirred solution of *N*-(cyclopropylmethyl)-4-(3-pyridyl)aniline (45 mg, 0.2 mmol) and **50** (35 mg, 0.2 mmol) in DMF (0.5 mL) was added T3P (50% in EtOAc) (238 μL, 0.4 mmol), followed by pyridine (48 μL, 0.6 mmol). The mixture was stirred at rt for 14 h, then directly purified by RP-HPLC to afford a colorless solid (50 mg, 0.13 mmol, 65%). ¹H NMR (400 MHz, CDCl₃) δ 8.88 (d, *J* = 2.4 Hz, 1H), 8.66 (dd, *J* = 4.8, 1.6 Hz, 1H), 8.04 (d, *J* = 8.4 Hz, 1H), 7.92 (dt, *J* = 7.9, 2.0 Hz, 1H), 7.70 (d, *J* = 8.3 Hz, 2H), 7.55 – 7.40 (m, 5H), 7.36 (ddd, *J* = 8.1, 6.5, 1.4 Hz, 1H), 5.23 (s, 2H), 3.67 (d, *J* = 7.3 Hz, 2H), 1.08 – 0.96 (m, 1H), 0.54 – 0.45 (m, 2H), 0.23 – 0.14 (m, 2H); ¹³C NMR (101 MHz, CDCl₃) δ 165.02, 149.46, 148.54, 146.28, 141.00, 138.96, 135.57, 134.84, 134.04, 129.54, 129.24, 127.95, 124.23, 124.09, 120.34, 110.19, 54.68, 50.36, 10.04, 4.18; Purity 95% by LCMS (Method A) *t*_R = 1.59 min, *m/z* = 384.18 [M+H]⁺; HRMS calculated for C₂₃H₂₁N₅O [M+H]⁺ 384.1830, found 384.1813.

2-(1H-Benzo[d][1,2,3]triazol-1-yl)-N-(cyclobutylmethyl)-N-(4-(pyridin-3-yl)phenyl)acetamide (24).

Step 1. N-(Cyclobutylmethyl)-4-(3-pyridyl)aniline.: To a solution of cyclobutanecarbaldehyde (0.04 mL, 0.50 mmol) and **51** (104 mg, 0.61 mmol) in DCE (5 mL) was added NaBH(OAc)₃ (161 mg, 0.76 mmol) and the mixture stirred for 1 h at rt Sat. aq. NH₄Cl (30 mL) was added and DCE layer separated. The aqueous layer was extracted with DCM (3 × 10 mL) and concentrated, purified by flash chromatography to afford as a light-yellow solid (110 mg, 0.46 mmol, 92%). ¹H NMR (400 MHz, CDCl₃) δ 8.80 (s, 1H), 8.48 (dd, *J* = 4.9, 1.7 Hz, 1H), 7.82 (dt, *J* = 8.1, 1.9 Hz, 1H), 7.42 (d, *J* = 8.7 Hz, 2H), 7.31 (dd, *J* = 7.9, 4.9 Hz, 1H), 6.69 (d, *J* = 8.7 Hz, 2H), 3.18 (d, *J* = 7.3 Hz, 2H), 2.68 – 2.54 (m, 1H), 2.21 – 2.09 (m, 2H), 2.02 – 1.87 (m, 3H), 1.83 – 1.70 (m, 3H).

Step 2. 2-(1H-Benzo[d][1,2,3]triazol-1-yl)-N-(cyclobutylmethyl)-N-(4-(pyridin-3-yl)phenyl)acetamide.: To a stirred solution of *N*-(cyclobutylmethyl)-4-(3-pyridyl)aniline (48 mg, 0.2 mmol) and **50** (35 mg, 0.2 mmol) in DMF (0.5 mL) was added T3P (50% in EtOAc) (238 μL, 0.4 mmol), followed by pyridine (48 μL, 0.6 mmol). The mixture was stirred at rt for 13 h, then directly purified by RP-HPLC to afford a colorless solid (30 mg, 0.08 mmol, 38%). ¹H NMR (400 MHz, MeOD) δ 8.85 (d, *J* = 2.4 Hz, 1H), 8.60 – 8.54 (m, 1H), 8.15 (dt, *J* = 8.2, 2.0 Hz, 1H), 7.97 (d, *J* = 8.4 Hz, 1H), 7.83 (d, *J* = 8.1 Hz, 2H), 7.64 (d, *J* = 8.4 Hz, 1H), 7.61 – 7.49 (m, 4H), 7.41 (t, *J* = 7.7 Hz, 1H), 5.39 (s, 2H), 3.87 (d, *J* = 7.6 Hz, 2H), 2.64 – 2.51 (m, 1H), 2.10 – 1.97 (m, 2H), 1.97 – 1.81 (m, 2H), 1.78 – 1.67 (m, 2H); ¹³C NMR (101 MHz, CDCl₃) δ 165.20, 149.33, 148.40, 146.29, 140.92, 138.85, 135.62, 134.97, 134.03, 129.28 (two peaks overlap), 127.96, 124.24, 124.15, 120.35, 110.21, 55.14, 50.38, 34.01, 26.54, 18.64; Purity 95% by LCMS (Method A) *t*_R = 1.70 min, *m/z* = 398.20 [M+H]⁺; HRMS calculated for C₂₄H₂₃N₅O [M+H]⁺ 398.1986, found 398.1969.

2-(1*H*-Benzo[*d*][1,2,3]triazol-1-yl)-*N*-(cyclopentylmethyl)-*N*-(4-(pyridin-3-yl)phenyl)acetamide (25).

Step 1. *N*-(Cyclobutylmethyl)-4-(3-pyridyl)aniline: To a solution of cyclopentanecarbaldehyde (0.05 mL, 0.50 mmol) and **51** (104 mg, 0.61 mmol) in DCE (5 mL) was added NaBH(OAc)₃ (161 mg, 0.76 mmol) and the mixture stirred for 1 h at rt. Sat. aq. NH₄Cl (30 mL) was added and DCE layer separated. The aqueous layer was extracted with EtOAc (3 × 10 mL) and concentrated. Purification by flash chromatography afforded a light yellow solid (126 mg, 0.20 mmol, 99%). LCMS (Method A) t_R = 1.55 min, *m/z* = 253.09 [M+H]⁺.

Step 2. 2-(1*H*-benzo[*d*][1,2,3]triazol-1-yl)-*N*-(cyclopentylmethyl)-*N*-(4-(pyridin-3-yl)phenyl)acetamide.: To an ice-cold solution of **50** (53 mg, 0.30 mmol) and Et₃N (0.08 mL, 0.60 mmol) in DCM (1 mL) was added HATU (114 mg, 0.30 mmol) and the mixture stirred for 30 min before the addition of *N*-(cyclopentylmethyl)-4-(3-pyridyl)aniline (51 mg, 0.20 mmol) in a single portion. The mixture was stirred for 20 h at rt then washed with water, brine, and concentrated. Purification by flash chromatography afforded title compound as a colorless solid (69.1 mg, 0.17 mmol, 84%). ¹H NMR (400 MHz, MeOD) δ 8.85 (d, *J* = 2.4 Hz, 1H), 8.60 – 8.54 (m, 1H), 8.15 (dt, *J* = 8.0, 2.0 Hz, 1H), 7.97 (d, *J* = 8.4 Hz, 1H), 7.84 (d, *J* = 8.4 Hz, 2H), 7.69 – 7.59 (m, 3H), 7.60 – 7.50 (m, 2H), 7.41 (t, *J* = 7.7 Hz, 1H), 5.42 (s, 2H), 3.79 (d, *J* = 7.7 Hz, 2H), 2.19 – 2.06 (m, 1H), 1.82 – 1.71 (m, 2H), 1.69 – 1.50 (m, 4H), 1.35 – 1.24 (m, 2H); ¹³C NMR (101 MHz, CDCl₃) δ 165.29, 149.47, 148.54, 146.25, 140.96, 138.86, 135.54, 134.81, 134.03, 129.30, 129.23, 127.95, 124.22, 124.08, 120.31, 110.19, 54.82, 50.40, 38.25, 30.65, 25.52; Purity 95% by LCMS (Method A) t_R = 1.81 min, *m/z* = 412.21 [M+H]⁺; HRMS calculated for C₂₅H₂₅N₅O [M+H]⁺ 412.2143, found 412.2125.

2-(1*H*-Benzo[*d*][1,2,3]triazol-1-yl)-*N*-(4-(pyridin-3-yl)phenyl)-*N*-((tetrahydrofuran-3-yl)methyl)acetamide (26).

Step 1. 4-(3-Pyridyl)-*N*-(tetrahydrofuran-3-ylmethyl)aniline.: To a solution of tetrahydrofuran-3-carbaldehyde (50% aq., 91 μL, 0.50 mmol) and **51** (98 mg, 0.58 mmol) in DCE (5 mL) was added NaBH(OAc)₃ (148 mg, 0.70 mmol) and the mixture stirred for 1 h at rt. Saturated aq. NH₄Cl (30 mL) was added and DCE layer separated. The aqueous layer was extracted with EtOAc (3 × 10 mL) and concentrated. Purification by flash chromatography afforded a yellow oil (114 mg, 0.45 mmol, 90%). LCMS (Method A) t_R = 1.15 min, *m/z* = 255.08 [M+H]⁺.

Step 2. 2-(1*H*-Benzo[*d*][1,2,3]triazol-1-yl)-*N*-(4-(pyridin-3-yl)phenyl)-*N*-((tetrahydrofuran-3-yl)methyl)acetamide.: To a stirred solution of 4-(3-pyridyl)-*N*-(tetrahydrofuran-3-ylmethyl)aniline (51 mg, 0.2 mmol) and **50** (35 mg, 0.2 mmol) in DMF (0.5 mL) was added T3P (50% in EtOAc) (238 μL, 0.4 mmol), followed by pyridine (48 μL, 0.6 mmol). The mixture was stirred at rt for 16 h, then washed with water (20 mL) and brine (20 mL). Purification by flash chromatography afforded a colorless solid (47 mg, 0.11 mmol, 57%). ¹H NMR (400 MHz, CDCl₃) δ 8.88 (s, 1H), 8.67 (d, *J* = 4.8 Hz, 1H), 8.05 (d, *J* = 8.4 Hz, 1H), 7.95 (d, *J* = 8.1 Hz, 1H), 7.71 (d, *J* = 8.3 Hz, 2H), 7.53 – 7.45 (m, 3H), 7.42 (d, *J* = 8.1 Hz, 2H), 7.40 – 7.33 (m, 1H), 5.29 – 5.17 (m, 2H), 3.99 (dd, *J* = 13.5, 7.7

Hz, 1H), 3.90 – 3.68 (m, 4H), 3.51 – 3.43 (m, 1H), 2.59 – 2.48 (m, 1H), 2.06 – 1.94 (m, 1H), 1.68 – 1.64 (m, 1H); ¹³C NMR (101 MHz, CDCl₃) δ 165.61, 149.54, 148.48, 146.26, 140.75, 139.18, 135.41, 134.88, 133.98, 129.54, 129.09, 128.06, 124.32, 124.14, 120.40, 110.04, 71.59, 68.00, 52.86, 50.32, 38.45, 30.46; Purity 95% by LCMS (Method A) t_R = 1.44 min, m/z = 414.19 [M+H]⁺; HRMS calculated for C₂₄H₂₃N₅O₂ [M+H]⁺ 414.1935, found 414.1936.

2-(Benzotriazol-1-yl)-N-[4-(3-pyridyl)phenyl]-N-(thiazol-4-ylmethyl)acetamide (27).

Step 1. 4-(3-Pyridyl)-N-(thiazol-4-ylmethyl)aniline.: To a solution of **51** (34 mg, 0.20 mmol) and thiazole-4-carbaldehyde (25 mg, 0.22 mmol) in DCM (1 mL) was added AcOH (50 μL) and stirred for 30 min before the addition of NaBH(OAc)₃ (64 mg, 0.30 mmol). The mixture was stirred for 16 h, then diluted with DCM and washed with sat. aq. NaHCO₃, concentrated and purified by ISCO flash chromatography (0–100% EtOAc in hexanes) to afford a cream colored solid (47 mg, 0.18 mmol, 88%). LCMS (Method A) t_R = 1.13 min, m/z = 268.01 [M+H]⁺.

Step 2. 2-(Benzotriazol-1-yl)-N-[4-(3-pyridyl)phenyl]-N-(thiazol-4-ylmethyl)acetamide.: To a solution of 4-(3-pyridyl)-N-(thiazol-4-ylmethyl)aniline (47 mg, 0.18 mmol) and **50** (31 mg, 0.18 mmol) in DMF (1 mL) was added T3P (50% in DMF, 0.21 mL, 0.35 mmol) and pyridine (43 μL, 0.53 mmol). The mixture was stirred at rt for 16 h, then filtered and purified by preparative RP-HPLC. The free base was obtained by SCX-II chromatography (eluant 2N NH₃/MeOH) affording a colorless solid (27 mg, 0.06 mmol, 36%). ¹H NMR (400 MHz, MeOH-*d*₄) δ 8.99 (s, 1H), 8.82 (s, 1H), 8.61 – 8.52 (m, 1H), 8.12 (d, *J* = 8.0 Hz, 1H), 7.99 (d, *J* = 8.4 Hz, 1H), 7.77 (d, *J* = 8.0 Hz, 2H), 7.71 (d, *J* = 8.4 Hz, 1H), 7.60 – 7.47 (m, 6H), 7.43 (t, *J* = 7.7 Hz, 1H), 5.50 (s, 2H), 5.18 (s, 2H); ¹³C NMR (101 MHz, DMSO-*d*₆) δ 165.61, 154.83, 152.81, 149.31, 148.20, 145.46, 140.95, 134.92, 134.70, 134.19, 129.38, 128.66, 127.61, 124.37, 124.26, 119.42, 117.47, 111.58, 50.00, 49.50; Purity 95% by LCMS (Method A) t_R = 1.24 min, m/z = 427.13 [M+H]⁺; HRMS calculated for C₂₃H₁₈N₆OS [M+H]⁺ 427.1336, found 427.1339.

2-(Benzotriazol-1-yl)-N-[(3-chlorophenyl)methyl]-N-[4-(3-pyridyl)phenyl]acetamide (28).

Step 1. N-[(3-Chlorophenyl)methyl]-4-(3-pyridyl)aniline.: To a solution of **51** (34 mg, 0.20 mmol) and 3-chlorobenzaldehyde (25 μL, 0.22 mmol) in DCM (1 mL) was added AcOH (50 μL) and stirred for 30 min before the addition of NaBH(OAc)₃ (64 mg, 0.30 mmol). The mixture was stirred for 16 h, then diluted with DCM and washed with sat. aq. NaHCO₃. Concentration and purification by ISCO flash chromatography (0–100% EtOAc in hexanes) afforded a cream colored solid (51 mg, 0.17 mmol, 86%). LCMS (Method A) t_R = 1.63 min, m/z = 295.02 [M+H]⁺.

Step 2. 2-(Benzotriazol-1-yl)-N-[(3-chlorophenyl)methyl]-N-[4-(3-pyridyl)phenyl]acetamide.: To a solution of N-[(3-chlorophenyl)methyl]-4-(3-pyridyl)aniline (51 mg, 0.17 mmol) and **50** (30 mg, 0.17 mmol) in DMF (1 mL) was added T3P (50% in DMF, 206 μL, 0.35 mmol) and pyridine (42 μL, 0.52 mmol). The mixture was

stirred at rt for 16 h, then filtered and purified by preparative RP-HPLC. The free base was obtained after SCX-II chromatography (eluent 2N NH₃/MeOH) affording a colorless solid (48 mg, 0.11 mmol, 61%). ¹H NMR (400 MHz, DMSO-*d*₆) δ 8.93 (s, 1H), 8.59 (d, *J* = 4.8 Hz, 1H), 8.11 (d, *J* = 8.0 Hz, 1H), 8.04 (d, *J* = 8.4 Hz, 1H), 7.86 (d, *J* = 8.1 Hz, 2H), 7.82 (d, *J* = 8.4 Hz, 1H), 7.64 (d, *J* = 8.0 Hz, 2H), 7.55 (t, *J* = 7.7 Hz, 1H), 7.50 (dd, *J* = 7.9, 4.8 Hz, 1H), 7.44 – 7.31 (m, 4H), 7.26 (d, *J* = 6.1 Hz, 1H), 5.55 (s, 2H), 4.98 (s, 2H); ¹³C NMR (101 MHz, DMSO-*d*₆) δ 166.19, 149.33, 148.20, 145.44, 140.58, 139.92, 137.49, 134.83, 134.69, 134.20, 133.58, 130.80, 129.24, 128.74, 128.17, 127.83, 127.63, 127.07, 124.36, 124.28, 119.43, 111.57, 52.49, 49.98; Purity 95% by LCMS (Method A) *t*_R = 1.60 min, *m/z* = 454.14 [M+H]⁺; HRMS calculated for C₂₆H₂₀ClN₅O [M+H]⁺ 454.1429, found 454.1445.

2-(Benzotriazol-1-yl)-*N*-[(3-chloro-4-fluoro-phenyl)methyl]-*N*-[4-(3-pyridyl)phenyl]acetamide (29).

Step 1: *N*-[(3-Chloro-4-fluoro-phenyl)methyl]-4-(3-pyridyl)aniline.: 3-chloro-4-fluorobenzaldehyde (35 mg, 0.22 mmol) and **51** (34 mg, 0.20 mmol) were dissolved in DCM:AcOH (0.2 M, 20:1) and stirred for 30 min at 23 °C. To the mixture, NaBH(OAc)₃ (63.6 mg, 0.30 mmol) was added and stirred at 23 °C for 18 h. The reaction mixture was diluted with DCM and washed with sat. aq. NaHCO₃. The organic layer was dried (Na₂SO₄), filtered, and concentrated *in vacuo*. The resulting residue was purified by ISCO automated flash chromatography (4 g, 0–100% EtOAc in hexanes) to afford a cream colored solid (19 mg, 0.06 mmol, 30%). LCMS (Method A), *t*_R = 1.86 min, *m/z* = 313.09 [M+H]⁺.

Step 2: 2-(Benzotriazol-1-yl)-*N*-[(3-chloro-4-fluoro-phenyl)methyl]-*N*-[4-(3-pyridyl)phenyl]acetamide.: Pyridine (14 μL, 0.17 mmol) and T3P (50% in DMF) (78 μL, 0.12 mmol) were added to a solution of *N*-[(3-chloro-4-fluoro-phenyl)methyl]-4-(3-pyridyl)aniline (18 mg, 0.06 mmol) and **50** (11 mg, 0.06 mmol) in DMF (0.5 mL, 0.2 M) and stirred at 23 °C for 18 h. The concentrated reaction mixture was purified by preparative RP-HPLC (5–50% MeCN in H₂O, 0.1% TFA), pure fractions were combined and concentrated *in vacuo*. The free base was obtained by SCX-II chromatography (load/wash MeOH, elution with 2N NH₃ in MeOH) to afford the title compound as a colorless solid (7.5 mg, 0.02 mmol, 28%). ¹H NMR (400 MHz, CD₃OD) δ 9.02 (d, *J* = 2.3 Hz, 1H), 8.74 (dd, *J* = 5.5, 1.5 Hz, 1H), 8.61 – 8.54 (m, 1H), 7.98 (d, *J* = 8.5 Hz, 1H), 7.91 (dd, *J* = 8.1, 5.5 Hz, 1H), 7.83 (d, *J* = 8.4 Hz, 2H), 7.69 (d, *J* = 8.4 Hz, 1H), 7.59 – 7.52 (m, 1H), 7.50 – 7.34 (m, 4H), 7.24 – 7.13 (m, 2H), 5.49 (s, 2H), 4.99 (s, 2H); ¹³C NMR (101 MHz, DMSO-*d*₆) δ 165.71, 157.68, 155.23, 148.85, 147.71, 144.97, 139.96, 137.06, 134.86, 134.82, 134.33, 134.21, 133.71, 130.02, 128.81, 128.28, 127.15, 123.88, 119.46, 119.28, 118.95, 116.97, 116.76, 111.09, 51.42, 49.51; ¹⁹F NMR (376 MHz, CD₃OD) δ –112.43; Purity 95% by LCMS (Method A) *t*_R = 1.86 min, *m/z* = 472.13 [M+H]⁺; HRMS calculated for C₂₆H₁₉ClFN₅O [M+H]⁺ 472.1335, found 472.1345.

2-(Benzotriazol-1-yl)-*N*-[(3,4-dichlorophenyl)methyl]-*N*-[4-(3-pyridyl)phenyl]acetamide (30).

Step 1: *N*-[(3,4-Dichlorophenyl)methyl]-4-(3-pyridyl)aniline.: 3,4-Dichlorobenzaldehyde (39 mg, 0.22 mmol) and **51** (34 mg, 0.20 mmol) were dissolved in DCM:AcOH (0.2 M,

20:1) and stirred for 30 min at rt. To the mixture, NaBH(OAc)₃ (63.6 mg, 0.30 mmol) was added and stirred at rt for 18 h. The reaction mixture was diluted with DCM and washed with sat. aq. NaHCO₃. The organic layer was dried (Na₂SO₄), filtered, and concentrated *in vacuo*. The resulting residue was purified by ISCO flash chromatography (4 g, 0–100% EtOAc in hexanes) to afford *N*-[(3,4-dichlorophenyl)methyl]-4-(3-pyridyl)aniline as a cream colored solid (40 mg, 0.12 mmol, 61%). LCMS (Method A) t_R = 1.93 min, *m/z* = 329.06 [M+H]⁺.

Step 2: 2-(Benzotriazol-1-yl)-*N*-[(3,4-dichlorophenyl)methyl]-*N*-[4-(3-pyridyl)phenyl]acetamide.: Pyridine (29 μL, 0.36 mmol) and T3P (50% in DMF) (160 μL, 0.24 mmol) were added to a solution of *N*-[(3,4-dichlorophenyl)methyl]-4-(3-pyridyl)aniline (39 mg, 0.12 mmol) and **50** (23 mg, 0.13 mmol, 1.1 eq.) in DMF (0.6 mL, 0.2 M) and stirred at rt for 18 h. The reaction mixture was purified directly by preparative RP-HPLC (5–50% MeCN in H₂O, 0.1% TFA). The product containing fractions were combined and concentrated *in vacuo*. The free base was obtained by SCX-II chromatography (load/wash MeOH, elution with 2N NH₃ in MeOH) to afford the title compound as a colorless solid (36 mg, 0.07 mmol, 62%). ¹H NMR (400 MHz, CD₃OD) δ 9.02 (d, *J* = 2.3 Hz, 1H), 8.74 (dd, *J* = 5.5, 1.5 Hz, 1H), 8.57 (dd, *J* = 6.1, 4.1 Hz, 1H), 7.98 (d, *J* = 8.4 Hz, 1H), 7.92 (dd, *J* = 8.1, 5.4 Hz, 1H), 7.87 – 7.80 (m, 2H), 7.69 (d, *J* = 8.4 Hz, 1H), 7.58 – 7.53 (m, 1H), 7.51 – 7.39 (m, 5H), 7.20 (d, *J* = 8.3 Hz, 1H), 5.50 (s, 2H), 5.00 (s, 2H); ¹³C NMR (101 MHz, DMSO-*d*₆) δ 166.23, 158.89, 158.53, 146.78, 145.79, 145.45, 140.92, 138.57, 137.69, 135.88, 134.17, 131.54, 131.10, 130.45, 130.41, 129.32, 128.98, 128.82, 127.65, 125.47, 124.30, 119.44, 111.58, 51.91, 50.00; Purity 95% by LCMS (Method A) t_R = 1.93 min, *m/z* = 488.10 [M+H]⁺; HRMS calculated for C₂₆H₁₉Cl₂N₅O [M+H]⁺ 488.1039, found 488.1048.

2-(Benzotriazol-1-yl)-*N*-[(3-chloro-5-fluoro-phenyl)methyl]-*N*-[4-(3-pyridyl)phenyl]acetamide (31).

Step 1: *N*-[(3-Chloro-5-fluoro-phenyl)methyl]-4-(3-pyridyl)aniline.: 3-Chloro-5-fluorobenzaldehyde (35 mg, 0.22 mmol) and **51** (34 mg, 0.20 mmol) were dissolved in DCM:AcOH (0.2 M, 20:1) and stirred for 30 min at 23 °C. To the mixture, NaBH(OAc)₃ (64 mg, 0.30 mmol) was added and stirred at rt for 18 h. The reaction mixture was diluted with DCM and washed with sat. aq. NaHCO₃. The organic layers were dried (Na₂SO₄), filtered, and concentrated *in vacuo*. The resulting residue was purified by ISCO automated flash chromatography (4 g, 0–100% EtOAc in hexanes) to afford a colorless solid (56 mg, 0.18 mmol, 90%). LCMS (Method A) t_R = 1.87 min, *m/z* = 313.09 [M+H]⁺.

Step 2: 2-(Benzotriazol-1-yl)-*N*-[(3-chloro-5-fluoro-phenyl)methyl]-*N*-[4-(3-pyridyl)phenyl]acetamide.: Pyridine (40 μL, 0.50 mmol) and T3P (50% in DMF) (224 μL, 0.33 mmol) were added to a solution of *N*-[(3-chloro-5-fluoro-phenyl)methyl]-4-(3-pyridyl)aniline (52 mg, 0.17 mmol) and **50** (32 mg, 0.18 mmol) in DMF (0.8 mL) and stirred at rt for 18 h. The reaction mixture was purified directly by preparative RP-HPLC (5–50% MeCN in H₂O, 0.1% TFA). The product containing fractions were combined and concentrated *in vacuo*. The free base was obtained by SCX-II chromatography (load/wash MeOH, elution with 2N NH₃ in MeOH) to afford title compound as a colorless solid (26

mg, 0.06 mmol, 33%). ¹H NMR (400 MHz, CD₃OD) δ 8.81 (s, 1H), 8.56 (d, *J* = 4.8 Hz, 1H), 8.11 (dt, *J* = 7.9, 2.0 Hz, 1H), 7.98 (d, *J* = 8.4 Hz, 1H), 7.76 (d, *J* = 8.4 Hz, 2H), 7.68 (d, *J* = 8.4 Hz, 1H), 7.54 (dd, *J* = 8.3, 5.9 Hz, 2H), 7.49 – 7.38 (m, 3H), 7.17 – 7.09 (m, 2H), 7.02 (d, *J* = 9.3 Hz, 1H), 5.51 (s, 2H), 5.00 (s, 2H); ¹³C NMR (101 MHz, DMSO-*d*₆) δ 166.38, 163.87, 161.41, 149.15, 148.04, 145.45, 142.12, 142.04, 140.55, 137.47, 134.91, 134.47, 134.36, 134.17, 129.17, 128.80, 127.62, 124.44, 124.28, 119.43, 115.53, 115.28, 114.22, 114.00, 111.59, 52.19, 50.01; ¹⁹F NMR (376 MHz, CD₃OD) δ –110.58; Purity 95% by LCMS (Method A) *t*_R = 1.87 min, *m/z* = 472.13 [M+H]⁺; HRMS calculated for C₂₆H₁₉ClFN₅O [M+H]⁺ 472.1335, found 472.1343.

2-(Benzotriazol-1-yl)-N-[(3,5-dichlorophenyl)methyl]-N-[4-(3-pyridyl)phenyl]acetamide (32).

Step 1: N-[(3,5-Dichlorophenyl)methyl]-4-(3-pyridyl)aniline.: Compound **51** (34 mg, 0.20 mmol) and 3,5-dichlorobenzaldehyde (39 mg, 0.22 mmol) were dissolved in DCM:AcOH (0.2 M, 20:1) and stirred for 30 min at 23 °C. To the mixture, NaHB(OAc)₃ (64 mg, 0.30 mmol) was added and stirred at rt for 18 h. The reaction mixture was diluted with DCM and washed with sat. aq. NaHCO₃. The organic layers were dried (Na₂SO₄), filtered, and concentrated *in vacuo*. The resulting residue was purified by ISCO automated flash chromatography (4 g, 0–100% EtOAc in hexanes) to afford a colorless solid (65 mg, 0.20 mmol, 99%). LCMS (Method A) *t*_R = 1.95 min, *m/z* = 329.06 [M+H]⁺.

Step 2: 2-(Benzotriazol-1-yl)-N-[(3,5-dichlorophenyl)methyl]-N-[4-(3-pyridyl)phenyl]acetamide.: Pyridine (46 μL, 0.57 mmol) and T3P (50% in DMF) (258 μL, 0.38 mmol) were added to a solution of N-[(3,5-dichlorophenyl)methyl]-4-(3-pyridyl)aniline (63 mg, 0.19 mmol) and **50** (37 mg, 0.21 mmol) in DMF (1 mL) and stirred at rt for 1 h. The reaction mixture was purified directly by preparative RP-HPLC (5–50% MeCN in H₂O, 0.1% TFA). The product containing fractions were combined and concentrated *in vacuo*. The free base was obtained by SCX-II chromatography (load/wash MeOH, elution with 2N NH₃ in MeOH) to afford the title compound as a beige powder (76 mg, 0.16 mmol, 81%). ¹H NMR (400 MHz, DMSO-*d*₆) δ 8.93 (d, *J* = 2.4 Hz, 1H), 8.59 (dd, *J* = 4.6, 1.7 Hz, 1H), 8.11 (d, *J* = 7.7 Hz, 1H), 8.03 (d, *J* = 8.4 Hz, 1H), 7.87 (d, *J* = 8.0 Hz, 2H), 7.80 (d, *J* = 8.4 Hz, 1H), 7.67 (d, *J* = 8.0 Hz, 2H), 7.58 – 7.46 (m, 3H), 7.43 – 7.35 (m, 3H), 5.56 (s, 2H), 4.98 (s, 2H); ¹³C NMR (101 MHz, DMSO-*d*₆) δ 166.42, 149.34, 148.21, 145.45, 141.80, 140.49, 134.81, 134.70, 134.57, 134.15, 129.14, 128.79, 127.62, 127.53, 127.05, 124.37, 124.29, 119.44, 111.57, 52.09, 50.03; Purity 95% by LCMS (Method A) *t*_R = 1.95 min, *m/z* = 488.10 [M+H]⁺; HRMS calculated for C₂₆H₁₉Cl₂N₅O [M+H]⁺ 488.1039, found 488.1049.

2-(Benzotriazol-1-yl)-N-[(3-chloro-5-methyl-phenyl)methyl]-N-[4-(3-pyridyl)phenyl]acetamide (33).

Step 1. N-[(3-chloro-5-methyl-phenyl)methyl]-4-(3-pyridyl)aniline.: Compound **51** (34 mg, 0.20 mmol) and 3-chloro-5-methyl-benzaldehyde (28 μL, 0.22 mmol) were taken in DCM (1mL) and acetic acid (0.05 mL) and stirred for 30 min before the addition of NaHB(OAc)₃ (64 mg, 0.30 mmol) and stirred for 18 h at rt. The mixture was diluted with DCM and washed with sat. aq. NaHCO₃. The organic layers were separated and concentrated to dryness. Purification by ISCO automated flash chromatography (4 g, 0–

100% EtOAc in hexanes) afforded a straw-colored oil (54 mg, 0.17 mmol, 87%). LCMS (Method A) $t_R = 1.94$ min, $m/z = 309.12$ [M+H]⁺.

Step 2. 2-(Benzotriazol-1-yl)-N-[(3-chloro-5-methyl-phenyl)methyl]-N-[4-(3-pyridyl)phenyl]acetamide.:

To a solution of *N*-[(3-chloro-5-methyl-phenyl)methyl]-4-(3-pyridyl)aniline (54 mg, 0.17 mmol) and **50** (31 mg, 0.17 mmol) in DMF (1 mL) was added T3P (50% in EtOAc, 0.21 mL, 0.35 mmol) and pyridine (43 μ L, 0.53 mmol). The mixture was stirred at rt for 16 h, then filtered and purified by preparative RP-HPLC. The free base was obtained by SCX-II chromatography (eluant 2N NH₃/MeOH) affording a colorless solid (39 mg, 0.08 mmol, 48%). ¹H NMR (400 MHz, DMSO-*d*₆) δ 8.93 (s, 1H), 8.60 (d, $J = 4.9$ Hz, 1H), 8.12 (d, $J = 8.0$ Hz, 1H), 8.04 (d, $J = 8.4$ Hz, 1H), 7.86 (d, $J = 8.1$ Hz, 2H), 7.81 (d, $J = 8.4$ Hz, 1H), 7.64 (d, $J = 8.1$ Hz, 2H), 7.55 (t, $J = 7.6$ Hz, 1H), 7.50 (dd, $J = 8.0, 4.8$ Hz, 1H), 7.40 (t, $J = 7.6$ Hz, 1H), 7.16 (d, $J = 8.4$ Hz, 2H), 7.06 (s, 1H), 5.55 (s, 2H), 4.94 (s, 2H), 2.29 (s, 3H); ¹³C NMR (101 MHz, DMSO) δ 166.18, 151.21, 149.32, 148.20, 145.45, 140.64, 139.64, 137.47, 134.84, 134.69, 134.16, 133.33, 129.19, 128.73, 128.23, 127.63, 125.14, 124.37, 124.29, 119.44, 111.55, 52.47, 50.00, 21.12; Purity 95% by LCMS (Method A) $t_R = 1.91$ min, $m/z = 468.16$ [M+H]⁺; HRMS calculated for C₂₇H₂₂ClN₅O [M+H]⁺ 468.1586, found 468.1592.

2-(Benzotriazol-1-yl)-N-[(5-chloro-3-pyridyl)methyl]-N-[4-(3-pyridyl)phenyl]acetamide (34).

Step 1. N-[(5-Chloro-3-pyridyl)methyl]-4-(3-pyridyl)aniline.: Compounds **51** (34 mg, 0.20 mmol) and 5-chloropyridine-3-benzaldehyde (31 mg, 0.22 mmol) were taken in DCM (1 mL) and acetic acid (0.05 mL) and stirred for 30 min before the addition of NaHB(OAc)₃ (64 mg, 0.30 mmol) and stirred for 18 h at rt. The mixture was diluted with DCM and washed with sat. aq. NaHCO₃. The organic layers were separated and concentrated to dryness. Purification by ISCO flash chromatography (4 g, 0–100% EtOAc in hexanes) afforded a cream colored solid (53 mg, 0.18 mmol, 90%). LCMS (Method A) $t_R = 1.45$ min, $m/z = 296.10$ [M+H]⁺.

Step 2. 2-(Benzotriazol-1-yl)-N-[(5-chloro-3-pyridyl)methyl]-N-[4-(3-pyridyl)phenyl]acetamide.:

To a solution of *N*-[(5-chloro-3-pyridyl)methyl]-4-(3-pyridyl)aniline (53 mg, 0.18 mmol) and **50** (32 mg, 0.17 mmol) in DMF (1 mL) was added T3P (50% in EtOAc, 0.21 mL, 0.35 mmol) and pyridine (43 μ L, 0.53 mmol). The mixture was stirred at rt for 16 h, then filtered and purified by preparative RP-HPLC. The free base was obtained by SCX-II chromatography (eluant 2N NH₃/MeOH) affording a colorless solid (42 mg, 0.09 mmol, 52%). ¹H NMR (400 MHz, DMSO-*d*₆) δ 8.94 (d, $J = 2.5$ Hz, 1H), 8.60 (dd, $J = 4.8, 1.7$ Hz, 1H), 8.55 (d, $J = 2.5$ Hz, 1H), 8.46 (s, 1H), 8.12 (d, $J = 8.0$ Hz, 1H), 8.03 (d, $J = 8.4$ Hz, 1H), 7.91 – 7.85 (m, 3H), 7.82 (d, $J = 8.4$ Hz, 1H), 7.69 (d, $J = 8.0$ Hz, 2H), 7.59 – 7.48 (m, 2H), 7.40 (t, $J = 7.6$ Hz, 1H), 5.54 (s, 2H), 5.03 (s, 2H); ¹³C NMR (101 MHz, DMSO-*d*₆) δ 166.36, 149.36, 148.21, 147.97, 147.65, 145.44, 140.39, 137.63, 135.86, 134.86, 134.81, 134.72, 134.18, 131.41, 129.30, 128.84, 127.63, 124.37, 124.29, 119.43, 111.61, 50.22, 50.01; Purity 95% by LCMS (Method A) $t_R = 1.59$ min, $m/z = 455.14$ [M+H]⁺; HRMS calculated for C₂₅H₁₉ClN₆O [M+H]⁺ 455.1382, found 455.1393.

2-(1*H*-Benzo[d][1,2,3]triazol-1-yl)-*N*-(3-chlorobenzyl)-*N*-(4-(2-oxo-1,2-dihydropyridin-3-yl)phenyl)acetamide (35).

Step 1. 4-Bromo-*N*-[(3-chlorophenyl)methyl]aniline (58): To a solution of 3-chlorobenzaldehyde (1.13 mL, 10.0 mmol) and 4-bromoaniline (2.06 g, 12.0 mmol) in DCE (50 mL) was added NaHB(OAc)₃ (2.76 g, 13.0 mmol) and the mixture stirred for 2 h at rt. Saturated aq. NH₄Cl (50 mL) was added and the DCE layer separated. The aqueous layer was extracted with EtOAc (3 × 30 mL) and concentrated. Purification by ISCO automated flash chromatography afforded a tan oil (2.0 g, 6.74 mmol, 67%). ¹H NMR (400 MHz, CDCl₃) δ 7.36 (s, 1H), 7.34 – 7.21 (m, 6H), 6.51 (d, *J* = 8.8 Hz, 2H), 4.32 (s, 2H).

Step 2. *N*-[(3-Chlorophenyl)methyl]-4-(2-fluoro-3-pyridyl)aniline: To a vial containing 4-bromo-*N*-[(3-chlorophenyl)methyl]aniline (415 mg, 1.4 mmol), 2-fluoropyridine-3-boronic acid (237 mg, 1.68 mmol), Pd(dppf)Cl·DCM (57 mg, 0.07 mmol) and K₂CO₃ (386.99 mg, 2.8 mmol) was added dioxane (3.5 mL) and water (0.7 mL). The mixture was heated to 100 °C for 20 h. The mixture was diluted with EtOAc and washed with water, brine, then dried over Na₂SO₄ and concentrated. The mixture was purified by ISCO automated flash chromatography to afford title intermediate (157 mg, 0.50 mmol, 36%). ¹H NMR (400 MHz, CDCl₃) δ 8.10 (dt, *J* = 4.9, 1.6 Hz, 1H), 7.81 (ddd, *J* = 9.6, 7.4, 2.0 Hz, 1H), 7.42 (dd, *J* = 8.6, 1.8 Hz, 2H), 7.38 (s, 1H), 7.27 (d, *J* = 2.8 Hz, 3H), 7.22 (ddd, *J* = 6.9, 4.8, 1.8 Hz, 1H), 6.71 (d, *J* = 8.2 Hz, 2H), 4.38 (s, 2H).

Step 3. 3-[4-[(3-Chlorophenyl)methylamino]phenyl]-1*H*-pyridin-2-one (59): To a solution of *N*-[(3-chlorophenyl)methyl]-4-(2-fluoro-3-pyridyl)aniline (94 mg, 0.30 mmol) in dioxane (1 mL) was added conc. aq. HCl (0.2 mL, 2.4 mmol) and the mixture stirred for 16 h at 80 °C. The reaction was allowed to cool to room temperature, neutralized with sat. aq. NaHCO₃, extracted with EtOAc, concentrated, and purified by ISCO automated flash chromatography to afford the title intermediate (87 mg, 0.28 mmol, 93%). LCMS (Method A) *t*_R = 1.90 min, *m/z* = 311.10 [M+H]⁺.

Step 4. 2-(1*H*-Benzo[d][1,2,3]triazol-1-yl)-*N*-(3-chlorobenzyl)-*N*-(4-(2-oxo-1,2-dihydropyridin-3-yl)phenyl)acetamide: To a stirred solution of **59** (49 mg, 0.16 mmol) and **50** (28 mg, 0.16 mmol) in DMF (0.5 mL) was added T3P (50% in EtOAc, 189 μL, 0.32 mmol), followed by pyridine (38 μL, 0.48 mmol). The mixture was stirred at rt for 16 h. Purification by preparative RP-HPLC afforded a colorless solid (36 mg, 0.08 mmol, 49%). ¹H NMR (400 MHz, CD₃OD) δ 7.99 (d, *J* = 8.5 Hz, 1H), 7.80 – 7.72 (m, 3H), 7.69 (d, *J* = 8.4 Hz, 1H), 7.57 (t, 1H), 7.49 – 7.40 (m, 2H), 7.37 (d, *J* = 8.6 Hz, 2H), 7.33 – 7.25 (m, 3H), 7.19 (s, 1H), 6.50 (t, *J* = 6.8 Hz, 1H), 5.47 (s, 2H), 4.98 (s, 2H); ¹³C NMR (101 MHz, CDCl₃) δ 165.63, 163.89, 146.29, 140.65, 139.82, 138.83, 137.84, 134.95, 134.75, 134.04, 130.73, 130.27, 130.03, 129.27, 128.42, 128.34, 128.07, 127.46, 124.29, 120.41, 110.06, 107.66, 53.60, 50.22; Purity 95% by LCMS (Method A) *t*_R = 2.01 min, *m/z* = 470.14 [M+H]⁺; HRMS calculated for C₂₆H₂₀ClN₅O₂ [M+H]⁺ 470.1389, found 470.1389.

***N*-(4-(1*H*-Pyrazol-4-yl)phenyl)-2-(1*H*-benzo[d][1,2,3]triazol-1-yl)-*N*-(3-chlorobenzyl)acetamide (36).**

Step 1. *N*-[(3-chlorophenyl)methyl]-4-(1-tetrahydropyran-2-ylpyrazol-4-yl)aniline (60).

To a vial containing 4-bromo-*N*-[(3-chlorophenyl)methyl]aniline (138 mg, 0.47 mmol), 1-(tetrahydro-2*H*-pyran-2-yl)-4-(4,4,5,5-tetramethyl-1,3,2-dioxaborolan-2-yl)-1*H*-pyrazole (155 mg, 0.56 mmol), Pd(dppf)Cl·DCM (19 mg, 0.02 mmol) and K₂CO₃ (129 mg, 0.93 mmol) was added dioxane (1.2 mL) and water (0.12 mL). The mixture was heated to 100 °C for 16 h. The mixture was diluted with EtOAc and washed with water, brine, then dried over Na₂SO₄ and concentrated to dryness. The resulting crude material was purified by ISCO automated flash chromatography to afford a pale-yellow oil (74 mg, 0.20 mmol, 43%). LCMS (Method B) t_R = 1.36 min, m/z = 311.10 [M+H]⁺.

Step 2. 2-(benzotriazol-1-yl)-*N*-[(3-chlorophenyl)methyl]-*N*-[4-(1-tetrahydropyran-2-ylpyrazol-4-yl)phenyl]acetamide.

To a stirred solution of **60** (74 mg, 0.2 mmol) and **50** (35 mg, 0.20 mmol) in DMF (1 mL) was added T3P (50% in EtOAc, 238 μL, 0.40 mmol), followed by pyridine (48 μL, 0.60 mmol). The mixture was stirred at 60 °C for 20 h, then washed with water (20 mL) and extracted with EtOAc. The combined organic layers were purified by ISCO automated flash chromatography to afford the title intermediate (77 mg, 0.15 mmol, 73%). LCMS (Method A) t_R = 2.30 min, m/z = 527.20 [M+H]⁺.

Step 3. *N*-(4-(1*H*-pyrazol-4-yl)phenyl)-2-(1*H*-benzo[d][1,2,3]triazol-1-yl)-*N*-(3-chlorobenzyl)acetamide.

To a solution of 2-(benzotriazol-1-yl)-*N*-[(3-chlorophenyl)methyl]-*N*-[4-(1-tetrahydropyran-2-ylpyrazol-4-yl)phenyl]acetamide (77 mg, 0.15 mmol) in THF (1.5 mL) was added 1N aq. HCl (1.5 mL, 1.5 mmol) and the mixture stirred for 16 h at rt. The reaction was allowed to cool to rt, neutralized with sat. aq. NaHCO₃, extracted with EtOAc, concentrated, and purified by ISCO automated flash chromatography to afford title compounds as a colorless solid (41 mg, 0.09 mmol, 63%). ¹H NMR (400 MHz, CD₃OD) δ 8.07 – 7.89 (m, 3H), 7.71 – 7.64 (m, 3H), 7.55 (t, *J* = 7.7 Hz, 1H), 7.43 (t, *J* = 7.7 Hz, 1H), 7.33 – 7.23 (m, 5H), 7.20 – 7.14 (m, 1H), 5.45 (s, 2H), 4.95 (s, 2H); ¹³C NMR (101 MHz, CDCl₃) δ 165.60, 146.27, 138.71, 138.51, 134.76, 134.01, 133.95, 131.76, 130.26, 129.42, 129.09, 128.48, 128.09, 127.78, 127.59, 124.34, 121.70, 120.41, 110.06, 53.57, 50.18; Purity 95% by LCMS (Method A) t_R = 2.04 min, m/z = 443.14 [M+H]⁺; HRMS calculated for C₂₄H₁₉ClN₆O [M+H]⁺ 443.1393, found 443.1385.

***2*-(Benzotriazol-1-yl)-*N*-[(3-chlorophenyl)methyl]-*N*-[3-methoxy-4-(1*H*-pyrazol-4-yl)phenyl]acetamide (37).**

Step 1. 4-Bromo-*N*-[(3-chlorophenyl)methyl]-3-methoxy-aniline (54). A mixture of 3-chlorobenzaldehyde (216 μL, 1.91 mmol) and 4-bromo-3-methoxyaniline (350 mg, 1.73 mmol) in DCM (8.25 mL) and AcOH (0.41 mL) was stirred for 30 min at rt before the addition of NaBH(OAc)₃ (551 mg, 2.60 mmol). The mixture was stirred for an additional 18 h at rt. Saturated aq. NH₄Cl (50 mL) was added and the crude residue extracted with DCM, concentrated and purified by ISCO automated flash chromatography to afford a straw-colored oil (470 mg, 1.44 mmol, 83%). LCMS (Method B) t_R = 1.85 min, m/z = 325.99 [M+H]⁺; ¹H NMR (400 MHz, CDCl₃) δ 7.37 (s, 1H), 7.33–7.18 (m, 4H), 6.21 (d, *J* = 2.5 Hz, 1H), 6.15 (dd, *J* = 8.4, 2.3 Hz, 1H), 4.32 (s, 2H), 3.81 (s, 3H).

Step 2. 2-Benzotriazol-1-yl)-N-(4-bromo-3-methoxy-phenyl)-N-[(3-

chlorophenyl)methyl]acetamide (56).: To a stirred solution of **54** (465 mg, 1.42 mmol) and **50** (265 mg, 1.50 mmol) in THF (7 mL) was added T3P (50% in EtOAc, 1.70 mL, 2.85 mmol), followed by pyridine (344 μ L, 4.27 mmol). The mixture was stirred at 60 °C for 20 h, then diluted with water (20 mL) and extracted with EtOAc. The combined organic layers were washed with brine, concentrated and purified by flash chromatography to afford a colorless solid (651 mg, 1.34 mmol, 94%). LCMS (Method B) t_R = 1.81 min, m/z = 485.03 [M+H]⁺; ¹H NMR (400 MHz, CDCl₃) δ 8.06 (d, J = 8.4 Hz, 1H), 7.59 (d, J = 8.2 Hz, 1H), 7.54–7.47 (m, 2H), 7.43–7.35 (m, 1H), 7.32–7.19 (m, 2H), 7.13–7.06 (m, 1H), 6.64 (dd, J = 8.2, 2.3 Hz, 1H), 6.47 (d, J = 2.3 Hz, 1H), 5.24 (s, 2H), 4.85 (s, 2H), 3.79 (s, 3H).

Step 3. 2-(Benzotriazol-1-yl)-N-[(3-chlorophenyl)methyl]-N-[3-methoxy-4-(1H-

pyrazol-4-yl)phenyl]acetamide.: A vial was charged with 2-(benzotriazol-1-yl)-N-(4-bromo-3-methoxy-phenyl)-N-[(3-chlorophenyl)methyl]acetamide (100 mg, 0.21 mmol), 4-(4,4,5,5-tetramethyl-1,3,2-dioxaborolan-2-yl)-1H-pyrazole (48 mg, 0.25 mmol) and Pd(dppf)Cl₂-DCM (8.3 mg, 0.01 mmol). Dioxane (1.0 mL) and 2M aq. K₂CO₃ (0.2 mL) were then added and the resulting solution purged with argon for 15 min. The mixture was then heated to 110 °C and stirred vigorously. After 18 h, the resulting mixture was cooled to rt, filtered through celite, concentrated, and purified by preparative RP-HPLC (5–95% MeCN in H₂O, 0.1% TFA) to afford a colorless solid (2.6 mg, 5.5 μ mol, 3%). ¹H NMR (400 MHz, CD₃OD) δ 7.98 (s, 2H), 7.87 (d, J = 8.4 Hz, 1H), 7.55 (t, J = 8.5 Hz, 2H), 7.43 (t, J = 7.7 Hz, 1H), 7.35 – 7.27 (m, 1H), 7.23 – 7.16 (m, 3H), 7.11 – 7.04 (m, 1H), 6.82 – 6.74 (m, 2H), 5.39 (s, 2H), 4.85 (s, 2H), 3.75 (s, 3H); ¹³C NMR (101 MHz, CD₃OD) δ 166.3, 156.8, 139.0, 138.5, 134.0, 133.81 132.8, 129.7, 128.6, 128.1, 127.52, 127.48, 127.1, 124.2, 120.2, 118.4, 111.1, 110.2, 54.7, 52.5, 49.5; Purity 95% by LCMS (Method A) t_R = 2.10, m/z = 473.15 [M+H]⁺; HRMS calculated for C₂₅H₂₁ClN₆O₂ [M+H]⁺ 473.1487, found 473.1497.

2-(Benzotriazol-1-yl)-N-[(3-chlorophenyl)methyl]-N-[2-methoxy-4-(1H-pyrazol-4-yl)phenyl]acetamide (38).

Step 1. 4-Bromo-N-[(3-chlorophenyl)methyl]-2-methoxy-aniline (55).: To a solution of 3-chlorobenzaldehyde (200 μ L, 1.77 mmol) and 4-bromo-2-methoxyaniline (325 mg, 1.61 mmol) in DCM (7.7 mL) and AcOH (0.4 mL) was stirred for 30 min at rt before the addition of NaBH(OAc)₃ (511 mg, 2.41 mmol). The mixture was stirred for an additional 18 h at rt. Saturated aq. NH₄Cl (50 mL) was added and the crude residue extracted with DCM, concentrated and purified by ISCO automated flash chromatography to afford a straw-colored oil (446 mg, 1.37 mmol, 85%). LCMS (Method B) t_R = 2.05 min, m/z = 325.99 [M+H]⁺; ¹H NMR (400 MHz, CDCl₃) δ 7.35 (s, 1H), 7.31 – 7.19 (m, 3H), 6.92 (dd, J = 8.4, 2.1 Hz, 1H), 6.89 (d, J = 2.1 Hz, 1H), 6.37 (d, J = 8.4 Hz, 1H), 4.76 (br s, 1H), 4.32 (s, 2H), 3.87 (s, 3H).

Step 2. 2-(Benzotriazol-1-yl)-N-(4-bromo-2-methoxy-phenyl)-N-[(3-

chlorophenyl)methyl]acetamide (57).: To a stirred solution of **55** (440 mg, 1.35 mmol) and **50** (251 mg, 1.41 mmol) in THF (7 mL) was added T3P (50% in EtOAc, 1.60 mL, 2.69 mmol), followed by pyridine (326 μ L, 4.04 mmol). The mixture was stirred at 60 °C for 20 h, then diluted with water (20 mL) and extracted with EtOAc. The combined

organic layers were washed with brine, concentrated and purified by ISCO automated flash chromatography to afford a colorless solid (507 mg, 1.04 mmol, 77%). LCMS (Method B) $t_R = 1.83$ min, $m/z = 485.04$ [M+H]⁺; ¹H NMR (400 MHz, CDCl₃) δ 8.05 (d, $J = 8.4$ Hz, 1H), 7.56 – 7.45 (m, 2H), 7.42 – 7.33 (m, 1H), 7.29 – 7.01 (m, 6H), 6.84 (d, $J = 8.3$ Hz, 1H), 5.30 (s, 2H), 5.22 (d, $J = 16.6$ Hz, 1H), 5.11 (d, $J = 16.6$ Hz, 1H), 5.01 (d, $J = 14.3$ Hz, 1H), 4.52 (d, $J = 14.3$ Hz, 1H), 3.78 (s, 3H).

Step 3. 2-(Benzotriazol-1-yl)-N-[(3-chlorophenyl)methyl]-N-[2-methoxy-4-(1H-

pyrazol-4-yl)phenyl]acetamide.: A vial was charged with **57** (100 mg, 0.21 mmol), 4-(4,4,5,5-tetramethyl-1,3,2-dioxaborolan-2-yl)-1H-pyrazole (48 mg, 0.25 mmol) and Pd(dppf)Cl₂·DCM (8.3 mg, 0.01 mmol). Dioxane (1.0 mL) and 2M aq. K₂CO₃ (0.2 mL) were then added and the resulting solution purged with argon for 15 min. The mixture was then heated to 110 °C and stirred vigorously. After 18 h, the resulting mixture was cooled to rt, filtered through celite, concentrated, and purified by preparative RP-HPLC (5–95% MeCN in H₂O, 0.1% TFA) to afford a colorless solid (2.5 mg, 5.3 μ mol, 3%). ¹H NMR (400 MHz, CD₃OD) δ 7.96 (s, 2H), 7.88 (d, $J = 8.4$ Hz, 1H), 7.53 – 7.42 (m, 2H), 7.38 – 7.29 (m, 1H), 7.23 (d, $J = 1.8$ Hz, 1H), 7.20 – 7.10 (m, 4H), 7.06 (d, $J = 8.1$ Hz, 1H), 7.04 – 6.99 (m, 1H), 5.34 (d, $J = 17.0$ Hz, 1H), 5.19 (d, $J = 17.0$ Hz, 1H), 4.86 (d, $J = 14.5$ Hz, 1H), 4.62 (d, $J = 14.5$ Hz, 1H), 3.79 (s, 3H); ¹³C NMR (101 MHz, CD₃OD) δ 167.0, 155.3, 138.9, 138.8, 135.6, 133.7, 129.8, 129.4, 128.7, 127.5, 127.4, 127.2, 125.8, 124.2, 118.5, 118.1, 110.1, 109.4, 55.1, 51.9, 49.3; Purity 95% by LCMS (Method A) $t_R = 2.13$, $m/z = 473.15$ [M+H]⁺; HRMS calculated for C₂₅H₂₁ClN₆O₂ [M+H]⁺ 473.1487, found 473.1476.

2-(Benzotriazol-1-yl)-N-[(3-chlorophenyl)methyl]-N-[6-(1H-pyrazol-4-yl)-3-pyridyl]acetamide (39).

Step 1. 6-(1-Tetrahydropyran-2-yl)pyrazol-4-yl)pyridin-3-amine, (64).: 1-

(Tetrahydro-2H-pyran-2-yl)-4-(4,4,5,5-tetramethyl-1,3,2-dioxaborolan-2-yl)-1H-pyrazole (560 mg, 2.01 mmol), 6-chloropyridin-3-amine (388 mg, 3.02 mmol), potassium carbonate (3.02 mL, 6.04 mmol) and SPhos Pd G2 (72 mg, 0.10 mmol) were combined in 1-butanol (5.3 mL) in a sealed-tube and degassed under a stream of argon for 20 mins followed by heating at 100 °C for 16 h. The reaction mixture was filtered through celite, washed with EtOAc (10 mL), concentrated under reduced pressure and purified by ISCO automated flash chromatography (24 g, 0–8 % MeOH in DCM) to afford a viscous oil (414 mg, 1.69 mmol, 84%). LCMS (Method A) $t_R = 1.30$ min, $m/z = 245.13$ [M+H]⁺; ¹H NMR (400 MHz, CD₃OD) δ 8.15 (s, 1H), 7.95 (d, $J = 2.8$ Hz, 1H), 7.92 (s, 1H), 7.42 (d, $J = 8.5$ Hz, 1H), 7.11 (dd, $J = 8.5, 2.8$ Hz, 1H), 5.41 (dd, $J = 10.0, 2.3$ Hz, 1H), 4.10 – 4.00 (m, 1H), 3.74 (td, $J = 11.2, 3.1$ Hz, 1H), 2.21 – 2.08 (m, 1H), 2.08 – 1.98 (m, 2H), 1.84 – 1.55 (m, 3H).

Step 2. N-[(3-Chlorophenyl)methyl]-6-(1-tetrahydropyran-2-yl)pyrazol-4-yl)pyridin-3-

amine (66).: Compound **64** (114 mg, 0.47 mmol) and 3-chlorobenzaldehyde (0.05 mL, 0.43 mmol) were taken in DCM (4 mL) and stirred for 15 min. NaHB(OAc)₃ (135 mg, 0.64 mmol) was added at rt and stirring continued for 16 h. To the reaction mixture sat. aq. NaHCO₃ (5 ml) was added. The resulting residue was extracted with DCM (2 × 10 mL), dried over sodium sulfate, concentrated to dryness and then purified by ISCO automated flash chromatography (12 g, 0–3 % MeOH in DCM) to afford a viscous oil (96 mg, 0.26

mmol, 61%). LCMS (Method A) $t_R = 1.84$ min, $m/z = 369.14$ $[M+H]^+$; 1H NMR (400 MHz, CD_3OD) δ 8.13 (s, 1H), 7.90 (s, 1H), 7.88 (d, $J = 2.8$ Hz, 1H), 7.42 (d, $J = 9.3$ Hz, 2H), 7.34 – 7.28 (m, 2H), 7.28 – 7.21 (m, 1H), 7.01 (dd, $J = 8.7, 2.8$ Hz, 1H), 5.40 (dd, $J = 10.0, 2.4$ Hz, 1H), 4.38 (s, 2H), 4.04 (d, $J = 11.7$ Hz, 1H), 3.79 – 3.68 (m, 1H), 2.20 – 2.07 (m, 1H), 2.06 – 1.99 (m, 2H), 1.83 – 1.56 (m, 3H).

Step 3. 2-(Benzotriazol-1-yl)-N-[(3-chlorophenyl)methyl]-N-[6-(1H-pyrazol-4-yl)-3-pyridyl]acetamide (39).

To a stirred solution of **50** (1.10 g, 6.24 mmol) in DCM (20 mL) was added pyridine (0.60 mL, 7.48 mmol) and cyanuric fluoride (0.64 mL, 7.48 mmol) sequentially at rt and continued stirring for 1 h. The precipitated solid was filtered and washed with DCM (10 mL). The filtrate was concentrated to afford crude 2-(benzotriazol-1-yl)acetyl fluoride that was immediately dissolved in anhydrous THF (12 mL). To this was added a solution of **66** (230 mg, 0.62 mmol) and Et_3N (0.91 mL, 6.55 mmol) in THF (2 mL). The reaction mixture was stirred at 60 °C for 16 h. Water (20 mL) was added followed by extraction with EtOAc (25 mL x 2). The organic layer was dried over Na_2SO_4 , concentrated under reduced pressure, and passed quickly through a flash column using 0–10 % MeOH in DCM to afford an impure intermediate, 2-(benzotriazol-1-yl)-N-[(3-chlorophenyl)methyl]-N-[6-(1-tetrahydropyran-2-ylpyrazol-4-yl)-3-pyridyl]acetamide (212 mg), which was further treated with 5 mL of 4:1 mixture of MeOH and 4 N HCl in dioxane at rt for 40 min. To the reaction mixture EtOAc (15 mL) was added followed by washing with sat. $NaHCO_3$. The organic layer was dried over Na_2SO_4 , concentrated under reduced pressure and purified by ISCO automated flash chromatography (24 g, 0–6 % MeOH in DCM) to afford desired product as a yellow solid (60 mg, 0.13 mmol, 22 % over 2 steps). 1H NMR (400 MHz, $DMSO-d_6$) δ 13.11 (s, 1H), 8.59 (d, $J = 2.6$ Hz, 1H), 8.36 (s, 1H), 8.08 (s, 1H), 8.03 (d, $J = 8.3$ Hz, 1H), 7.92 – 7.85 (m, 1H), 7.81 (dd, $J = 14.2, 8.3$ Hz, 2H), 7.55 (t, $J = 7.7$ Hz, 1H), 7.40 (t, $J = 7.7$ Hz, 1H), 7.33 (d, $J = 3.3$ Hz, 3H), 7.21 (d, $J = 6.7$ Hz, 1H), 5.54 (s, 2H), 4.94 (s, 2H); ^{13}C NMR (101 MHz, $DMSO-d_6$) δ 165.89, 151.92, 148.94, 144.98, 139.11, 137.55, 136.57, 133.71, 133.58, 133.11, 130.36, 128.03, 127.49, 127.17, 126.95, 123.85, 123.82, 121.42, 120.02, 118.96, 111.11, 51.88, 49.48; Purity 95% by LCMS (Method A) $t_R = 1.89$, $m/z = 443.13$ $[M+H]^+$; HRMS calculated for $C_{23}H_{18}ClN_7O$ $[M+H]^+$ 443.1334, found 443.1344.

2-(Benzotriazol-1-yl)-N-[(3-chlorophenyl)methyl]-N-[5-(1H-pyrazol-4-yl)-2-pyridyl]acetamide (40).

Step 1. 5-(1-Tetrahydropyran-2-ylpyrazol-4-yl)pyridin-2-amine (65). 1-(Tetrahydro-2H-pyran-2-yl)-4-(4,4,5,5-tetramethyl-1,3,2-dioxaborolan-2-yl)-1H-pyrazole (560 mg, 2.01 mmol), 2-amino-5-chloropyridine (388 mg, 3.02 mmol), potassium carbonate (2 M, 3.02 mL, 6.04 mmol) and XPhos Pd G2 (79 mg, 0.10 mmol) were combined in dioxane (5.3 mL) in a sealed-tube and degassed under a stream of argon for 20 mins followed by heating at 100 °C for 16 h. The reaction mixture was filtered through celite, washed with EtOAc (10 mL), concentrated under reduced pressure and purified by ISCO automated flash chromatography (24 g, 0–7% MeOH in DCM) to afford an off-white solid (479 mg, 1.96 mmol, 97%). LCMS (Method A) $t_R = 1.32$ min, $m/z = 245.13$ $[M+H]^+$; 1H NMR (400 MHz, CD_3OD) δ 8.12 (d, $J = 2.4$ Hz, 1H), 8.06 (s, 1H), 7.79 (s, 1H), 7.67 (dd, $J = 8.6, 2.4$ Hz, 1H),

6.62 (d, $J=8.6$ Hz, 1H), 5.40 (dd, $J=10.2, 2.4$ Hz, 1H), 4.09 – 4.00 (m, 1H), 3.73 (td, $J=11.2, 3.0$ Hz, 1H), 2.21 – 2.09 (m, 1H), 2.09 – 1.98 (m, 2H), 1.84 – 1.57 (m, 3H).

Step 2. *N*-[(3-Chlorophenyl)methyl]-5-(1-tetrahydropyran-2-ylpyrazol-4-yl)pyridin-2-amine (67): Intermediate **65** (133 mg, 0.55 mmol) from above and 3-chlorobenzaldehyde (0.06 mL, 0.50 mmol) were taken in DCM (4 mL) and stirred for 15 min. NaHB(OAc)₃ (158 mg, 0.75 mmol) was added at rt and stirring was continued for 16 h. The reaction mixture was quenched with sat. aq. NaHCO₃ solution (5 ml), the aqueous layer was extracted with DCM (2 × 10 mL), dried over Na₂SO₄, concentrated under reduced pressure and purified by ISCO automated flash chromatography (12 g, 0–3% MeOH in DCM) to afford a colorless solid (100 mg, 0.27 mmol, 54 %). LCMS (Method A) $t_R = 1.80$ min, $m/z = 369.14$ [M+H]⁺; ¹H NMR (400 MHz, CD₃OD) δ 8.16 (d, $J=2.3$ Hz, 1H), 8.04 (s, 1H), 7.78 (s, 1H), 7.65 (dd, $J=8.7, 2.3$ Hz, 1H), 7.38 – 7.34 (m, 1H), 7.28 (dd, $J=4.2, 2.0$ Hz, 2H), 7.28 – 7.20 (m, 1H), 6.58 (d, $J=8.7$ Hz, 1H), 5.40 (dd, $J=10.1, 2.4$ Hz, 1H), 4.52 (s, 2H), 4.08–4.01 (m, 1H), 3.77–3.69 (m, 1H), 2.22 – 1.96 (m, 3H), 1.81 – 1.56 (m, 3H).

Step 3. 2-(Benzotriazol-1-yl)-*N*-[(3-chlorophenyl)methyl]-*N*-[5-(1H-pyrazol-4-yl)-2-pyridyl]acetamide: To a stirred solution of **50** (1.44 g, 8.13 mmol) in DCM (20 mL) was added pyridine (0.79 mL, 9.76 mmol) and cyanuric fluoride (0.84 mL, 9.76 mmol) sequentially at room temperature and continued stirring for 1 h. The precipitated solid was filtered and washed with DCM (10 mL). The filtrate was concentrated to get crude 2-(benzotriazol-1-yl)acetyl fluoride that was immediately dissolved in anhydrous THF (12 mL). To this was added a solution of **67** (300 mg, 0.81 mmol) and Et₃N (1.19 mL, 8.54 mmol) in THF (2 mL). The reaction mixture was stirred at 60 °C for 16 h. Water (20 mL) was added followed by extraction with EtOAc (25 mL × 2). The organic layer was dried over Na₂SO₄, concentrated under reduced pressure, and passed quickly through the flash column using 0–10 % MeOH in DCM to afford a impure intermediate 2-(benzotriazol-1-yl)-*N*-[(3-chlorophenyl)methyl]-*N*-[5-(1-tetrahydropyran-2-ylpyrazol-4-yl)-2-pyridyl]acetamide (364 mg) which was further treated with 5 mL of 4:1 mixture of MeOH and 4 N HCl in dioxane at room temperature for 40 min. To the reaction mixture EtOAc (15 mL) was added followed by washing with sat. aq. NaHCO₃, dried over Na₂SO₄, concentrated under reduced pressure, and purified by ISCO automated flash chromatography (24 g, 0–4% MeOH in DCM) to afford desired product as a yellow solid (150 mg, 0.33 mmol, 41 % over 2 steps). ¹H NMR (400 MHz, CD₃OD) δ 8.78 (d, $J=2.4$ Hz, 1H), 8.21 – 8.01 (m, 3H), 7.97 (d, $J=8.4$ Hz, 1H), 7.69 (d, $J=8.4$ Hz, 1H), 7.59 – 7.51 (m, 1H), 7.43 (d, $J=7.6$ Hz, 1H), 7.39 (d, $J=8.2$ Hz, 1H), 7.34 (s, 1H), 7.32 – 7.18 (m, 3H), 5.73 (s, 2H), 5.11 (s, 2H); ¹³C NMR (101 MHz, CD₃OD) δ 168.24, 152.24, 147.13, 146.52, 140.36, 137.02, 135.49, 135.19, 131.14, 129.10, 128.93, 128.73, 127.51, 125.72, 125.62, 122.08, 119.89, 119.06, 111.64, 111.41, 109.89, 52.27, 45.71; Purity 95% by LCMS (Method A) $t_R = 1.98$, $m/z = 443.13$ [M+H]⁺; HRMS calculated for C₂₃H₁₈ClN₇O [M+H]⁺ 443.1334, found 443.1323.

***N*-(4-(1*H*-imidazol-4-yl)phenyl)-2-(1*H*-benzo[*d*][1,2,3]triazol-1-yl)-*N*-(3-chlorobenzyl)acetamide (41).**

Step 1. 2-(benzotriazol-1-yl)-*N*-(4-bromophenyl)-*N*-[(3-chlorophenyl)methyl]acetamide (61): To a stirred solution of intermediate **58** (1.48 g, 5.0 mmol) and acid **50** (886 mg, 5

mmol) in THF (25 mL) was added T3P (50% in EtOAc, 5.95 mL, 10 mmol), followed by pyridine (1.21 mL, 15 mmol). The mixture was stirred at rt for 16 h, then diluted with water (20 mL) and extracted with EtOAc. The combined organic layers were washed with brine, concentrated, and purified by ISCO automated flash chromatography to afford a colorless solid (1.58 g, 3.46 mmol, 69%). LCMS (Method B) $t_R = 2.40$ min, $m/z = 457.03$ [M+H]⁺.

Step 2. 2-(benzotriazol-1-yl)-N-[(3-chlorophenyl)methyl]-N-[4-(4,4,5,5-tetramethyl-1,3,2-dioxaborolan-2-yl)phenyl]acetamide (62).: To a vial containing **61** (228 mg, 0.50 mmol), bis(pinacolato)diboron (152 mg, 0.60 mmol), Pd(dppf)Cl₂·DCM (20 mg, 0.03 mmol) and KOAc (221 mg, 2.25 mmol) was added dioxane (2.5 mL). The mixture was heated to 100 °C for 16 h. The mixture was diluted with EtOAc and washed with water, brine, then dried over Na₂SO₄ and concentrated. The mixture was purified by ISCO automated chromatography to afford a cream colored solid (176 mg, 0.35 mmol, 70%). LCMS (Method A) $t_R = 2.53$ min, $m/z = 503.21$ [M+H]⁺.

Step 3. 2-(benzotriazol-1-yl)-N-[(3-chlorophenyl)methyl]-N-[4-(1-tritylimidazol-4-yl)phenyl]acetamide.: To a vial containing **62** (127 mg, 0.25 mmol), 4-bromo-1-tritylimidazole (90 mg, 0.23 mmol), Pd(PPh₃)₄ (40 mg, 0.15 mmol) and K₂CO₃ (64 mg, 0.46 mmol) was added dioxane (1.9 mL) and water (0.4 mL). The mixture was degassed with argon, heated to 100 °C for 16 h. The mixture was diluted with EtOAc and washed with water, brine, then dried over Na₂SO₄ and concentrated. The mixture was purified by ISCO automated chromatography to afford the desired intermediate (100 mg, 0.15 mmol, 63%). LCMS (Method B) $t_R = 1.53$ min, $m/z = 685.25$ [M+H]⁺.

Step 4. N-(4-(1H-imidazol-4-yl)phenyl)-2-(1H-benzol[d][1,2,3]triazol-1-yl)-N-(3-chlorobenzyl)acetamide.: To 2-(Benzotriazol-1-yl)-N-[(3-chlorophenyl)methyl]-N-[4-(1-tritylimidazol-4-yl)phenyl]acetamide (100 mg, 0.15 mmol) in MeOH (1.5 mL) was added AcOH (170 μL, 3.0 mmol) and the mixture stirred for 2 h at 65 °C. The reaction was allowed to cool to rt, concentrated, and purified by preparative RP-HPLC to afford a colorless solid (30 mg, 0.07 mmol, 45%). ¹H NMR (400 MHz, DMSO-*d*₆) δ 12.42 (br s, 1H), 8.04 (d, *J* = 8.4 Hz, 1H), 7.87 (d, *J* = 8.1 Hz, 2H), 7.82 (d, *J* = 8.4 Hz, 1H), 7.78 (s, 1H), 7.69 (s, 1H), 7.56 (t, *J* = 7.7 Hz, 1H), 7.46 (d, *J* = 8.1 Hz, 2H), 7.40 (t, *J* = 7.7 Hz, 1H), 7.35–7.29 (m, 3H), 7.21 (d, *J* = 6.8 Hz, 1H), 5.49 (s, 2H), 4.92 (s, 2H); ¹³C NMR (101 MHz, DMSO-*d*₆) δ 165.7, 145.0, 139.5, 137.8, 137.6, 136.3, 134.3, 133.8, 133.0, 130.3, 128.4, 127.9, 127.3, 127.2, 126.8, 125.5, 123.8, 119.0, 115.2, 111.1, 52.0, 49.3; Purity 95% by LCMS (Method A) $t_R = 1.80$ min, $m/z = 443.14$ [M+H]⁺; HRMS calculated for C₂₄H₁₉ClN₆O [M+H]⁺ 443.1393, found 443.1375.

N-[(3-Chlorophenyl)methyl]-N-[4-(1H-pyrazol-4-yl)phenyl]-2-(3-pyridyl)acetamide (42).—To a solution of N-[(3-Chlorophenyl)methyl]-4-(1-tetrahydropyran-2-yl)pyrazol-4-ylaniline, **60** (37 mg, 0.1 mmol) in THF (1 mL), was added 3-pyridylacetic acid (14 mg, 0.1 mmol), T3P (50% in EtOAc, 0.18 mL, 0.30 mmol) and DIPEA (52 μL, 0.30 mmol) and the mixture stirred at 65 °C for 16 h. The mixture was concentrated, then re-dissolved in HCl (4.0 M in dioxane, 1 mL) and stirred at 60 °C for 1 h. The mixture was concentrated

and purified by RP-HPLC (20–100% MeCN in H₂O, 0.1% TFA) and free-base obtained by washing product with sat. aq. K₂CO₃, affording the title compound as a colorless solid (18 mg, 0.04 mmol, 47%). ¹H NMR (400 MHz, DMSO-*d*₆) δ 8.74 (d, *J* = 5.4 Hz, 1H), 8.67 (s, 1H), 8.27 (d, *J* = 8.0 Hz, 1H), 8.10 (br s, 2H), 7.88 (dd, *J* = 8.0, 5.5 Hz, 1H), 7.68 (d, *J* = 8.0 Hz, 2H), 7.38 – 7.25 (m, 5H), 7.20 (d, *J* = 6.6 Hz, 1H), 4.91 (s, 2H), 3.77 (s, 2H); ¹³C NMR (101 MHz, DMSO-*d*₆) δ 169.49, 158.88, 158.52, 145.80, 144.83, 142.20, 140.38, 139.28, 135.59, 133.46, 133.36, 130.69, 129.20, 128.33, 127.70, 127.26, 126.60, 126.06, 120.68, 117.84, 114.92, 52.26, 37.61; Purity 95% by LCMS (Method A) t_R = 1.71, *m/z* = 403.13 [M+H]⁺; HRMS calculated for C₂₃H₁₉ClN₄O [M+H]⁺ 403.1320, found 403.1340.

***N*-[(3-Chlorophenyl)methyl]-*N*-[4-(1*H*-pyrazol-4-yl)phenyl]-2-pyrimidin-5-yl-acetamide (43).**—To a solution of *N*-[(3-chlorophenyl)methyl]-4-(1-tetrahydropyran-2-ylpyrazol-4-yl)aniline, **60** (37 mg, 0.1 mmol) in THF (1 mL), was added 2-pyrimidin-5-ylacetic acid (14 mg, 0.1 mmol), T3P (50% in EtOAc, 0.18 mL, 0.30 mmol) and DIPEA (52 μL, 0.30 mmol) and the mixture stirred at 65 °C for 16 h. The mixture was concentrated, then re-dissolved in HCl (4.0 M in dioxane, 1 mL) and stirred at 60 °C for 1 h. The mixture was concentrated and purified by RP-HPLC (20–100% MeCN in H₂O, 0.1% TFA) and free-base obtained by washing product with sat. aq. K₂CO₃, affording the title compound as a colorless solid (9 mg, 0.02 mmol, 23%). ¹H NMR (400 MHz, CD₃OD) δ 9.04 (s, 1H), 8.61 (s, 2H), 8.03 (s, 2H), 7.68 (d, *J* = 8.2 Hz, 2H), 7.32 – 7.26 (m, 3H), 7.18 (d, *J* = 8.2 Hz, 3H), 4.95 (s, 2H), 3.66 (s, 2H); ¹³C NMR (101 MHz, CD₃OD) δ 170.15, 157.57, 156.10, 139.32, 139.07, 133.96, 133.48, 130.23, 129.68, 128.75, 128.40, 127.37, 126.84, 126.48, 121.06, 52.38, 35.30; Purity 95% by LCMS (Method A) t_R = 1.84, *m/z* = 404.13 [M+H]⁺; HRMS calculated for C₂₂H₁₈ClN₅O [M+H]⁺ 404.1273, found 404.1289.

Supplementary Material

Refer to Web version on PubMed Central for supplementary material.

Acknowledgements

The authors thank J. Scott Daniels, PhD and Matthew J. Vergne, PhD at Lipscomb University College of Pharmacy for their assistance and analytic support for the metabolite ID studies. This research used resources of the Advanced Photon Source, a U.S. Department of Energy (DOE) Office of Science User Facility operated for the DOE Office of Science by Argonne National Laboratory under Contract No. DE-AC02-06CH11357. Use of the LS-CAT Sector 21 was supported by the Michigan Economic Development Corporation and the Michigan Technology Tri-Corridor (Grant 085P1000817).

Funding

We thank Lerner Research Institute for lab start-up support and Cleveland Clinic Philanthropy and an anonymous donor for a generous donation to support COVID related capital purchases for this research to S.R.S. This work was partly supported by: grant no. CA200422, CA251275, AI140718, AI140705, AI140705S1, AI152190, DE023926, DE027888, DE028521, KGM9942011, and the Betsy B. deWindt endowment to J.U.J.

Abbreviations Used

3CL^{pro}	3C-like protease
CoV	coronavirus

CPE	cytopathic effect
MERS	Middle East respiratory syndrome
MLPCN	Molecular Libraries Probe Production Centers Network
SARS	severe acute respiratory syndrome
SC1	SARS-CoV-1
SC2	SARS-CoV-2

References

- (1). Myint SH Human Coronavirus Infections. In *The Coronaviridae*; Siddell SG, Ed.; Springer US: Boston, MA, 1995; pp 389–401.
- (2). McIntosh K; Dees JH; Becker WB; Kapikian AZ; Chanock RM Recovery in Tracheal Organ Cultures of Novel Viruses from Patients with Respiratory Disease. *Proc. Natl. Acad. Sci. U. S. A* 1967, 57 (4), 933–940. [PubMed: 5231356]
- (3). Ksiazek TG; Erdman D; Goldsmith CS; Zaki SR; Peret T; Emery S; Tong S; Urbani C; Comer JA; Lim W; Rollin PE; Dowell SF; Ling A; Humphrey CD; Shieh W-J; Guarner J; Paddock CD; Rota P; Fields B; DeRisi J; Yang J; Cox N; Hughes JM; LeDuc JW; Bellini WJ; Anderson LJ A Novel Coronavirus Associated with Severe Acute Respiratory Syndrome. *N. Engl. J. Med* 2003, 348 (20), 1953–1966. [PubMed: 12690092]
- (4). Drosten C; Günther S; Preiser W; van der Werf S; Brodt H-R; Becker S; Rabenau H; Panning M; Kolesnikova L; Fouchier RAM; Berger A; Burguière A-M; Cinatl J; Eickmann M; Escriou N; Grywna K; Kramme S; Manuguerra J-C; Müller S; Rickerts V; Stürmer M; Vieth S; Klenk H-D; Osterhaus ADME; Schmitz H; Doerr HW Identification of a Novel Coronavirus in Patients with Severe Acute Respiratory Syndrome. *N. Engl. J. Med* 2003, 348 (20), 1967–1976. [PubMed: 12690091]
- (5). WHO Emergencies preparedness, response - Update 49 - SARS case fatality ratio, incubation period.
- (6). Pyrc K; Berkhout B; van der Hoek L. The Novel Human Coronaviruses NL63 and HKU1. *J. Virol* 2007, 81 (7), 3051–3057. [PubMed: 17079323]
- (7). Fielding BC Human Coronavirus NL63: A Clinically Important Virus? *Future Microbiol.* 2011, 6 (2), 153–159. [PubMed: 21366416]
- (8). Middle East respiratory syndrome coronavirus (MERS-CoV) - United Arab Emirates <https://www.who.int/emergencies/emergency-events/item/2021-DON314>.
- (9). Liu G; Lee J-H; Parker ZM; Acharya D; Chiang JJ; van Gent M; Riedl W; Davis-Gardner ME; Wies E; Chiang C; Gack MU ISG15-Dependent Activation of the Sensor MDA5 Is Antagonized by the SARS-CoV-2 Papain-like Protease to Evade Host Innate Immunity. *Nat. Microbiol* 2021, 6, 467–478. [PubMed: 33727702]
- (10). WHO Coronavirus (COVID-19) Data Surveillance Dashboard <https://covid19.who.int/> (accessed Mar 29, 2021).
- (11). Wu F; Zhao S; Yu B; Chen YM; Wang W; Song ZG; Hu Y; Tao ZW; Tian JH; Pei YY; Yuan ML; Zhang YL; Dai FH; Liu Y; Wang QM; Zheng JJ; Xu L; Holmes EC; Zhang YZ A New Coronavirus Associated with Human Respiratory Disease in China. *Nature* 2020, 579 (7798), 265–269. [PubMed: 32015508]
- (12). Morse JS; Lalonde T; Xu S; Liu WR Learning from the Past: Possible Urgent Prevention and Treatment Options for Severe Acute Respiratory Infections Caused by 2019-NCoV. *ChemBioChem* 2020, 21 (5), 730–738. [PubMed: 32022370]
- (13). Dömling A; Gao L. Chemistry and Biology of SARS-CoV-2. *Chem* 2020, 6 (6), 1283–1295. [PubMed: 32529116]

- (14). Ghosh AK; Brindisi M; Shahabi D; Chapman ME; Mesecar AD Drug Development and Medicinal Chemistry Efforts toward SARS-Coronavirus and Covid-19 Therapeutics. *ChemMedChem* 2020, 15 (11), 907–932. [PubMed: 32324951]
- (15). Cannalire R; Cerchia C; Beccari AR; Di Leva FS; Summa V. Targeting SARS-CoV-2 Proteases and Polymerase for COVID-19 Treatment: State of the Art and Future Opportunities. *J. Med. Chem* 2020, doi.10.1021/acs.jmedchem.0c01140.
- (16). Gil C; Ginex T; Maestro I; Nozal V; Barrado-Gil L; Cuesta-Geijo MÁ; Urquiza J; Ramírez D; Alonso C; Campillo NE; Martínez A. COVID-19: Drug Targets and Potential Treatments. *J. Med. Chem* 2020, 63 (21), 12359–12386. [PubMed: 32511912]
- (17). Fan K; Wei P; Feng Q; Chen S; Huang C; Ma L; Lai B; Pei J; Liu Y; Chen J; Lai L. Biosynthesis, Purification, and Substrate Specificity of Severe Acute Respiratory Syndrome Coronavirus 3C-like Proteinase. *J. Biol. Chem* 2004, 279 (3), 1637–1642. [PubMed: 14561748]
- (18). Thiel V; Ivanov KA; Putics Á; Hertzog T; Schelle B; Bayer S; Weißbrich B; Snijder EJ; Rabenau H; Doerr HW; Gorbalenya AE; Ziebuhr J. Mechanisms and Enzymes Involved in SARS Coronavirus Genome Expression. *J. Gen. Virol* 2003, 84 (9), 2305–2315. [PubMed: 12917450]
- (19). Shi J; Wei Z; Song J. Dissection Study on the Severe Acute Respiratory Syndrome 3C-like Protease Reveals the Critical Role of the Extra Domain in Dimerization of the Enzyme. *J. Biol. Chem* 2004, 279, 24765–24773. [PubMed: 15037623]
- (20). Jacobs J; Grum-Tokars V; Zhou Y; Turlington M; Saldanha SA; Chase P; Egger A; Dawson ES; Baez-Santos YM; Tomar S; Mielech AM; Baker SC; Lindsley CW; Hodder P; Mesecar A; Stauffer SR Discovery, Synthesis, and Structure-Based Optimization of a Series of *N*-(*Tert*-Butyl)-2-(*N*-Arylamido)-2-(Pyridin-3-Yl) Acetamides (ML188) as Potent Noncovalent Small Molecule Inhibitors of the Severe Acute Respiratory Syndrome Coronavirus (SARS-CoV) 3CL. *J. Med. Chem* 2013, 56 (2), 534–546. [PubMed: 23231439]
- (21). Turlington M; Chun A; Tomar S; Egger A; Grum-Tokars V; Jacobs J; Daniels JS; Dawson E; Saldanha A; Chase P; Baez-Santos YM; Lindsley CW; Hodder P; Mesecar AD; Stauffer SR Discovery of *N*-(Benzo[1,2,3]Triazol-1-yl)-*N*-(Benzyl)AcetamidoPhenyl Carboxamides as Severe Acute Respiratory Syndrome Coronavirus (SARS-CoV) 3CLpro Inhibitors: Identification of ML300 and Noncovalent Nanomolar Inhibitors with an Induced-Fit Binding. *Bioorganic Med. Chem. Lett* 2013, 23 (22), 6172–6177.
- (22). Zhang C; Stone EA; Deshmukh M; Ippolito JA; Ghahremanpour MM; Tirado-rives J; Spasov KA; Zhang S; Takeo Y; Kudalkar SN; Liang Z; Isaacs F; Lindenbach B; Miller SJ; Anderson KS; Jorgensen WL Potent Noncovalent Inhibitors of the Main Protease of SARS-CoV-2 from Molecular Sculpting of the Drug Perampanel Guided by Free Energy Perturbation Calculations. *ACS Cent. Sci* 2021, 7 (3), 467–475. [PubMed: 33786375]
- (23). Kim Y; Lovell S; Tiew K-C; Mandadapu SR; Alliston KR; Battaile KP; Groutas WC; Chang K-O Broad-Spectrum Antivirals against 3C or 3C-Like Proteases of Picornaviruses, Noroviruses, and Coronaviruses. *J. Virol* 2012, 86 (21), 11754–11762. [PubMed: 22915796]
- (24). Hoffman RL; Kania RS; Brothers MA; Davies JF; Ferre RA; Gajiwala KS; He M; Hogan RJ; Kozminski K; Li LY; Lockner JW; Lou J; Marra MT; Mitchell LJ; Murray BW; Nieman JA; Noell S; Planken SP; Rowe T; Ryan K; Smith GJ; Solowiej JE; Steppan CM; Taggart B. Discovery of Ketone-Based Covalent Inhibitors of Coronavirus 3CL Proteases for the Potential Therapeutic Treatment of COVID-19. *J. Med. Chem* 2020, 63 (21), 12725–12747. [PubMed: 33054210]
- (25). Boras B; Jones RM; Anson BJ; Arenson D; Aschenbrenner L; Bakowski MA; Beutler N; Binder J; Chen E; Eng H; Hammond J; Hoffman R; Kadar EP; Kania R; Kimoto E; Kirkpatrick MG; Lanyon L; Lendy EK; Lillis JR; Luthra SA; Ma C; Noell S; Obach RS; O'Brien MN; O'Connor R; Ogilvie K; Owen D; Pettersson M; Reese MR; Rogers T; Rossulek MI; Sathish JG; Steppan C; Ticehurst M; Updyke LW; Zhu Y; Wang J; Chatterjee AK; Mesecar AD; Anderson AS; Allerton C. Discovery of a Novel Inhibitor of Coronavirus 3CL Protease as a Clinical Candidate for the Potential Treatment of COVID-19. *bioRxiv* 2020. doi.10.1101/2020.09.12.293498.
- (26). Zhang L; Lin D; Sun X; Curth U; Drosten C; Sauerhering L; Becker S; Rox K; Hilgenfeld R. Crystal Structure of SARS-CoV-2 Main Protease Provides a Basis for Design of Improved α -Ketoamide Inhibitors. *Science*, 2020, 368 (6489), 409–412. [PubMed: 32198291]

- (27). Anand K. Coronavirus Main Proteinase (3CLpro) Structure: Basis for Design of Anti-SARS Drugs. *Science*, 2003, 300 (5626), 1763–1767. [PubMed: 12746549]
- (28). Yang H; Yang M; Ding Y; Liu Y; Lou Z; Zhou Z; Sun L; Mo L; Ye S; Pang H; Gao GF; Anand K; Bartlam M; Hilgenfeld R; Rao Z. The Crystal Structures of Severe Acute Respiratory Syndrome Virus Main Protease and Its Complex with an Inhibitor. *Proc. Natl. Acad. Sci* 2003, 100 (23), 13190–13195. [PubMed: 14585926]
- (29). Douangamath A; Fearon D; Gehrtz P; Krojer T; Lukacik P; Owen CD; Resnick E; Strain-Damerell C; Aimon A; Ábrányi-Balogh P; Brandão-Neto J; Carbery A; Davison G; Dias A; Downes TD; Dunnelt L; Fairhead M; Firth JD; Jones SP; Keeley A; Keserü GM; Klein HF; Martin MP; Noble MEM; O'Brien P; Powell A; Reddi RN; Skyner R; Snee M; Waring MJ; Wild C; London N; von Delft F; Walsh MA Crystallographic and Electrophilic Fragment Screening of the SARS-CoV-2 Main Protease. *Nat. Commun* 2020, 11 (5047), doi.10.1038/s41467-020-18709-w.
- (30). Jin Z; Du X; Xu Y; Deng Y; Liu M; Zhao Y; Zhang B; Li X; Zhang L; Peng C; Duan Y; Yu J; Wang L; Yang K; Liu F; Jiang R; Yang X; You T; Liu X; Yang X; Bai F; Liu H; Liu X; Guddat LW; Xu W; Xiao G; Qin C; Shi Z; Jiang H; Rao Z; Yang H. Structure of Mpro from SARS-CoV-2 and Discovery of Its Inhibitors. *Nature* 2020, 582 (7811), 289–293. [PubMed: 32272481]
- (31). Dai W; Zhang B; Jiang XM; Su H; Li J; Zhao Y; Xie X; Jin Z; Peng J; Liu F; Li C; Li Y; Bai F; Wang H; Cheng X; Cen X; Hu S; Yang X; Wang J; Liu X; Xiao G; Jiang H; Rao Z; Zhang LK; Xu Y; Yang H; Liu H, Structure-based design of antiviral drug candidates targeting the SARS-CoV-2 main protease. *Science* 2020, 368 (6497), 1331–1335. [PubMed: 32321856]
- (32). Su HX; Yao S; Zhao WF; Li MJ; Liu J; Shang WJ; Xie H; Ke CQ; Hu HC; Gao MN; Yu KQ; Liu H; Shen JS; Tang W; Zhang LK; Xiao GF; Ni L; Wang DW; Zuo JP; Jiang HL; Bai F; Wu Y; Ye Y; Xu YC, Anti-SARS-CoV-2 activities in vitro of Shuanghuanglian preparations and bioactive ingredients. *Acta Pharmacol Sin* 2020, 41 (9), 1167–1177. [PubMed: 32737471]
- (33). Qiao J; Li YS; Zeng R; Liu FL; Luo RH; Huang C; Wang YF; Zhang J; Quan B; Shen C; Mao X; Liu X; Sun W; Yang W; Ni X; Wang K; Xu L; Duan ZL; Zou QC; Zhang HL; Qu W; Long YH; Li MH; Yang RC; Liu X; You J; Zhou Y; Yao R; Li WP; Liu JM; Chen P; Liu Y; Lin GF; Yang X; Zou J; Li L; Hu Y; Lu GW; Li WM; Wei YQ; Zheng YT; Lei J; Yang S, SARS-CoV-2 M(pro) inhibitors with antiviral activity in a transgenic mouse model. *Science* 2021, 371 (6536), 1374–1378. [PubMed: 33602867]
- (34). Lee TW; Cherney MM; Liu J; James KE; Powers JC; Eltis LD; James MNG Crystal Structures Reveal an Induced-Fit Binding of a Substrate-like Aza-Peptide Epoxide to SARS Coronavirus Main Peptidase. *J. Mol. Biol* 2007, 366 (3), 916–932. [PubMed: 17196984]
- (35). St. John SE; Tomar S; Stauffer SR; Mesecar AD Targeting Zoonotic Viruses: Structure-Based Inhibition of the 3C-like Protease from Bat Coronavirus HKU4 - The Likely Reservoir Host to the Human Coronavirus That Causes Middle East Respiratory Syndrome (MERS). *Bioorganic Med. Chem* 2015, 23 (17), 6036–6048.
- (36). Grum-Tokars V; Ratia K; Begaye A; Baker SC; Mesecar AD Evaluating the 3C-like Protease Activity of SARS-Coronavirus: Recommendations for Standardized Assays for Drug Discovery. *Virus Res.* 2008, 133 (1), 63–73. [PubMed: 17397958]
- (37). Uzunova K; Filipova E; Pavlova V; Vekov T. Insights into Antiviral Mechanisms of Remdesivir, Lopinavir/Ritonavir and Chloroquine/Hydroxychloroquine Affecting the New SARS-CoV-2. *Biomed. Pharmacother* 2020, 131 (May), 110668.
- (38). Wang M; Cao R; Zhang L; Yang X; Liu J; Xu M; Shi Z; Hu Z; Zhong W; Xiao G. Remdesivir and Chloroquine Effectively Inhibit the Recently Emerged Novel Coronavirus (2019-NCoV) in Vitro. *Cell Res.* 2020, 30 (3), 269–271. [PubMed: 32020029]
- (39). Xue X; Yang H; Shen W; Zhao Q; Li J; Yang K; Chen C; Jin Y; Bartlam M; Rao Z. Production of Authentic SARS-CoV Mpro with Enhanced Activity: Application as a Novel Tag-Cleavage Endopeptidase for Protein Overproduction. *J. Mol. Biol* 2007, 366 (3), 965–975. [PubMed: 17189639]
- (40). Tomar S; Johnston ML; John SES; Osswald HL; Nyalapatla PR; Paul LN; Ghosh AK; Denison MR; Mesecar AD Ligand-Induced Dimerization of Middle East Respiratory Syndrome (MERS)

- Coronavirus Nsp5 Protease (3CLpro): Implications for Nsp5 Regulation and the Development of Antivirals. *J. Biol. Chem* 2015, 290 (32), 19403–19422. [PubMed: 26055715]
- (41). Otwinowski Z; Minor W. Processing of X-Ray Diffraction Data Collected in Oscillation Mode. *Methods Enzymol.* 1997, 276, 307–326. [PubMed: 27754618]
- (42). McCoy AJ; Grosse-Kunstleve RW; Adams PD; Winn MD; Storoni LC; Read RJ Phaser Crystallographic Software. *J. Appl. Crystallogr* 2007, 40 (4), 658–674. [PubMed: 19461840]
- (43). Kneller DW; Phillips G; O'Neill HM; Jedrzejczak R; Stols L; Langan P; Joachimiak A; Coates L; Kovalevsky A. Structural Plasticity of SARS-CoV-2 3CL Mpro Active Site Cavity Revealed by Room Temperature X-Ray Crystallography. *Nat. Commun* 2020, 11 (1), 7–12. [PubMed: 31911587]
- (44). Moriarty NW; Grosse-Kunstleve RW; Adams PD Electronic Ligand Builder and Optimization Workbench (ELBOW): A Tool for Ligand Coordinate and Restraint Generation. *Acta Crystallogr. Sect. D Biol. Crystallogr* 2009, 65 (10), 1074–1080. [PubMed: 19770504]
- (45). Liebschner D; Afonine PV; Baker ML; Bunkoczi G; Chen VB; Croll TI; Hintze B; Hung LW; Jain S; McCoy AJ; Moriarty NW; Oeffner RD; Poon BK; Prisant MG; Read RJ; Richardson JS; Richardson DC; Sammito MD; Sobolev OV; Stockwell DH; Terwilliger TC; Urzhumtsev AG; Videau LL; Williams CJ; Adams PD Macromolecular Structure Determination Using X-Rays, Neutrons and Electrons: Recent Developments in Phenix. *Acta Crystallogr. Sect. D Struct. Biol* 2019, 75, 861–877. [PubMed: 31588918]
- (46). Emsley P; Lohkamp B; Scott WG; Cowtan K. Features and Development of Coot. *Acta Crystallogr. Sect. D Biol. Crystallogr* 2010, 66 (4), 486–501. [PubMed: 20383002]
- (47). Chuck CP; Chen C; Ke Z; Chi-Cheong Wan D; Chow HF; Wong KB Design, Synthesis and Crystallographic Analysis of Nitrile-Based Broad-Spectrum Peptidomimetic Inhibitors for Coronavirus 3C-like Proteases. *Eur. J. Med. Chem* 2013, 59, 1–6. [PubMed: 23202846]
- (48). Winn MD; Ballard CC; Cowtan KD; Dodson EJ; Emsley P; Evans PR; Keegan RM; Krissinel EB; Leslie AGW; Mccoy A; Mcnicholas SJ; Murshudov GN; Pannu NS; Potterton EA; Powell HR; Read RJ; Vagin A; Wilson KS Overview of the CCP4 Suite and Current Developments. *Acta Crystallogr. Sect. D* 2011, 67, 235–242. [PubMed: 21460441]
- (49). Shin WJ; Hara D; Gbormittah F; Chang H; Chang BS; Jung JU Development of Thermostable Lyophilized Sabin Inactivated Poliovirus Vaccine. *MBio* 2018, 9 (6), 1–13.
- (50). Shin W-J; Nam K-Y; Kim N-D; Kim S-H; No K-T; Seong B-L Identification of a Small Benzamide Inhibitor of Influenza Virus Using a Cell-Based Screening. *Chemotherapy* 2016, 61 (3), 159–166. [PubMed: 26821172]
- (51). Wang W; Shin WJ; Zhang B; Choi Y; Yoo JS; Zimmerman MI; Frederick TE; Bowman GR; Gross ML; Leung DW; Jung JU; Amarasinghe GK The Cap-Snatching SFTSV Endonuclease Domain Is an Antiviral Target. *Cell Rep.* 2020, 30 (1), 153–163.e5. [PubMed: 31914382]
- (52). Zientek M; Jiang Y; Youdim K; Obach RS In Vitro-In Vivo Correlation for Intrinsic Clearance for Drugs Metabolized by Human Aldehyde Oxidase. *Drug Metab. Dispos* 2010, 38 (8), 1322–1327 [PubMed: 20444863]
- (53). Obach RS Prediction of Human Clearance of Twenty-Nine Drugs from Hepatic Microsomal Intrinsic Clearance Data: An Examination of in Vitro Half-Life Approach and Nonspecific Binding to Microsomes. *Drug Metab. Dispos* 1999, 27 (11), 1350–1359. [PubMed: 10534321]
- (54). Turlington M; Chun A; Jacobs J; Dawson E; Daniels JS; Saldanha A; Chase P; Hodder P; Eggler A; Tokars V; Mesecar A; Lindsley CW; Stauffer SR Non-Covalent Triazole-Based Inhibitors of the SARS Main Proteinase 3CLpro; Probe Reports from the NIH Molecular Libraries Program, 2013.

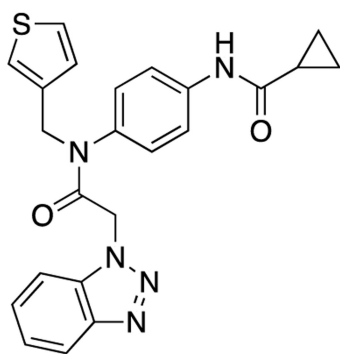
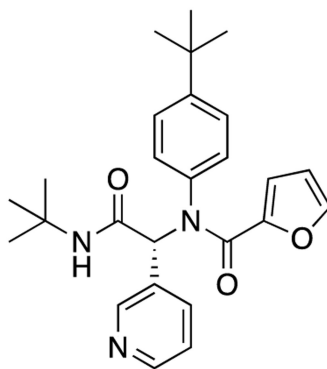
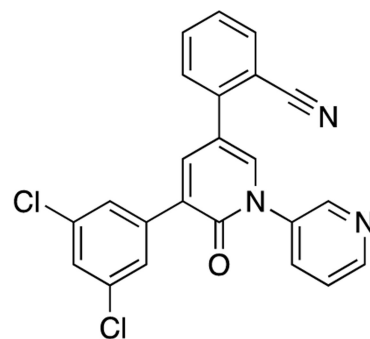
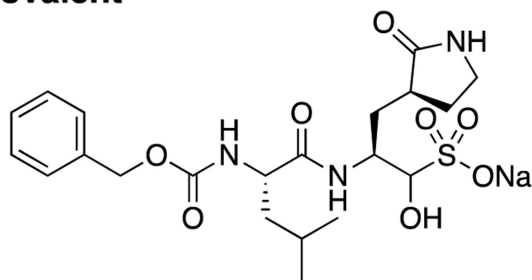
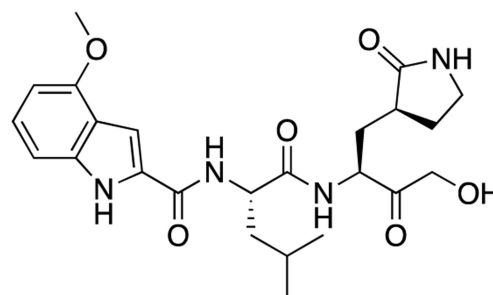
Non-Covalent**1**
ML300²¹**2**
ML188²⁰**3**²²**Covalent****4**
GC376²³**5**
PF-00835231²⁴

Figure 1.
Exemplary structures of reported 3CL^{pro} inhibitors for SARS-CoV-1 and SARS-CoV-2 using either a non-covalent (top) or covalent (bottom) mechanism of action.

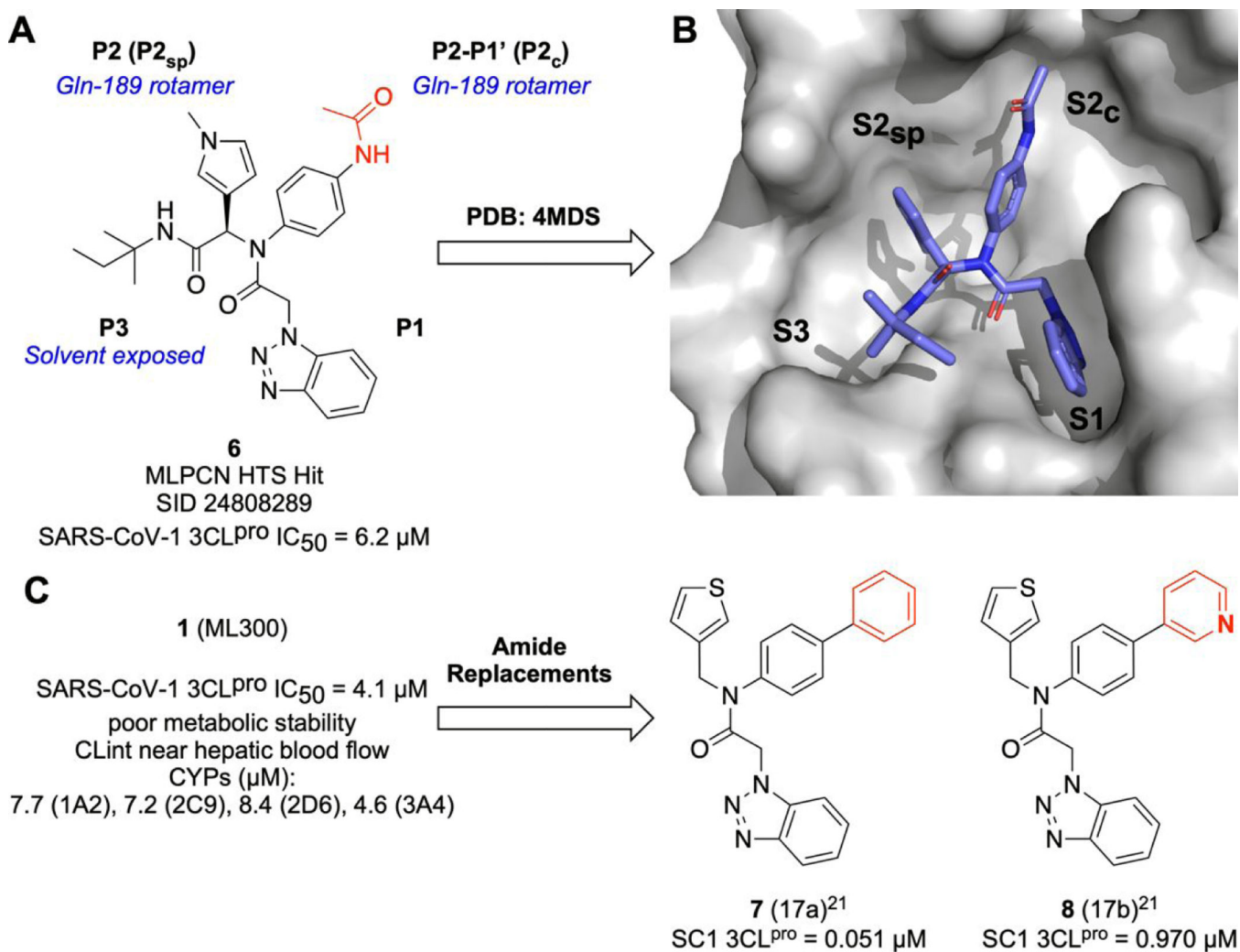


Figure 2. Non-canonical binding mode of MLPCN HTS compound **6** (SID 24808289) and evolution to ML300 and related bi-phenyl analogs **7** and **8** originally developed for SARS-CoV-1 3CL^{pro}. **A**) Schematic of binding mode of **6** orienting the binding site; **B**) Solvent accessible surface of SC1 3CL^{pro}:**6** complex, illustrating flexibility and reorganization of the binding pocket (PDB: 4MDS). **C**) Profile of **1** (ML300) and biaryl analogs **7** and **8**.

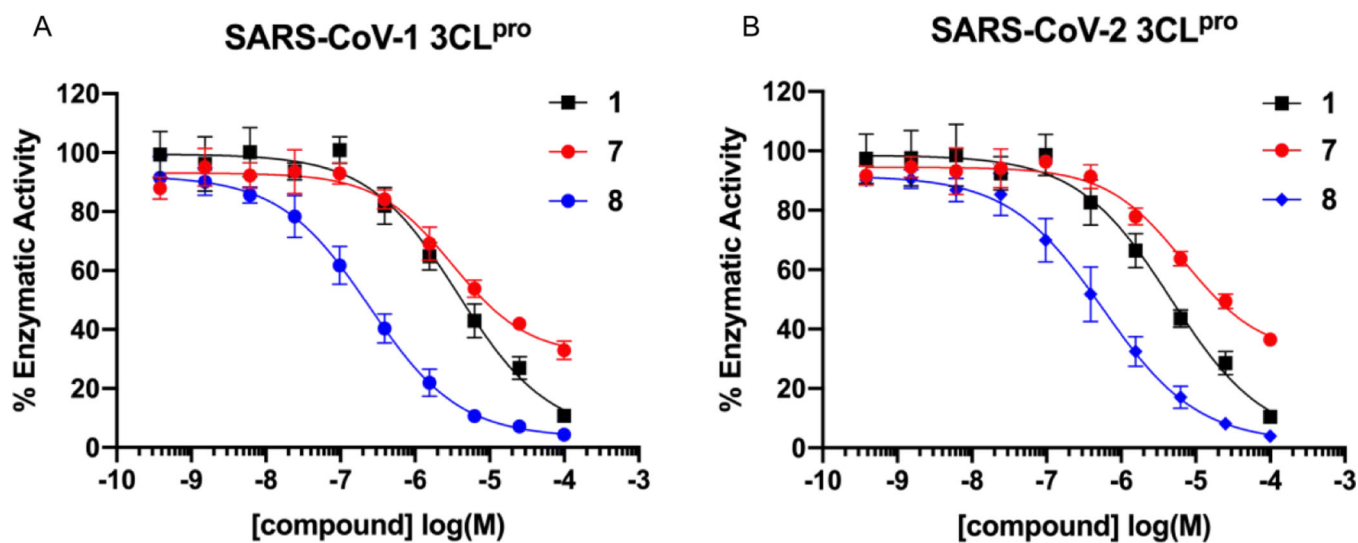


Figure 3.
3CL^{pro} concentration response curves for compounds **1**, **7** and **8**, against SC1 (A) and SC2 (B) enzymes.

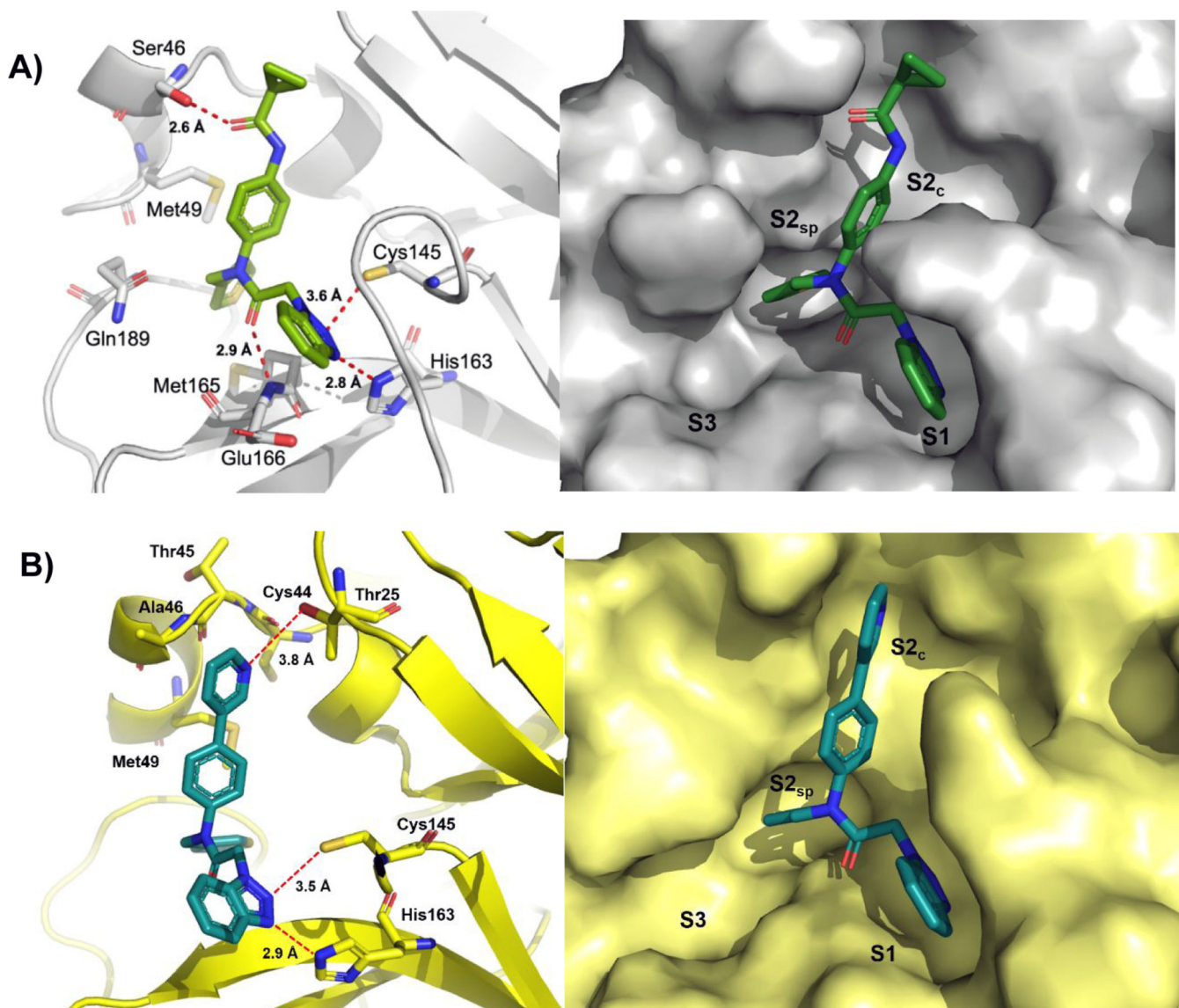


Figure 4.

A) X-ray co-crystal structure of **1** in complex with SC2 3CL^{Pro} (PDB: 7LME) and B) **8** in complex with SC1 3CL^{Pro} (PDB: 7LMH). Left panel: key residues are highlighted as sticks and interatomic distances depicted as dashes; right panel: solvent accessible surface with occupied and neighboring pockets labeled. Binding orientation of each inhibitor is the same in the active site of each monomer of the dimer in the asymmetric unit, only one active site is shown for clarity.

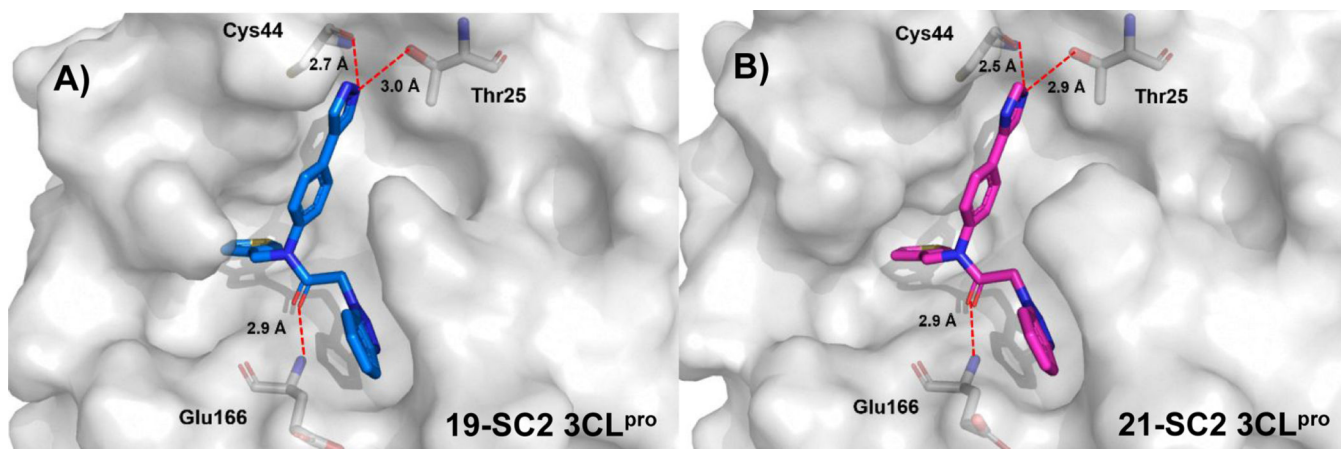
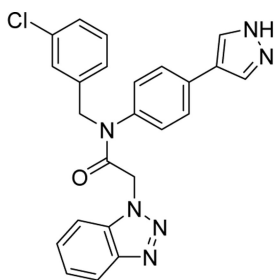
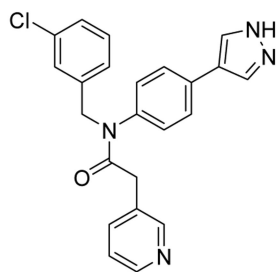


Figure 5. X-ray co-crystal structures of compounds **19** and **21**, select residues are shown as sticks with key hydrogen bonds shown as dashes. **A)** **19** in complex with SC2 3CL^{pro} (PDB: 7LMD); **B)** **21** in complex with SC2 3CL^{pro} (PDB: 7LMF)

**36**SC2 3CL^{pro} IC₅₀ = 0.270 μMhS9 CL_{int} = 436 mL/min/kgCL_{int} (h, r) = 2621, 5668 mL/min/kgf_u (h, r) = 0.1, - %MDCK-MDR1 P_{app} = 39.4 x10⁻⁶ cm/s

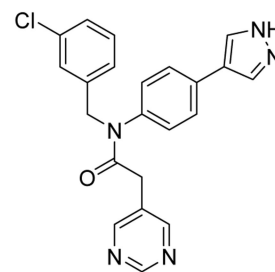
CYP's % inh @ 10 μM:

96% (3A4), 63% (2D6), 99% (2C9)

**42**SC2 3CL^{pro} IC₅₀ = 1.27 μMhS9 CL_{int} = 256 mL/min/kgCL_{int} (h, r) = 981, 3555 mL/min/kgf_u (h, r) = 0.4, 3.5 %MDCK-MDR1 P_{app} = 61.8 x10⁻⁶ cm/s

CYP's % inh @ 10 μM:

99% (3A4), 55% (2D6), 99% (2C9)

**43**SC2 3CL^{pro} IC₅₀ = 3.44 μMhS9 CL_{int} = 145 mL/min/kgCL_{int} (h, r) = 620, 3302 mL/min/kgf_u (h, r) = 1.8, 11 %MDCK-MDR1 P_{app} = 66.7 x10⁻⁶ cm/s

CYP's % inh @ 10 μM:

88% (3A4), 26% (2D6), 92% (2C9)

Figure 6.SC2 3CL^{pro} potency and DMPK profiles for lead benzotriazole **36**, **42**, and **43**.

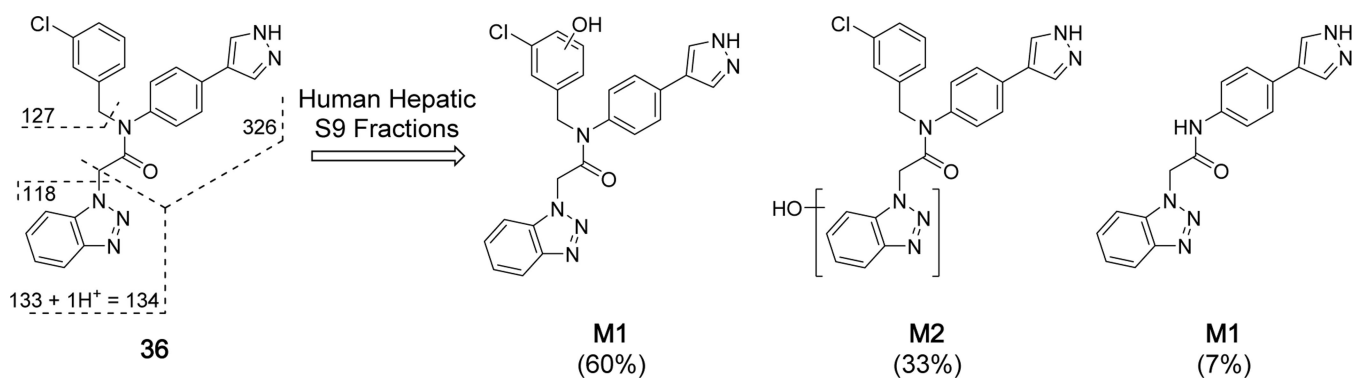


Figure 7. Soft-spot metabolite identification studies of **36** using human hepatic S9 fractions. Metabolite formation (%) is based on the total peak area of the three principle metabolites, M1, M2 and M3; see also Supplemental Table S2.

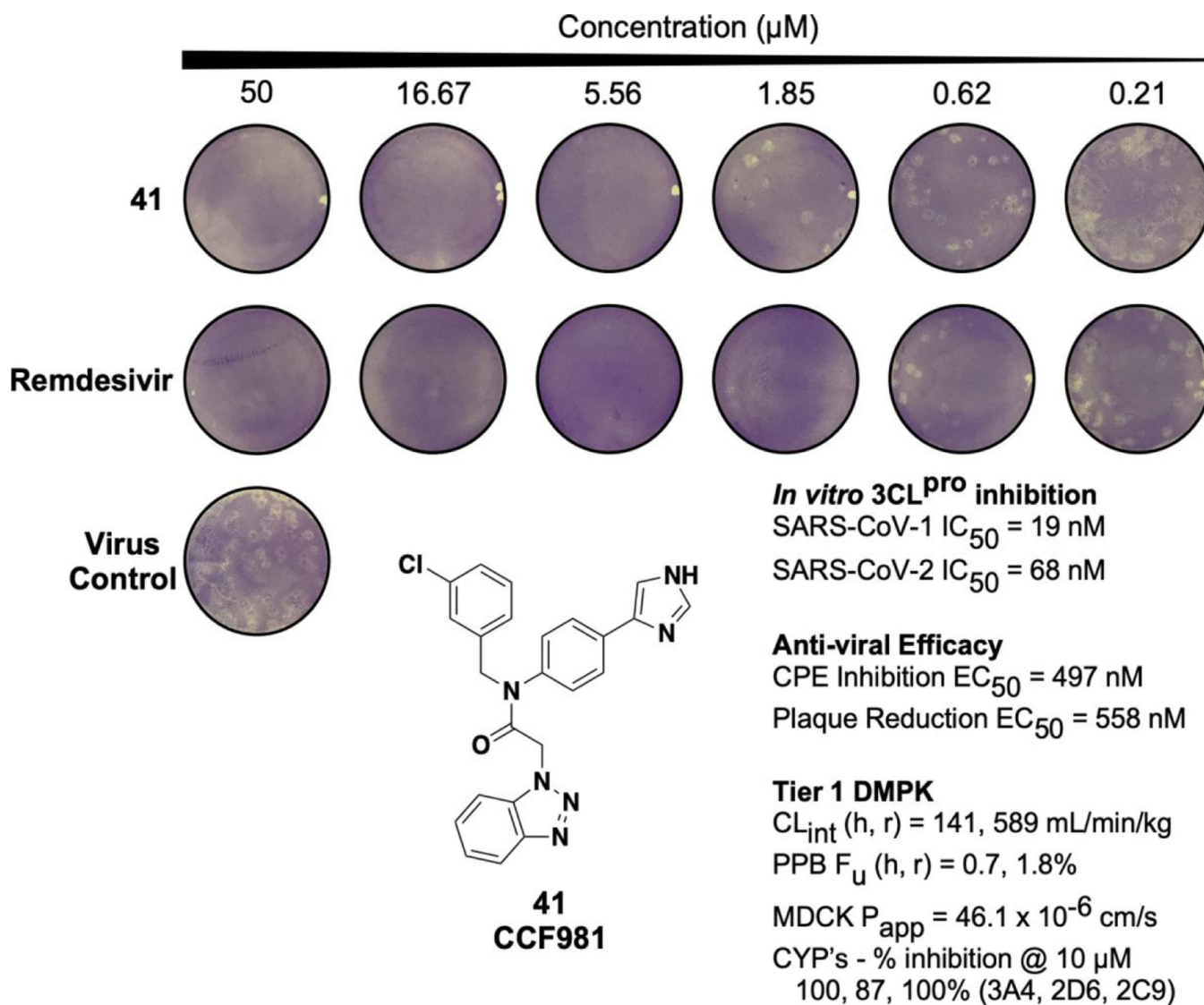
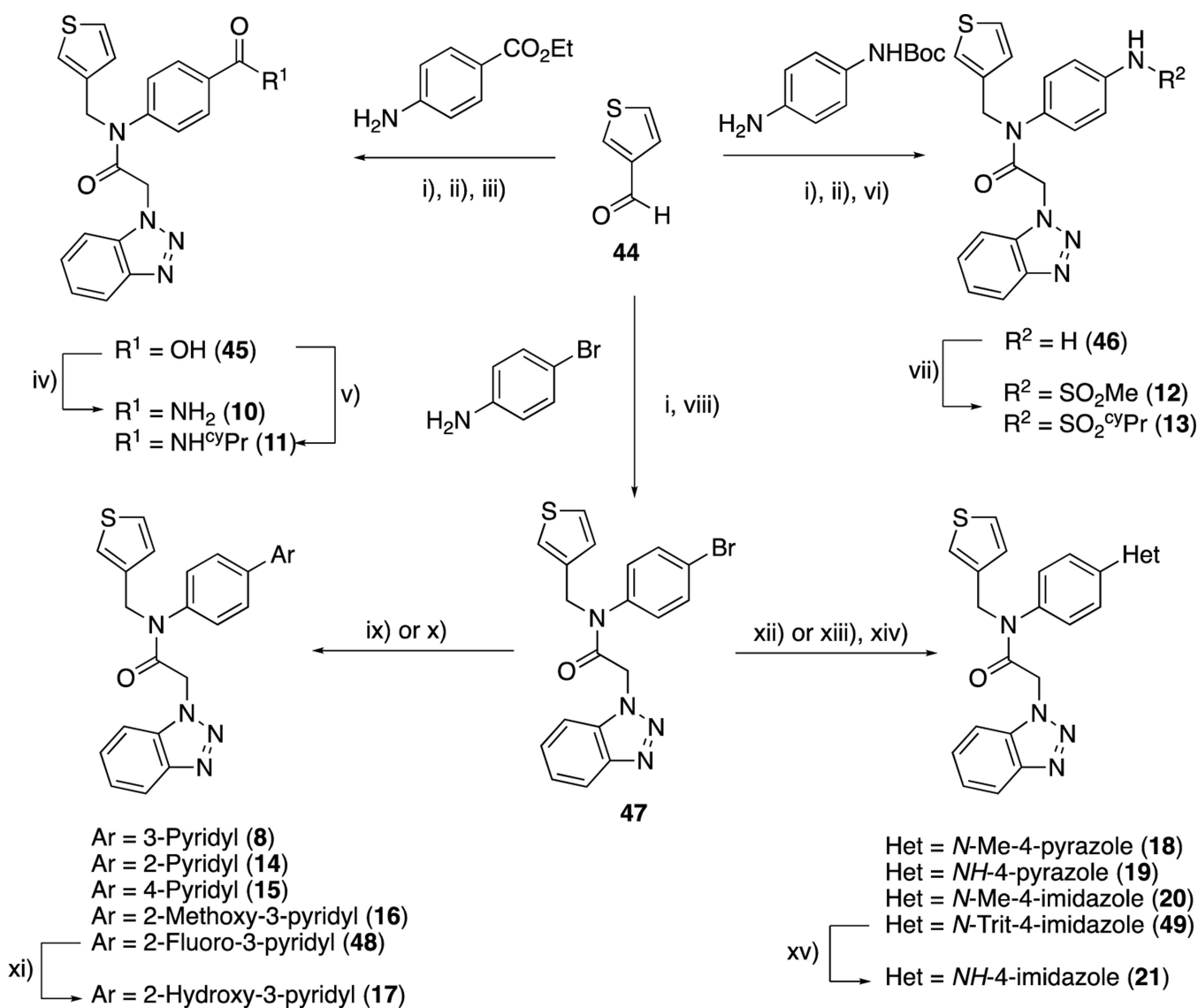
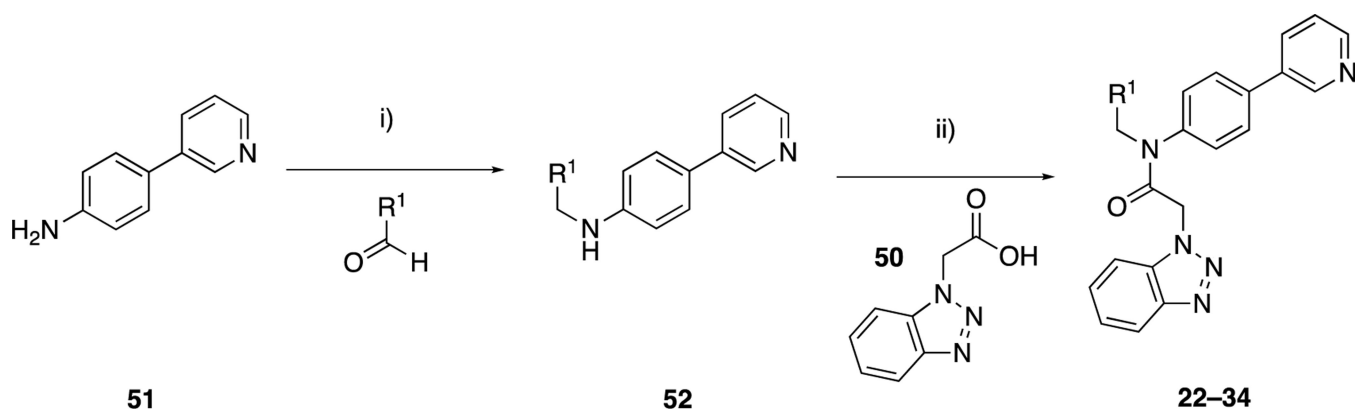


Figure 8.

Summary of data for compound **41** (CCF0058981). Images show antiviral activity of **41** and remdesivir against SARS-CoV-2 by plaque reduction assay. Vero E6 ACE2 cells were infected with approximately 50 plaque forming units per well of SARS-CoV-2. After 1 h incubation, the viral inoculum was removed, and the cells were overlaid with DMEM containing 1% low-melting agarose and indicated concentration of test compounds. At 3 days post-infection, the cells were fixed with 4% formaldehyde for at least 1 h. Overlay was then removed and cells were stained with 0.2% crystal violet containing 20% ethanol. The images are representatives of two repeats. Tier 1 DMPK data were obtained at Q² Solutions.

**Scheme 1.**

Synthesis of compounds **8–21**, from thiophene-3-carbaldehyde, **44**. Reagents and conditions: i) $\text{NaBH}(\text{OAc})_3$, AcOH, DCE, rt; ii) benzotriazole-1-acetic acid (**50**), T3P, EtOAc, rt; iii) LiOH , THF, rt; iv) NH_4Cl , EDC, HOBT, Et_3N , THF, rt; v) cyclopropylamine, COMU, DIPEA, DCM, rt; vi) TFA, DCM, rt; vii) $\text{R-SO}_2\text{Cl}$, Et_3N , DCM, rt; viii) **50**, HATU, Et_3N , DCM, rt; ix) $\text{ArB}(\text{OH})_2$, Pd(OAc)₂, dppf, CuCl, Cs₂CO₃, DMF, 100 °C; x) $\text{Ar-B}(\text{OH})_2$, Pd(PPh₃)₄, THF:H₂O, 100 °C; xi) aq. HCl, dioxane, 80 °C; xii) Ar-Bpin , Pd(dppf)Cl₂.DCM, K₂CO₃, dioxane, 100 °C; xiii) B_2pin_2 , Pd(dppf)Cl₂.DCM, KOAc, dioxane, 80 °C; xiv) 4-bromo-1-trityl-imidazole, Pd(dppf)Cl₂.DCM, K₂CO₃, dioxane, 100 °C; xv) AcOH, MeOH, 65 °C.

**Scheme 2.**

Synthesis of compounds **22-34**, varying the P2_{sp} substituent. Reagents and conditions: i) NaBH(OAc)₃, AcOH, DCE, rt; ii) T3P, pyridine, DMF, rt

MeOH, rt; xi) 1-THP-4-Bpin pyrazole, S/XPhos Pd G2, K₂CO₃, 1-BuOH, 100 °C; xii) **50**, cyanuric fluoride, pyridine, DCM, rt then **66** or **67**, Et₃N, THF 60 °C.

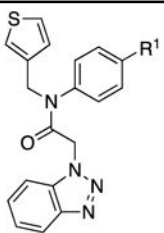
Author Manuscript

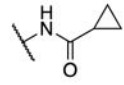
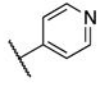
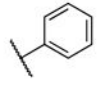
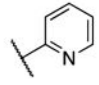
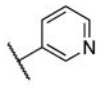
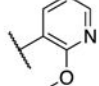
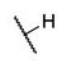
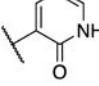
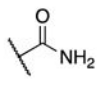
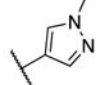
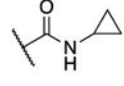
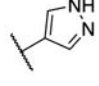
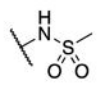
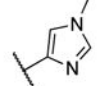
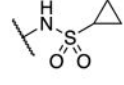
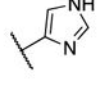
Author Manuscript

Author Manuscript

Author Manuscript

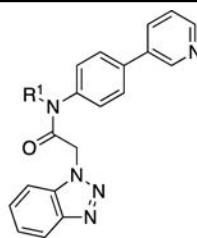
Table 1.

SARS-CoV-1 and SARS-CoV-2 3CL^{pro} inhibition data, exploring P2_c SAR


Compound	R ¹	^a SC1 3CL ^{pro} IC ₅₀ (μM)	^b SC2 3CL ^{pro} IC ₅₀ (μM)	Compound	R ¹	^a SC1 3CL ^{pro} IC ₅₀ (μM)	^b SC2 3CL ^{pro} IC ₅₀ (μM)
1 (ML300) ²¹		4.45 ± 0.26	4.99 ± 0.62	14		1.57 ± 0.60	2.09 ± 0.27
7 (17a) ²¹		16.82 ± 4.72	31.18 ± 4.65	15		0.90 ± 0.12	1.40 ± 0.21
8 (17b) ²¹		0.93 ± 0.05	0.95 ± 0.06	16		3.09 ± 0.52	5.07 ± 0.60
9		19.73 ± 3.01	18.87 ± 1.34	17		0.78 ± 0.15	0.92 ± 0.21
10		0.38 ± 0.04	0.44 ± 0.06	18		22.78 ± 1.87	20.39 ± 0.42
11		16.55 ± 0.44	15.94 ± 1.01	19		0.109 ± 0.020	0.106 ± 0.025
12		1.40 ± 0.41	1.61 ± 0.44	20		11.31 ± 1.52	9.55 ± 0.99
13		7.98 ± 0.42	8.77 ± 0.20	21		0.148 ± 0.038	0.063 ± 0.014

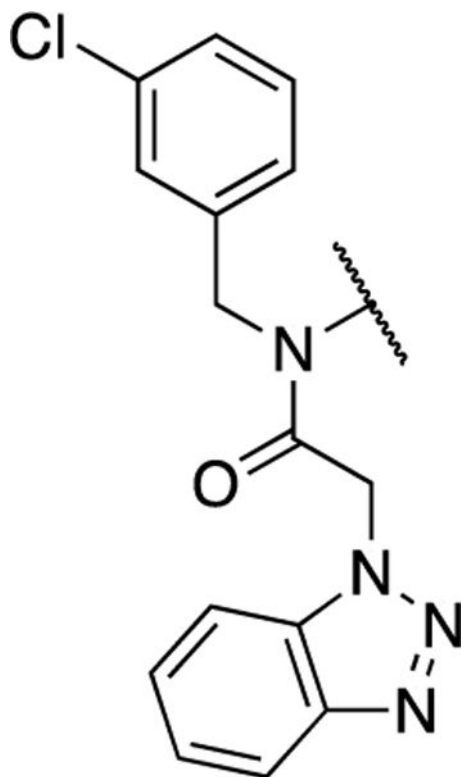
IC₅₀ values are average of at least 3 independent assays, each run as technical duplicates;^aSARS-CoV-1 3CL^{pro}^bSARS-CoV-2 3CL^{pro}.

Table 2.

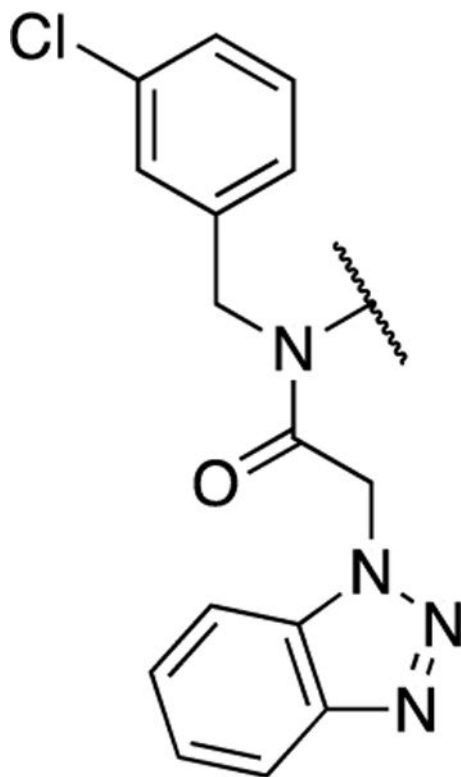
3CL^{pro} inhibition data, exploring P2_{sp} SAR

Compound	R ¹	^a SC1 3CL ^{pro} IC ₅₀ (μM)	^b SC2 3CL ^{pro} IC ₅₀ (μM)	Compound	R ¹	^a SC1 3CL ^{pro} IC ₅₀ (μM)	^b SC2 3CL ^{pro} IC ₅₀ (μM)
22		4.21 ± 0.19	4.62 ± 0.13	29		4.87 ± 1.87	8.53 ± 1.82
23		2.44 ± 0.39	2.51 ± 0.44	30		> 200	> 200
24		0.78 ± 0.06	0.83 ± 0.03	31		0.074 ± 0.01	0.119 ± 0.005
25		1.00 ± 0.21	1.16 ± 0.19	32		0.111 ± 0.018	0.176 ± 0.025
26		20.5 ± 1.59	23.0 ± 1.38	33		0.418 ± 0.065	0.312 ± 0.073
27		1.13 ± 0.26	1.59 ± 0.44	34		0.370 ± 0.105	0.540 ± 0.070
28		0.25 ± 0.07	0.39 ± 0.11				

IC₅₀ values are average of at least 3 independent assays, each run as technical duplicates;^aSARS-CoV-1 3CL^{pro}^bSARS-CoV-2 3CL^{pro}

Table 3.3CL^{pro} inhibition data, analogs exploring aniline-biaryl P2_c combinations

Compound	R ¹	^a SC1 3CL ^{pro} IC ₅₀ (μM)	^b SC2 3CL ^{pro} IC ₅₀ (μM)
35		0.657 ± 0.405	0.746 ± 0.098
36		0.334 ± 0.126	0.270 ± 0.067
37		0.206 ± 0.052	0.328 ± 0.027



Compound	R ¹	^a SC1 3CL ^{pro} IC ₅₀ (μM)	^b SC2 3CL ^{pro} IC ₅₀ (μM)
38		0.208 ± 0.077	0.197 ± 0.050
39		0.336 ± 0.065	0.333 ± 0.093
40		0.214 ± 0.063	0.171 ± 0.029
41		0.019 ± 0.005	0.068 ± 0.023

IC₅₀ values are average of at least 3 independent assays, each run as technical duplicates

^aSARSCoV-1 3CL^{PRO}

^bSARS-CoV-2 3CL^{PRO}

Author Manuscript

Author Manuscript

Author Manuscript

Author Manuscript

Table 4.Assessing antiviral efficacy of compounds, measuring *in vitro* viral replication.

Compound	CPE Inhibition Assay EC ₅₀ (μM)	Plaque Reduction Assay EC ₅₀ (μM)
Remdesivir	0.34 ± 0.01	0.43 ± 0.06
1 (ML300)	19.90 ± 6.32	28.15 ± 1.30
8	12.07 ± 0.31	14.55 ± 1.22
19	5.76 ± 1.96	7.63 ± 1.65
21	1.74 ± 0.19	1.75 ± 0.25
28	7.61 ± 1.43	11.14 ± 0.37
35	8.77 ± 1.14	16.69 ± 2.44
36	1.98 ± 0.24	3.31 ± 0.10
37	2.93 ± 0.28	3.24 ± 0.27
38	2.30 ± 0.33	2.01 ± 0.49
39	3.81 ± 0.18	4.65 ± 0.11
40	1.91 ± 0.30	3.39 ± 0.21
41	0.497 ± 0.009	0.558 ± 0.041